JPRS-JST-91-019
6 JUNE 1991

Foreign Broadcast Information Service 50 ANNIVERSARY 1941 - 1991

JPRS Report

Science & Technology

Japan

FORMATION OF, OUTLOOK FOR APPLICATIONS OF HIGH TEMPERATURE SUPERCONDUCTING THIN FILMS

JPRS-JST-91-019
6 JUNE 1991

SCIENCE & TECHNOLOGY
JAPAN

FORMATION OF, OUTLOOK FOR APPLICATIONS OF HIGH TEMPERATURE SUPERCONDUCTING THIN FILMS

916C1001 Tokyo HYOMEN KAGAKU SEMINA in Japanese 27-29 Jun 90 pp 1-154

[Selected papers presented at the 10th Surface Science Seminar held 27-29 Jun 90 in Tokyo, sponsored by the Surface Science Society of Japan]

CONTENTS

Outlook for High Temperature Superconductivity

916C1001A Tokyo HYOMEN KAGAKU SEMINA in Japanese 27-29 Jun 90 pp 1-11

[Article by Koichi Kitazawa, Faculty of Engineering, University of Tokyo]

[Text] **1. Introduction**

Even with the passage of three years since the discovery of high temperature superconductivity, a method to evaluate it has not yet been established. The reasons for this may be, first, that the superconductivity mechanism has not yet been explained, and, second, that various tasks remain to be resolved before the development of applications can be initiated. Nonetheless, a large number of facts have actually been uncovered in the interim. Oxide superconductors have broken fresh physical and chemical grounds on a very widespread basis. Moreover, their depth is so great that it does not seem possible that they can be unveiled during a mere several-year timespan.

One problem which was seriously questioned during the initial research period of high temperature superconductivity involved whether it was possible to raise the density of the critical current to a level that would be usable on a practical basis. Another problem involved the difficulties encountered when working on them which, since they were ceramic materials, were caused by their mechanical properties. As for the first problem, the situation has become such that at least a partially optimistic outlook is currently held. This is due to the circumstance that, as a result of advances in the processing technology, it may become possible to obtain properties comparable to those of metallic superconductors. However, substantial innovations in the processing technology are still required before the properties of this very impressive data can be obtained in their final form.

Concerning the applications of high temperature superconductivity, an impetuous pessimism and an unfounded optimism, which ignore the technological level, have dominated the mass media. As can be seen from past examples of the materials development, superconductivity applications have begun to proceed cautiously, yet steadily, and require a great deal of effort. In this article, problems related to high temperature superconductivity will be discussed, particularly from the surface interface standpoint.

Table 1. Classification of Copper Oxide Superconductors
(Focusing attention on laminated structures)

La_2CuO_4 (214) System	
Phase T $\{(La,Sr)O\}_2\{--\}CuO_2$	(40K) Octahedral coordination K_2NiF_4 structure, Sr7.5%)
Phase T′ $\{--\}\{(Nd,Ce)_2O_2\}CuO_2$	(27K) Planar 4 coordination Electron-doped type, Ce7.5%) Pr or Sm may be used instead of Nd, Th may be used instead of Ce
Phase T* $\{(La,Sr)O\}_2\{(Nd,Ce)_2O_2\}Cu_2O_4$	(27K) Pyramidal coordination Here, $\{MO\}_2$ and $\{M_2O_2\}$ correspond to the insertion layers of the rock salt type and the fluorite type, respectively
$(LNO)_2CaCu_2O_4$ System	
Phase 2126 $(La,Sr)_2CaCu_2O_6$	(60K) Pyramidal double-layer structure (SR40%)
$\{(CuO)_n\cdot(BaO)_2\}LnCu_2O_4$ System	
123 system $LnBa_2Cu_3O_7$	(90K) Double pyramidal layer/single chain layer (Ln is a rare-earth element excluding Pr,Ce, and Tb)
248 system $Y_2Ba_4Cu_8O_{16}$	(90K) Double pyramidal layer/double chain layer
247 system $Y_2Ba_4Cu_7O_{15}$	(85K) Double pyramidal layer/alternate single and double chain layers
$\{(CuO)\cdot(BaO)_2\}(Ln_2O_2)Cu_2O_u$	(43K) (Ln is Ce, Nd, Sm, or Eu) T, T′, composite 123 type
$(BiO\cdot SrO)_2Ca_{n-1}Cu_nO_{2n}$ system	(or $Bi_2Sr_2Ca_{n-1}Cu_nO_{2n+4}$)
n = 1 (0–20K), 2 (60–90K), 3 (110K),	For n equal to or greater than 4, it exists only in a thin film
$\{BiO\cdot(SrO)_2\}Ca_{n-1}Cu_nO_u$	The case of n=2 alone is synthesized in a thin film (85K)
$(BiO\cdot SrO)_2(Ln_2O_2)Cu_2O_u$	(40K) (Ln = Ce + Nd,Sm,Eu, or Gd)
$(TlO\cdot BaO)_2Ca_{n-1}Cu_nO_u$	(or $Tl_2Ba_2Ca_{n-1}Cu_nO_u$)
n = 1 (phase 2201, 90K), 2 (phase 2212, 110K), 3 (phase 2223, 125 K),	4 (phase 2234, 110K)
$\{TlO\cdot(BaO)_2\}Ca_{n-1}Cu_nO_u$	
n = 1 (phase 1201, 20K), 2 (1212 phase, 80K), 3 (phase 1223, 110K),	4 (phase 1234, 122K)
$\{(PbO)_2\cdot Cu\cdot SrO_2\}Y,Ca)_{n-1}Cu_nO_u$	or $(Pb,Cu)_3Sr_2(Y,Ca)_{n-1}Cu_nO_u$,
n = 1 (phase 3201, 30K, where (Sr,La) not (Y,Ca), 2 (phase 3212, 83K)	
$\{(PbO)\cdot Cu\cdot(SrO)_2\}(Y,Ca)_{n-1}Cu_nO_u$	or $(Pb,Cu)_2Sr_2(Y,Ca)Cu_2O_u$ (phase 2212)
n = 2 (32K)	
$\{(Pb,M)O\}(SrO)_2(Y,Ca)_{n-1}Cu_nO_u$	or $(Pb,M)(Sr,Ba)_2(Y,Ca)Cu_2O_u$ (phase 1212)
n = 2: M = Sr(53K), M = Cu(20K), M = Cu Ba is solid-dissolved to the Cu	or Sr site

2. Material and Structural Characteristics

As shown in Table 1, since the discovery of high temperature superconductivity in 1986, a great deal of effort has been expended toward the discovery of new materials, and numerous materials have been discovered. So far, all high temperature superconductors have layered structures that include a CuO_2 layer. The critical temperature of superconductors that do not include Cu is currently 40 K ($(Ba \cdot K)BiO_3$).

A CuO_2 layer exhibits a metallic conductivity, and the layer sandwiched between the CuO_2 layers demonstrates a property which is somewhat like that of an insulator. During the past three years, the insertion layers shown in Figure 1 have been discovered. The superconductors listed in Table 1 are constructed by these kinds of insertion layers and their combinations.

The most important properties determined by the insertion layer combinations are the critical temperature and the anisotropy of the superconducting properties. A superconductor's degree of anisotropy depends upon the extent to which the interaction between the adjacent CuO_2 layers is weakened by the disposition of the insertion layer. Strong anisotropy in an oxide superconductor is a double-edged sword, i.e., so far, no high temperature superconductor has been obtained without the use of an inserted insulating layer. However, the same strong anisotropy makes the use of the superconductor as a material very difficult, as will be described later. Granting that anisotropy is an indispensable factor with regard to superconductivity, it becomes necessary to establish measures to suppress the problems connected with anisotropy to the lowest possible level in order to overcome these problems through technical means.

The extent to which an insertion layer contributes to the anisotropy depends on the type of insertion layer. In insertion layers such as those containing Y or Ca, which do not contain oxygen ions, the interaction between the adjacent CuO_2 layers is relatively large. In other words, the electrons can move between the adjacent CuO_2 layers with a relatively large transition probability. On the other hand, insertion layers such as $(BiO)_2(SrO)_2$ or $(TiO)_2(BaO)_2$ reduce the transition probability to a substantial degree.

Because of this, anisotropy is the smallest in $YBa_2Cu_3O_7$ (123 or YBCO; T_c = 90 K) (it is about 25 in terms of the effective mass ratio of the carrier, and about 5 in terms of the H_{c2} ratio), while it is large in $Bi_2Sr_2Ca_{n-1}Cu_nO_{2n-4}$ (BSCCO; T_c = 117 K for n = 3) (above ratios are, respectively, 3000 and 35). This tending does not necessarily have a direct effect on the T_c, and the anisotropy of $(La,Sr)_2CuO_4$ (T_c = 40 K) with low T_c is stronger than that of YBCO. This is the reason for anticipating the discovery of substances with weaker anisotropies but higher T_cs than those of YBCO. For the time being, however, we have no choice but to consider profitable uses of the materials that have already been discovered.

The characteristics of the materials that are currently under development for applications are shown in Table 2. Since each has advantages and disadvantages, parallel development is under way.

a) Insertion layers with relatively high electron transition probability

□ Y 123 (other rare-earth elements can also be used), considered to have the highest transition probability

□ Ca 2126, and 2212, 2223, etc., of the Bi, Tl-system

□ (La, Ca) 3212 of the Pb system, 1212 of the Tl system, etc.

b) Insertion layers with low electron transition probability

○ $\begin{pmatrix} LnO \\ OLn \end{pmatrix}$ 214 (T phase, T^* phase)

□ $\begin{pmatrix} Ln \\ O\text{-}O \\ Ln \end{pmatrix}$

○ $\begin{pmatrix} OBa \\ CuO \text{ chain} \\ OBa \end{pmatrix}$ 123

○ $\begin{pmatrix} OBa \\ CuO \text{ chain} \\ CuO \text{ chain} \\ OBa \end{pmatrix}$ 247, 248

○ $\begin{pmatrix} OSr \\ BiO \\ BiO \\ OSr \end{pmatrix}$ or $\begin{pmatrix} OBa \\ TlO \\ TlO \\ OBa \end{pmatrix}$ Bi, Tl system (Pb replacement possible)
2201, 2212, 2223, 2234, 2222

○ $\begin{pmatrix} OSr \\ BiO \\ OSr \end{pmatrix}$ or $\begin{pmatrix} OBa \\ TlO \\ OBa \end{pmatrix}$ Bi system thin film 1212
Tl system 1201, 1212, 1223, 1234

○ $\begin{pmatrix} OSr \\ PbO \\ Cu \\ PbO \\ OSr \end{pmatrix}$ Pb system 3212, 3222 (NS)

○ $\begin{pmatrix} OSrOSr \\ PbO\text{-}Cu \\ Cu\text{-}PbO \\ OSrOSr \end{pmatrix}$ Pb system 2212

○ $\begin{pmatrix} OSrOSr \\ PbOCuO \\ OSrOSr \end{pmatrix}$ Pb system 2212, 1201

Figure 1. Various Kinds of Insertion Layers That Separate Laminated CuO_2 Layers

□: Does not supply a vertex oxygen

○: Supplies a vertex oxygen; NS: Nonsuperconductivity

Table 2. Materials Under Study for Applications

1) $Yba_2Cu_3O_7$	Most widely studied, high degree of freedom for thin film orientation
(90 K)	Tends to deteriorate with the escape of oxygen Somewhat defective in chemical stability (stable phase at high temperature) Coupling between grain boundaries is weak, but the pinning force is retained until high temperatures reached Has the least anisotropy
2) $Y_2Ba_4Cu_8O_{16}$	More stable than 1) at temperatures below about 800°C Oxygen is less likely to escape
(80~90 K)	Decomposes at high temperatures Larger anisotropy than 1) T_c can be raised to 90 K by Ca addition
3) $(Bi,Pb)_2Sr_2Ca_2Cu_3O_u$	Hard to put into a single phase
(107 K)	Problems in thin film quality, possible only for c-axis orientation Rapid drop in pinning force above 30~50 K Large J_c under strong magnetic field (above 20 T) below 20 K Problem involving weak grain boundary coupling is considerably better than that in 1) Very large anisotropy, strong cleavage
4) $Bi_2Sr_2CaCu_2O_u$	Easy orientation Can be put into a single phase easier than 3)
(80~90 K)	Somewhat stronger chemical stability than 1) Problem involving weak grain boundary coupling is improved over 3) Anisotropy is stronger than in 3), very strong cleavage T_c can be raised by reduction treatment or addition of Li Easy orientation Highest J_c for wire at 4.2 K and magnetic field above 20 T
5) $Tl_mBa_2Ca_{n-1}Cu_nO_u$	Hard to control process, with easy Tl evaporation
(90~125 K)	Problem involving weak grain boundary coupling is better than 1), but inferior to 3)
(m = 1 or 2)	Problems with thin film quality, orientation possible for c axis only Weak cleavage, orientation is harder than for 3) Slightly weaker anisotropy than 3) and 4) Low noise in SQUID

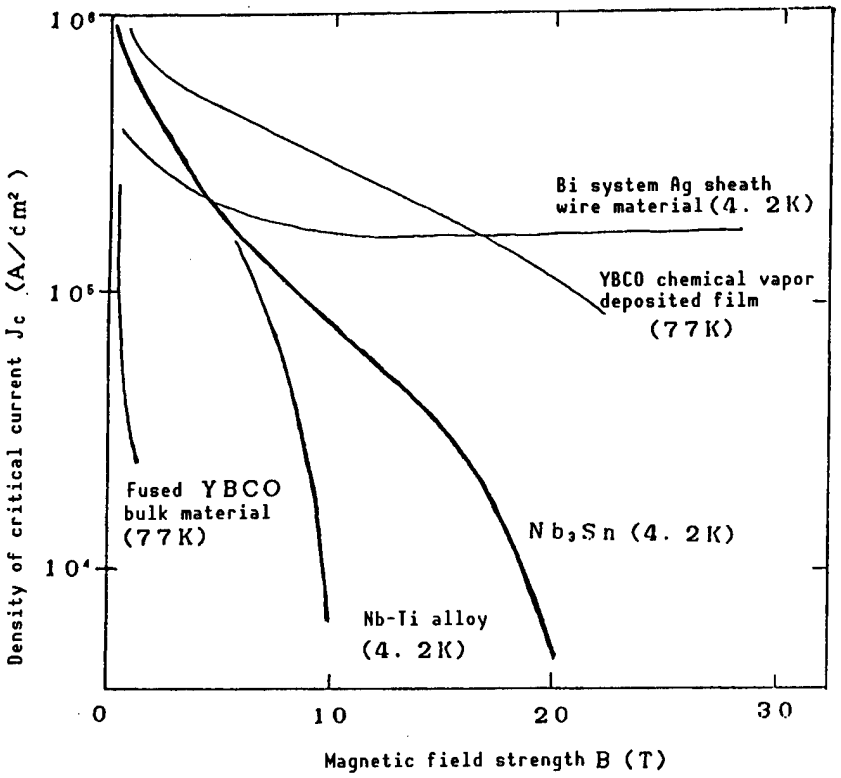

Figure 2. Comparison of Performance of Oxide and Metal Superconducting Materials

3. Critical Current

During the initial two years following the discovery of high temperature superconductivity, fairly strong pessimism prevailed regarding the critical current. However, with the progress in the process-related concepts, the very impressive data involving the critical current were updated in succession, and have already attained the level shown in Figure 2, i.e., as far as thin films are concerned, this impressive data (at 77 K) has reached a level comparable to that of metallic materials at 4.2 K. In addition, for materials used in wires and tapes, although short in length, the critical current density at 77 K may be said to have attained the level just short of the practical level.

On the other hand, proposals have been presented to try to use high temperature superconductors at 4.2 K or at around 20 K, for which cooling is fairly easy. At these temperatures, the critical current density of the high temperature superconductors has been found to be very excellent in that it hardly deteriorates, especially under a strong magnetic field, in comparison to that of metallic materials. One particularly promising application is in the generation of a magnetic field equal to or stronger than 20 T, which is said to be difficult to achieve with the superconducting magnet currently available.

Such progress owes much to the elimination of weak coupling. One of the biggest drawbacks of oxide superconductors is that the superconductivity is weakened on the interface of the polycrystalline particles, resulting in a drop of the critical current that traverses the grain boundary. Because of this, past efforts have mainly been directed toward the elimination of the grain boundaries exhibiting weak coupling, i.e., ways have been sought to orient the polycrystalline particles in the direction of the current passage. Typical examples of these efforts are seen in the film epitaxy, orientation by means of wire drawing that utilizes the anisotropic mechanical properties, orientation by means of the directional solidification of a molten body, etc. It has been shown that the deterioration in the critical current can be avoided to a fair extent by employing these techniques.

Needless to say, it is more convenient to modify the grain boundaries themselves and strengthen the coupling than to remove the grain boundaries. Although it has been suggested that grain boundary modification in this direction is possible in principle, methods for accomplishing this have not yet been found, so it will remain a future task.

Moreover, attempts to actively introduce pinning centers, in addition to the effort to remove the weak coupling, have made a large contribution to the substantial enhancement of the critical current. From the initial period on it was noticed that the critical current often obtained in thin films was larger than that of single crystals. In thin films, apparently some unintended pinning centers existed. It has recently been found that pinning centers can be obtained in the single crystals formed by the melt method through the introduction of fine precipitates or the introduction of defects by means of irradiation loss. No definitive conclusion has yet been reached as to what these pinning centers are. In YBCO, fine phase 211(Y_2BaCuO_4) precipitates CuO precipitates, clusters of oxygen voids, formation of fine defect regions due to irradiation loss, etc., are believed to represent powerful candidates.

As will be shown later, a very short coherence length of superconductivity is one feature of oxide superconductors. For this reason, it is anticipated that very fine pinning centers on the nanometer order, which is comparable to the coherence length, will be effective. Therefore, the time has come when the process design utilizing the full knowledge of the control of fine structures (nucleus formation, spinodal decomposition, recrystallization processes, etc.) accumulated during metallurgical and ceramic studies, is needed. In addition, the use of a transmission electron microscope is indispensable for the evaluation of fine defects. At any rate, the trend is for delicate fine structure control techniques to be developed, based on the fact that the introduction of pinning centers has been found to be effective.

4. Anisotropy

The problems due to the anisotropy originating from the above-mentioned layered structure can be better understood by contemplating the following concept. A high temperature superconductor resembles the laminated structure of a superconducting sheet with an atomic scale thickness and an insulating sheet, as mentioned above. Consequently, problems arise when a current is

passed in the direction perpendicular to these layers. Of course, a certain amount of tunneling current passes via the insulating layer, but it is inevitable that the critical current will be reduced to a large extent. This is the first problem.

Next, with the application of a magnetic field, when the magnetic flux lines and the layers are parallel, almost all of the magnetic flux lines will run through the inserted insulating layer due to the fact that it is difficult for the magnetic flux lines to enter the superconductor because of diamagnetism. Accordingly, a weak effect is exerted on the superconductor. This strengthens the critical magnetic field in that direction to a large extent. If, in this case, a current flows in the superconducting layer parallel to the magnetic field, the magnetic flux lines tend to move perpendicular to the layer (c axis). However, although the magnetic flux lines stay within the inserted insulating layer readily, they are less likely to stay within the superconducting layer, so they are trapped within the insulating layer. This effect is called the intrinsic pin effect. At any rate, the conditions I//ab and H//ab are the most favorable conditions for oxide conductors.

On the other hand, if an attempt is made to pass a current perpendicular to the layer, the magnetic flux lines receive the Lorentz force and tend to move in the direction that crosses the line of the current. When they move an electric resistance is generated. Since it is difficult to pin the magnetic flux lines so they cannot move within the inserted insulating layer, conditions I//c and H//ab are the most unfavorable conditions for oxide super-conductors. Accordingly, it is necessary to think of ways to avoid their use when these conditions prevail. For this reason, the materials must have a highly oriented state in which the layers are arrayed in the direction of the current.

However, even if one attempts to use a material so as to satisfy the first condition above as much as possible, a portion remains in which the magnetic distribution is not necessarily parallel to the layers. It becomes necessary to consider the case in which the magnetic field is perpendicular to the layers by passing a current through the layers. In this case, as shown in Figure 3, the magnetic flux lines tend to move, remaining perpendicular to the layers, but the pinning force will not act since they represent an energetically equivalent state wherever they are. Therefore, it becomes necessary to immobilize the magnetic flux lines by introducing a large number of inhomogeneous micro regions into the material. An inhomogeneous region introduced to immobilize the magnetic flux lines is called a pinning center. The pinning problem that is the most serious in oxide superconductors occurs in this case. The most suitable size for a pinning center is about the effective thickness of the magnetic flux lines that have crept in to the superconductor. This thickness corresponds to the thickness of the region of the superconductor damaged along the magnetic flux lines. This is the coherence length.

With the rise in the superconductors critical temperature, the coherence length is reduced. In oxide high temperature superconductors, this length is less than 10 Å. In other words, the most ideal oxide superconductor seems to require such superfine inhomogeneous regions. further, the coherence length in the direction of the c axis is less than several angstroms because of the anisotropy. This, in turn, gives rise to new problems.

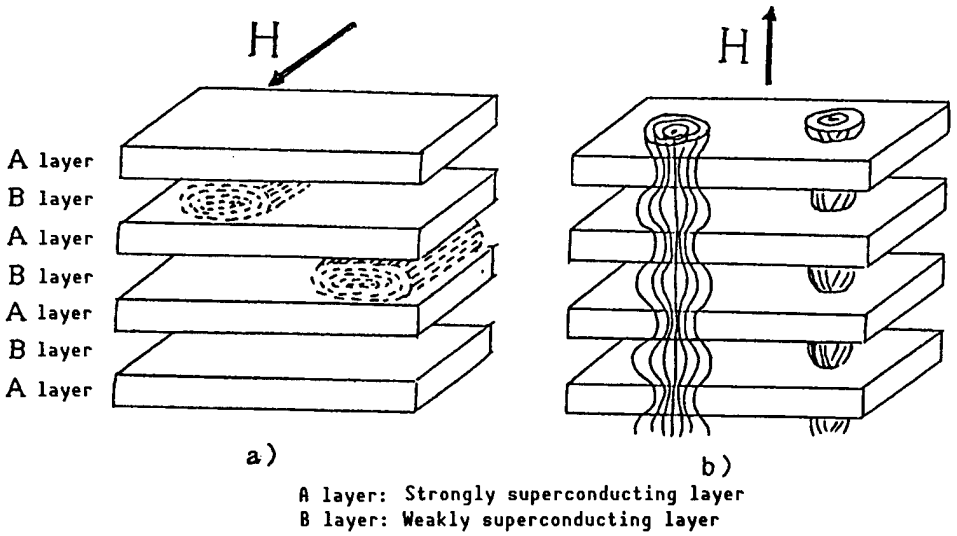

Figure 3. Quantized Magnetic Flux Lines Expected for a Laminated Layer Structure of Two Kinds of Strongly and Weakly Superconducting Layers
(a) The intrinsic pinning is not operative.
(b) The intrinsic pinning is expected to act in the vertical direction.
(The magnetic flux lines are energetically stable when they lie in the weakly superconducting layers.)

The coherence length (ξ_c) in the c-axis direction is about 3 Å for YBCO, and is estimated to be about 1~2 Å (this value is still smaller than the estimated value early on) for BSCCO. These values are smaller than a fraction of the lattice constant in the c-axis direction. Moreover, when one compares them with the value of about 200 Å for Nb, which is a typical metallic superconductor, one should be able to recognize the significant difference between these values. On the other hand, for the in-layer direction, ξ_{ab} is estimated at about 13 Å for both materials.

The quantity ξ is the size of the Cooper pair, or the minimum size at which superconductivity can appear, or the minimum size at which superconductivity breaks down. In terms of volume it corresponds to $\xi_o\xi_{ab}^2$, i.e., when a change occurs within a superconductor, it is the minimum volume at which the change takes place. If the energy per unit volume accompanying the change is denoted as E (the condensation energy of superconductivity), the change that occurs at the minimum volume is $\epsilon = E\xi_o\xi_{ab}^2$. It has been determined that the values of E for oxide superconductors and metals are comparable. Accordingly, the size of ϵ in an oxide superconductor should be smaller than that in a metal by several orders of magnitude, and is estimated at several millielectron volts.

The magnitude of thermal energy at the liquid nitrogen temperature, 77 K, is about 6 meV, which is close to the above-mentioned value. This means that a disturbance in the microscopic conductivity due to heat tends to take place at approximately 77 K. The manifestations of this phenomenon are being examined from various volume percentages, including the magnetic flux creep, melting magnetic flux lattice, fluctuations, Kosterliz-Thouless transition, etc., but their roots are essentially the same.

Such fluctuation phenomena due to heat are currently of concern at the "high temperature" of 77 K. This problem requires a quantitative thermostatical mechanical analysis, but sufficient understanding is not advanced and remains a scientific task to be solved in the future. However, the direction of the application development is relatively clear, and the applications hinge upon whether ξ_c can be made larger, or at what point it may be possible to suppress the fluctuations, by the introduction of as many pinning centers as possible, on the microscopic level.

Although the way to control ξ_c is not necessarily clear at the present time, some kind of modification of the carrier concentration or the above-mentioned insertion layer will be necessary.

5. Josephson Junction

To obtain a Josephson junction under controlled conditions is the basis for the application of superconducting electronics. It is not yet easy to achieve this for oxide superconductors. The reason for this is considered to be that the superconducting electron wave is confined to within the CuO_2 layer, and can seep out only to distances on the order of the coherence length. Moreover, this problem is particularly significant in the vertical direction (c-axis direction) of the layered film, along which film formation is normally easier. Accordingly, a future task for the filming process is whether it is possible to form a high quality film in an upright form (a-axis orientation). Such an a-axis-oriented film has already been realized to a certain degree, but it has slight defects involving surface flatness and film quality. Further, assuming that such a film is realized, the junction insulation barrier will be required to have a thickness on the order of an atomic layer. In other words, it looks as if the filming process will be required to be able to freely apply a technique something like atomic layer epitaxy.

Needless to say, it will be more than satisfactory if an isotropic new material can be discovered. However, at least for the time being, it would be unreasonable to expect that.

As a second best policy, for the time being, one may take the grain boundary junction approach. Since clean superconducting quantum interference device (SQUID) characteristics, free from hysteresis, have been obtained lately above 80 K by using a single grain boundary of a controlled YBCO thin film, a temporary practical level has been attained. On the individual element level, the goal may be said to have been achieved to a certain extent.

6. Weak Coupling

Although active use may be made of the kind of Josephson junction that is generated by the weakening of the superconductivity at the grain boundary, this approach involves generally troublesome problems.

The reasons for this seem to be related to the fact that the superconductivity is limited to approximately within the CuO_2 surface, the coherence length is short, on the order of the interatomic distance, and a grain boundary

potential barrier tends to be formed due to the fact that the carrier concentration is only one-tenth that of metals. Each of these factors represents a special property intrinsic to oxide superconductors, so its fundamental solution seems to present problems. The only possible solution is to lower the grain boundary potential to the vicinity of zero by adjusting it. The success of this approach hinges upon whether it is possible to satisfactorily control the grain boundary segregation (selective distribution of added elements), for which no successful record exists to date.

On the other hand, there is the position which seeks the cause of the weak grain boundary coupling in the presence of a second grain boundary phase or a grain boundary amorphous phase. In this case, by carefully removing these objects, a modification of the grain boundary will become possible. However, due to the difficulty encountered in characterizing a grain boundary as compared with a surface, research on this problem is destined to be postponed.

However, there exist examples of thin films in which the critical current density has attained a practical level, even though they are polycrystalline substances. Therefore, an improvement of the critical current density will be pursued for the time being, aimed at enhancing the orientability through trial and error.

7. Electronic Structure of High Temperature Superconductivity and Superconductive Mechanism

The mechanism of the high temperature superconductivity differs from that of metallic superconductivity, and it is often said that if it can be elucidated, a direction for the exploration of new materials and the basis for applications will be attainable. Of course, it is a correct argument, but from the standpoint of materials science and device development one has to be prepared, first of all, for the postponement of the elucidation of the mechanism. On the other hand, even if the mechanism is not firmly established, the Josephson junction characteristic between metallic superconductors and oxide superconductors has already been observed, and it has been confirmed that the superconductivity itself does not differ qualitatively from conventional superconductivity. Consequently, the only possible direction of research and development, for the time being, is to proceed by studying the quantitative differences of such characteristic parameters as the superconductive gap, penetration length, coherence length, etc., of metallic superconductors.

The reason for requiring time to elucidate the superconductivity mechanism is mainly due to the fact that it is still impossible to describe the electronic structure of normal conductors, which is a prerequisite for the question under discussion. The great success of semiconductors resides in the fortunate finding that a simple, straightforward and very rough approximate theory, called the band theory, was applicable. The concept of superconductivity heretofore was established on the basis of the Fermi liquid concept, which applies the band theory to metals by expansion. A substantial problem currently being encountered is that the Fermi liquid concept cannot be applied satisfactorily to oxide superconductors.

In other words, the strong interaction between electrons, which has so far been ignored, has to be considered explicitly. In the past, use was made of an approximation (one-electron approximation) in which the interaction was averaged, and which permitted the electron of interest to behave as a single electron in a potential incorporating the interaction. It has become clear that the interelectronic interaction in oxide superconductors is so strong that the above approximation is no longer permissible. Accordingly, first, a new concept is required that will replace the band theory and will be able to describe a many-electron system with strong electron correlation. This is a sufficiently difficult and interesting problem, which is challenging the theorists of solid-state physics. For this reason, various approaches are currently being developed, but their levels have not yet attained the levels which would enable the superconductivity critical temperature to be estimated quantitatively. Personnel who are participating in the practical development perhaps cannot afford to wait for such a theoretical development. Therefore, it will be necessary for us to develop research without presupposing the theoretical development, but instead using it as a hint by regarding it obliquely.

8. Conclusion

Problems involved in oxide superconductors are, for the most part, those related to surfaces and interfaces, as has been described above. Therefore, the future advances will largely depend on development in these fields. This is the reason that the active application by various kinds of surface analysis that have been accumulated are desired. In addition, layered structures in such material systems are such that it is to the point, in a sense, to think of them as laminated structures of the interfaces themselves. In that sense, studies based on surface and interface sciences are earnestly needed.

Predictions concerning oxide superconductors have always proceeded by pessimistic predictions being subsequently overturned by the actual results. This could be said to represent the luckiest situation for those who are involved in R&D. Moreover, products such as high frequency resonators, although small in size, have recently been put on the market. As for SQUID, too, it is expected that products that can satisfactorily produce cardiograms will be put on the market when combinations with coils become possible. On the other hand, in power applications, magnets that can generate superhigh magnetic fields, current leads, etc., are surfacing as the development targets. Steady and active efforts are expected to be continued toward full-scale application.

References

1. As a latest review including application development, see OYO BUTSURI, Vol 59 No 5, 1990.

2. The past development, especially the physical property aspect, is given in detail in issues of PARITY magazine (Maruzen Co.) published since 1987. Two issues of the magazine are available.

3. References to this article can be found on pp 553-570 of 1) above.

Crystal Structure of High Temperature Superconductors

916C1001B Tokyo HYOMEN KAGAKU SEMINA in Japanese 27-29 Jun 90 pp 13-26

[Article by Yoshio Matsui, Institute for Inorganic Materials Research, Science and Technology Agency]

[Text] **1. Introduction**

Since Bednorz and Muller's historical discovery,[1] research on oxide high temperature superconductors has entered its fifth year and the initial excitement seems to have gradually subsided. Since 1989, the T_c record has not been updated, but one example of a sensational topic was the discovery of electron injection type superconductors.[2] Since the oxide superconductors discovered so far are extremely diversified, it is impossible to state their characteristics in a word, but we can at least point out the following aspects:

(1) They contain copper (Cu) as a component element. In addition, a rare-earth element, an alkali-earth element, lead, bismuth, thallium, etc., are contained as important component elements. However, there are exceptional materials, such as (Ba,K) BiO_3.

(2) They have a perovskite-type structure (ABO_3) or a K_2NiF_4-type structure (A_2BO_4) as the base, to which positive replacements or oxygen defects are introduced (Figure 1).

(3) They have a two-dimensional layered structure.

(4) The oxygen defect plays an important role in the structural stability and superconductivity mechanism.

In this article, I will summarize the particularly interesting points from a crystalline structure viewpoint by paying attention to the yttrium and bismuth-system superconductors that are most promising for future applications from among the oxide superconductors reported so far. It should be mentioned that the data reported in this article are mainly those obtained by means of a superhigh resolution transmission type electron microscope by the author's group.[3-7]

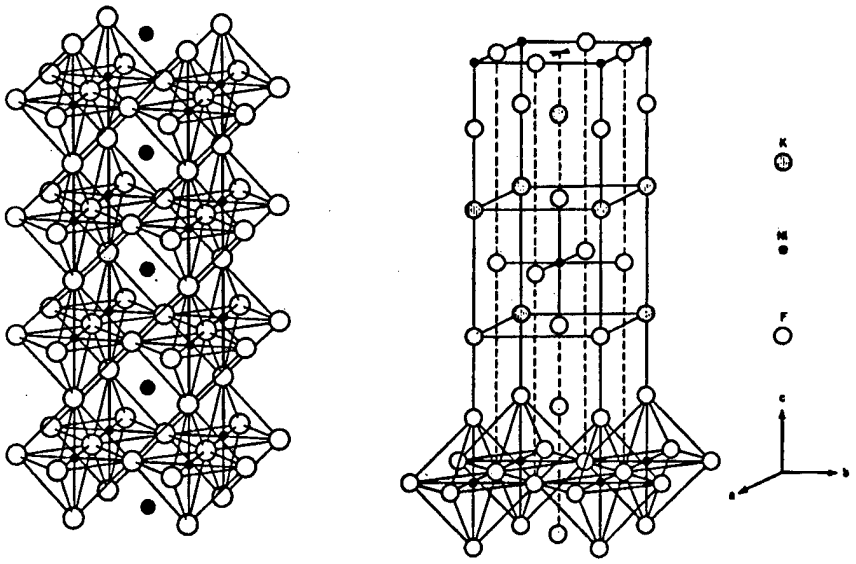

(b)●: positive ion
at site A; •: positive
ion at site B;
○: oxygen

Figure 1. Perovskite Structure (Left) and K_2NiF_4-Type Structure (Right)

2. Y-Ba-Cu-O System Superconductors and Related Materials[3]

2.1 Basic Structure of $Ba_2YCu_3O_y$[8]

The crystalline structure of the 90 K-phase $Ba_2YCu_3O_y$ (1-2-3) discovered by Chu, et al., (Figure 2), has, as is well known, a form in which site A of the perovskite structure takes on a regular array with the triple frequency of ..Ba, Ba, Y, Ba, Ba, Y.. (c~3a~11.69A). In addition, all of the oxygen atoms on the Y plane drop off, so that the copper atoms (Cu_2) above and below the Y plane are surrounded in a pyramidal form by oxygen atoms. On the other hand, oxygen atoms selectively drop off from the Cu_1 plane between the two Ba planes along the a axis. Because of this, a one-dimensional chain ..O-Cu_1-O.. is formed in the direction of the b axis. In addition, the b axis (3.88 Å), and an orthorhombic system is formed. The array of positive ions along the c axis becomes similar to

Ba Cu_1 Ba Cu_2 Y Cu_2 Ba Cu_1 Ba

When it is heated further, oxygens on the one-dimensional chain are dropped one after another, and a phase transition takes place at about 600°C, forming a tetragonal system with equivalent a and b axes and losing the superconducting capability.

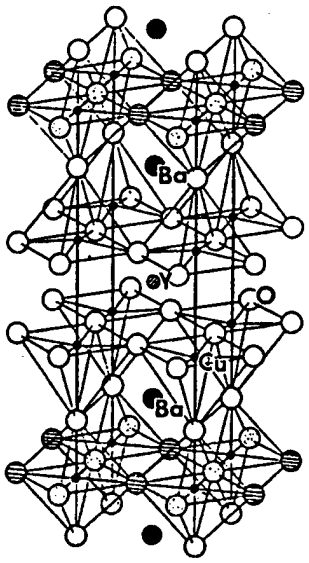

Figure 2. Crystalline Structure of $Ba_2YCu_3O_y$[8]

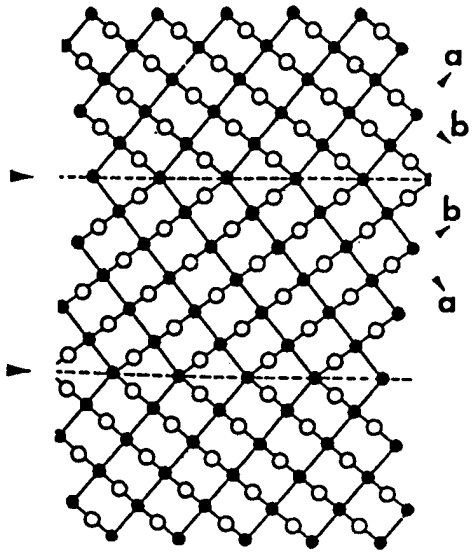

Figure 3. Schematic Model Diagram for Twinning[3]

2.2 Twinning

In the actual synthesis of the $Ba_2YCu_3O_y$ superconductor, a process which is the reverse of the above occurs. Namely, a thorough reaction occurs in the stable region of the tetragonal system at high temperatures, then a thorough annealing occurs at the stable region of the orthorhombic system at low temperatures, attaining superconductivity by taking oxygen into the structure. In this case, since the probability of oxygen entering the structure along the a axis or along the b axis is exactly equal, a {110} twinning structure is formed, as shown schematically in Figure 3. Figure 4 [not reproduced] gives an example of twinning observed by an electron microscope dark field of vision. In the upper part the twin plane is (1-10), while in the lower part it is (110). Since their discovery it has been suspected that the twinning may serve as a pinning center for the superconductor, but no definitive conclusion has yet been reached.

2.3 Orthorhombic II Phase[9]

The existence of a phase with a thermal conductivity of about 60 K between the orthorhombic system (y~6.9, superconducting phase) and the tetragonal phase (y~6.4, nonsuperconducting) of $Ba_2YCu_3O_y$ was reported by Cava, et al.,[10] and is generally referred to as the "orthorhombic II phase." The oxygen content of this phase is estimated to be about 6.6, and it has been thought to have a structure intermediate between the orthorhombic and tetragonal systems. However, a close observation of the electron beam diffraction pattern (left part of Figure 5) reveals that weak diffuse scattering occurs along the a^* direction and the period is approximately doubled on the a axis. This is believed to have formed due to the loss of oxygen above every other one-dimensional chain mentioned above, that is, a regular array of one-dimensional chains (see the right part of Figure 5). In this manner, the orthorhombic II

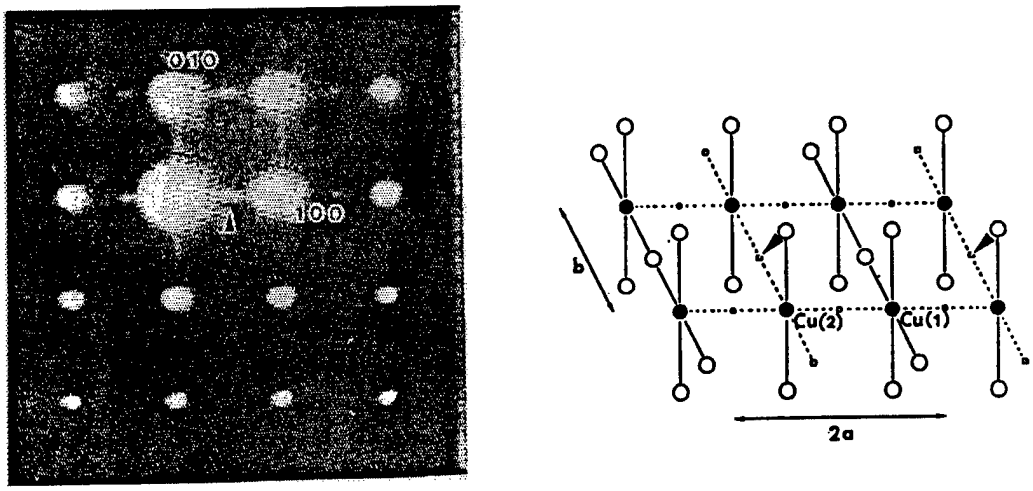

Figure 5. Electron Diffraction Image of Orthorhombic II Phase (Left) and the Corresponding Model (Right)

phase can be regarded as a structure in which the orthorhombic system (superconducting phase) and the tetragonal system (nonsuperconducting phase) are alternated in the a-axis direction on the unit cell level. That the superlattice reflection is broad is considered to be due to the irregularity that the one-dimensional chains losing oxygen may not necessarily be occurring strictly for every other chain, but rather for every third chain or, conversely, that one-dimensional chains are occurring consecutively.

2.4 90-Degree Domain Structure

By replacing Y or Ba in $Ba_2YCu_3O_y$ with another positive ion, sometimes a new fine structure, called "90° domain," is produced. For example, when Y is replaced by La or Nd with a larger ion radius, a structure is obtained whose high resolution electron microscopic image is like that shown in Figure 6(a). This is due to the fact that the c axis of a certain domain is brought into contact in parallel with the a or b axis of an adjacent domain, as shown schematically in Figure 6(b). In other words, formed domains are formed whose c-axis directions differ, respectively, by 90° from the x, y, and z directions. In order for such a fine structure to be realizable, it seems to be necessary to keep the relationship $c = 3a = 3b$ as strictly as possible. The result of regarding the parameters $r_a = (a-c/3)/a$ and $r_b = (b-c/3)/b$ as the measure of the misfit is shown in Figure 7. In $Ba_2YCu_3O_y$, the "misfit" for both axes is large, with $c<a/3$ and $c<b/3$, so the 90° domain is hard to generate. However, when Y is replaced by La or Nd with a large ionic radius, the c axis is relatively elongated, producing the relationships $c \sim a/3$ and $c \sim b/3$, so that the 90° domains become very clearly observable. Recently, the author and his colleagues found that the formation of the 90°domain is facilitated by the sequential replacement of the Ba site by Sr. As shown in Table 1, when the Sr replacement rate is lower than 30 percent, the superconductor has principally the {110} twinning structure, while the principal body becomes the 90° domain

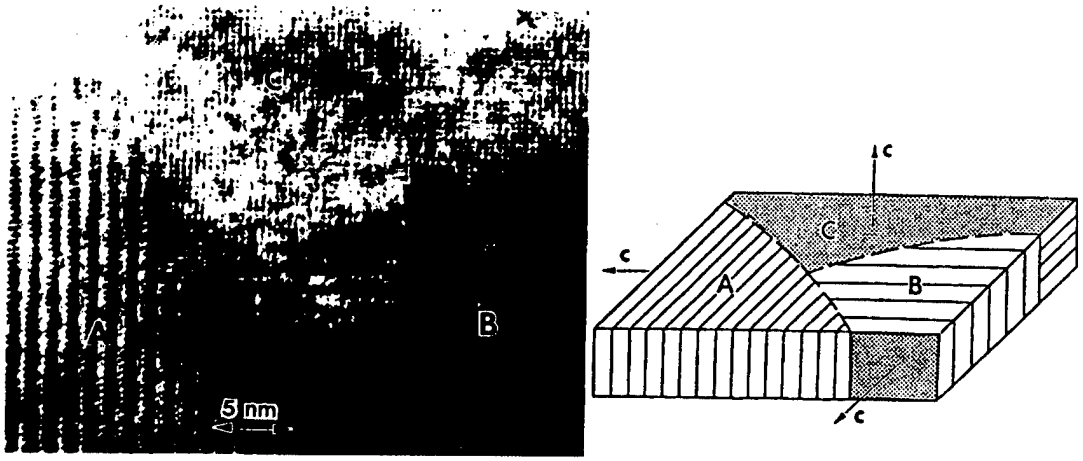

Figure 6. TEM Image and Schematic Diagram of 90° Domain Structure ($Ba_{1.8}Nd_{1.2}Cu_3O_y$)[11]
The direction of the c axis of the three regions A, B, and C differs by 90° from that of the adjacent region.

Table 1. Changes in the Formation Ratio of Twinning and 90° Domain by Adding Sr to $Ba_2YCu_3O_y$

x.	Twinning	90° domain
0	Y	N
0.2	Y	N
0.4	Y	Y,N
0.6	Y	Y
0.8	Y,N	Y
1.0	N	Y
1.2	N	Y

Y: Observed frequently.
Y,N: Observed but not so often.
N: Never or seldom observed.

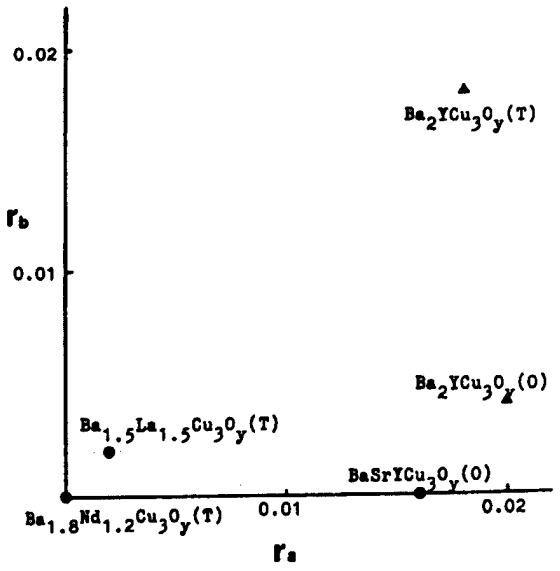

Figure 7. Relationship Between Misfit Factors (r_a, r_b) and the Formation of 90° Domain

for the rate higher than 30 percent. This can be understood by the fact that when the Sr replacement rate is higher than 30 percent, the relationship $b = c/3$ is nearly perfectly valid, making it possible for the c and b axes to make contact in parallel without "misfit" (Figure 8). In this manner, the replacement of an element not only delicately affects the crystal structure, but also the fine structure.

As was mentioned earlier, $Ba_2YCu_3O_y$ itself does not have the 90° domain. However, this is true only in the "bulk" obtained by a solid reaction, while the 90° domain is frequently observed in the "thin film" obtained by sputtering, etc. For example, Tomita, et al.,[13] carried out a transmission electron microscope (TEM) observation of the cross section of $Ba_2YCu_3O_y$ on $SrTiO_3$, and showed that the thin film consists of three domains, A to C, in which the direction of the c axis is parallel (domain A), rising toward the right at 45° (B) and rising toward the left at 45° (C), with respect to the junction plane. In other words, the c axes of the three domains are mutually orthogonal and basically form "90° domains" in the above. It is thought that this might be caused by the replacement effect of Sr, which has diffused into the thin film from the substrate. However, the result of interface analysis by SIMS, etc., is said to show almost no diffusion of Sr. Accordingly, why the formation of the 90° domain structure is facilitated in the thin film has been left to be solved in the future.

2.5 Plane Defect and $Ba_2YCu_4O_y$ (1-2-4) Phase

Of late, the $Ba_2YCu_4O_y$ (1–2–4), which has a structure obtainable by inserting one additional Cu layer into $Ba_2YCu_3O_y$, has been drawing attention.[14] Originally, this structure was found in a high resolution electron microscopic image as a partial plane defect structure in the 1–2–3 compound.[15]

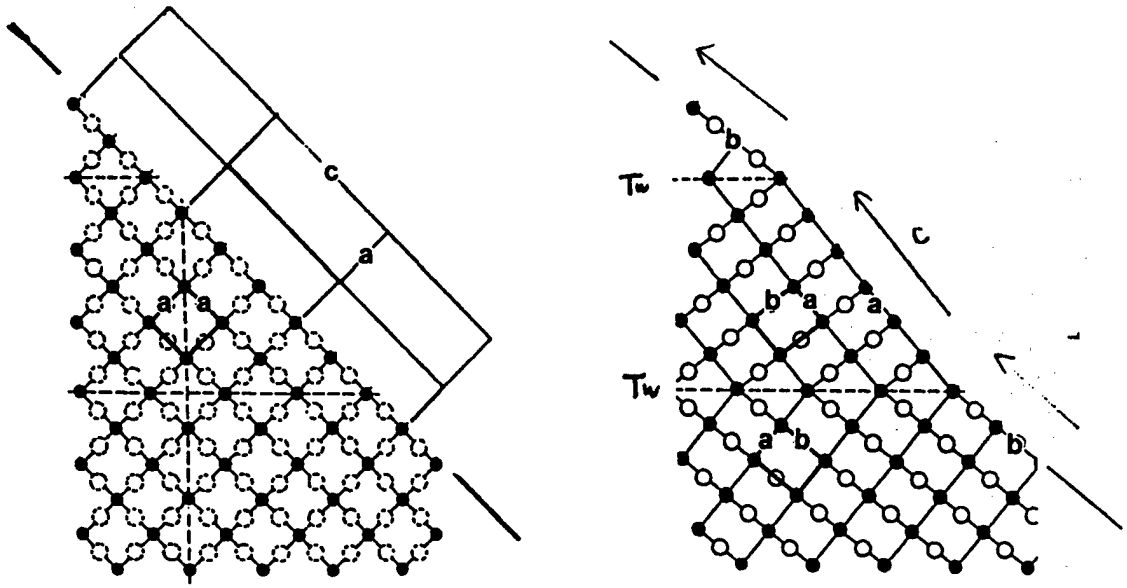

Figure 8. When There Is No Twin Structure (Left), the Formation of a 90° Domain Is Facilitated, But When There Is a Twin Structure (Right), a 90° Domain Is Less Easily Formed, Because the {100} Crystal Plane Is Formed in Zigzag Fashion

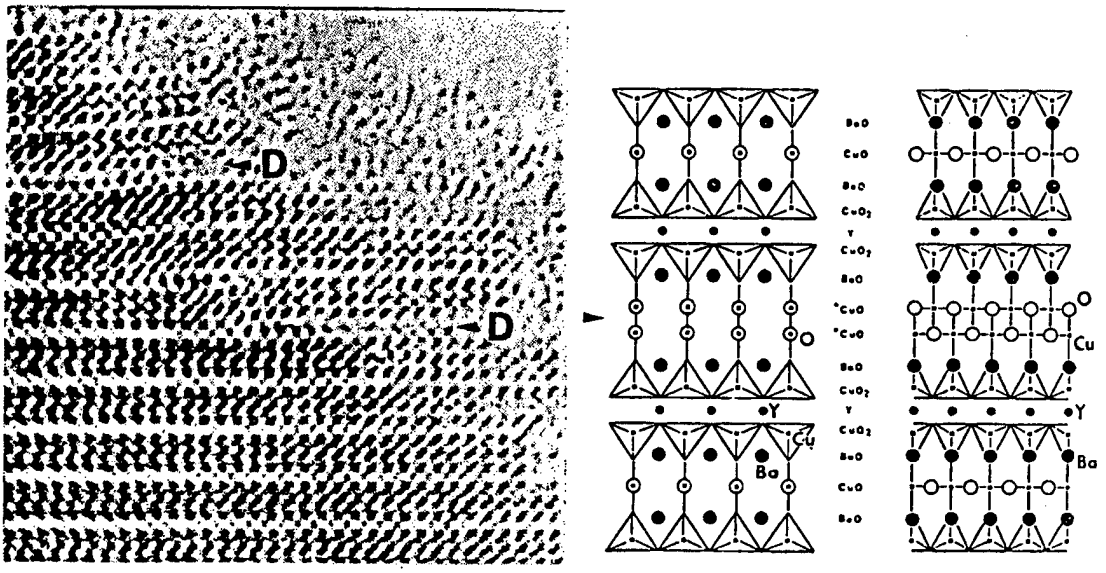

Figure 9. (Left) an HRTEM Image of $Ba_2YCu_3O_y$ Surface Defects and (Right) a Model[15]

An example of this is shown in Figure 9 (left part), in which the perpendicular distance between the Ba layers increases from about 4.3 Å to about 6 Å in the portion indicted by an arrow (denoted by D). It can be seen that the number of copper layers has been increased to two. The structure of the plane defect portion is shown schematically in Figure 9 (right part). Upper and lower one-dimensional CuO chains are joined to form a double chain. Since the

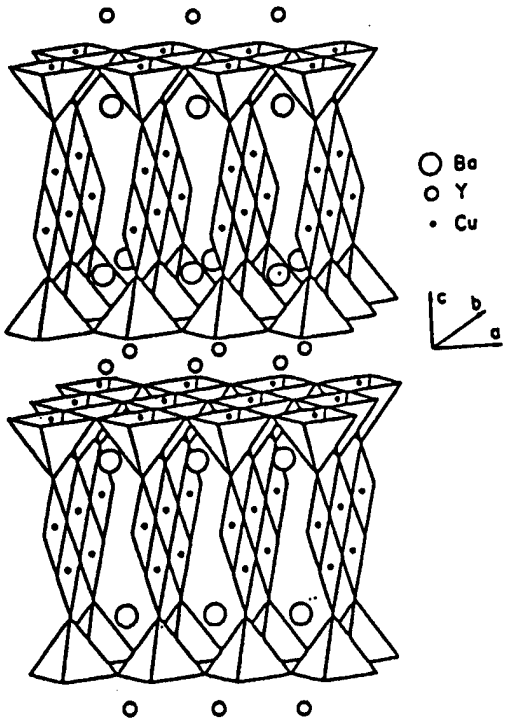

Figure 10. Model Diagram for 1-2-4 Structure

upper and lower chains shift with each other by b/2, the copper atoms on the double chain are arrayed in zigzag fashion in the direction of the b axis.

If all of the one-dimensional chains are replaced by double chains, the compound $Ba_2YCu_4O_y$, which has a new structure (Figure 10), will be formed, but such a compound will not exist as a stable phase, at least not under normal atmospheric pressure. However, that this compound could exist in a thin film was first discovered by a group at Stanford University. Subsequently, it was reported that the compound 1-2-4 can be synthesized relatively easily in the solid phase reaction as well by employing high pressure oxygen. Because of the fact that the T_c of phase 1-2-4 is about 80 K, which is somewhat lower than that of phase 1-2-3, and because of the difficulties accompanying its synthesis, as mentioned above, phase 1-2-4 did not draw too much attention in the beginning. However, after a very recent report that the T_c approaches 90 K, which is comparable to that of phase 1-2-3, by replacing some (several percent) of the Y with Ca, phase 1-2-4 suddenly began to draw attention.[16] Phase 1-2-4 has such characteristics as 1) it lacks the orthorhombic-tetragonal system change caused by the balance of oxygen, and 2) it is not mixed with the {110} twinning, which differ from those of phase 1-2-3. As to point 1), this is due to the difficulty found in removing oxygen from the rigid double chain structure formed via oxygen. On the other hand, as for point 2), this is believed to be due to the geometrical impossibility of forming the {110} twinning structure because the atoms, including the metallic atoms, above and below the double chain change by b/2. As in the above, although phase 1-2-4 is difficult to synthesize, once it is formed it is very stable. In contrast, phase 1-2-3 can be synthesized relatively easily, but its drawback is that it lacks stability, such as phase transition and structure deterioration.

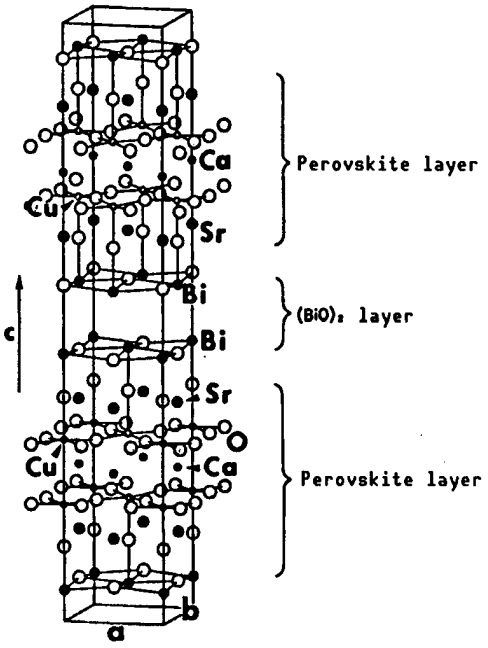

Figure 11. Mean Structural Model for Phase 2212

As in the above, in spite of their similarities in the composition and structure of phase 1-2-3 and phase 1-2-4, they have characteristics that are contrasting. It will be very interesting to see which of the two is developed as a practical material in the future.

3. Bi-Sr-Ca-Cu-O System Superconductors and Their Related Substances[5-7]

3.1 Fundamental Structure

A bismuth-system superconductor was discovered first by Akimitsu, et al.,[17] and Michel, et al.,[18] in the Bi-Sr-Cu-O system, but since its T_c is 20 K at the most, they did not attract too much attention. However, Maeda, et al.,[19] discovered that new high temperature superconductors with T_cs higher than 100 K could be obtained by adding Ca to the above system. The sample produced by Maeda, et al., is said to be a mixture of two compounds whose ideal compositions are $Bi_2Sr_2Ca_2Cu_3O_y$ (T_c ~110 K; phase 2223) and $Bi_2Sr_2CaCu_2O_y$ (T_c ~80 K; phase 2212). Since phase 2212 is relatively easy to synthesize, its structure analysis by X-ray was carried out immediately.

The model by Tarascon, et al.,[20] is shown in Figure 11. In the bismuth composite oxides known heretofore, an oxygen plane exists between two Bi layers, forming a "Bi_2O_2" layer.21 In bismuth system superconductors, oxygen exists on the same level as Bi, and a $(BiO)_2$ layer is formed by the gentle overlapping of two (BiO) planes, which is an outstanding characteristic of the system. Between two $(BiO)_2$ phases a perovskite layer with two copper layers exists, where each of the copper atoms is surrounded by oxygen in pyramidal form. On the other hand, phase 2223, with a T_c of 110 K, has perovskite layers with three layers of copper.

The copper atoms on the first and the third layers have pyramidal coordination, but the central copper atoms (on the second layer) have a planar four coordination. Further, in the $Bi_2Sr_2CuO_y$ (phase 2201) discovered first by Akimitsu, et al., the perovskite layer contains only one layer of copper atoms with an octahedral six coordination. As in the above, the T_c tends to increase with an increase in the number of copper layers within the perovskite layer and with the reduction in the coordination number of the oxygen. For this reason, the synthesis of phase 2234, having a perovskite layer with four layers of copper, and its T_c value have become of interest. Phase 2234 has been obtained in the form of a thin film by a vapor phase method, but its T_c is about 90 K lower than that of phase 2223.[22]

3.2 Intergrowth Defect

Analogous to many of the layered composite oxides, the bismuth-system superconductors sometimes include "intergrowth defects" in which structures of different phases coexist on the unit cell level. The phase where this is especially conspicuous is the high temperature phase (2223) with a T_c of 110 K. The high temperature phase is synthesizable only under extremely limited conditions, and, moreover, the 002 peak in its powder X-ray diffraction pattern is very broad. A high resolution electron microscopic image (projected in the [110] direction of the fundamental structure) is shown in Figure 12 [not reproduced].[23] It can be seen that four layers of copper (corresponding to phase 2234) and two layers of copper (corresponding to phase 2212) are inserted at a fairly high rate, in addition to the perovskite layers (indicated by numeral 3) with three layers of copper, which is intrinsic for phase 2223.

A report does not seem to exist concerning the success achieved in obtaining phase 2223 with no intergrowth by a solid phase reaction method. Later, Takano, et al.,[24] discovered that it was possible to manufacture phase 2223 with almost no intergrowth defects by adding lead (Pb). Lately, the expression of phase 2223 on the high temperature phase of the bismuth system in many cases refers to a phase to which Pb has been added without specifically mentioning it. It should also be noted that the addition of lead very strongly affects the modulation structure that will be described later.

3.3 Modulated Structure

(a) Modulated Structure of Phase 2212

In the previous section we saw the "fundamental structure" of bismuth-system superconductors. The most conspicuous characteristic of these superconductors is the existence of "modulated structures" resulting from the periodic displacement of atoms from the fundamental structure.[25-27] In Figure 13(a) [not reproduced] a b^*-c^* electron beam diffraction pattern of phase 2212 is shown in which satellite reflections are observed in addition to the strong fundamental reflections that can be explained in terms of Tarascon's fundamental structure. The intensity of the satellite reflections is strong in the vicinity of the fundamental reflections and decreases rapidly as one moves away from them.

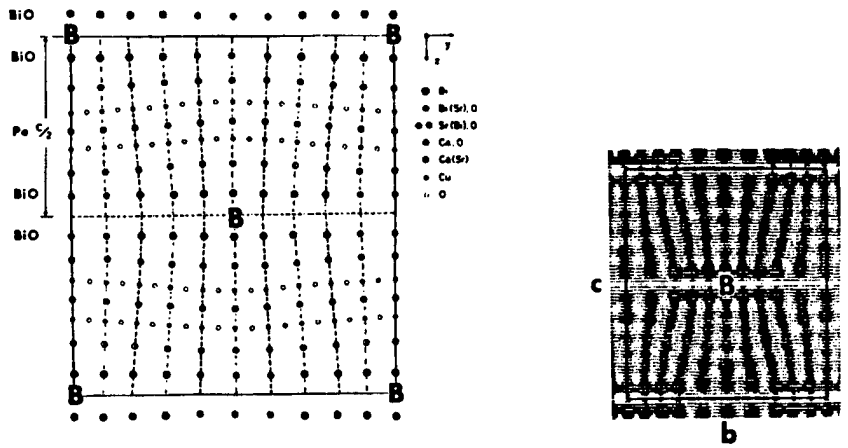

Figure 14. Model Diagram[5] for Modulated Structure and the Result of Computer Simulation[28]

In other words, the satellite reflections of the first and second orders are strong, but the third and higher order reflections are extremely weak. This suggests that the satellite reflections are caused by the periodic displacement of the atomic positions. In order to confirm this directly, the result of photographing the corresponding high resolution electron microscopic image is shown in Figure 13(b) [not reproduced]. The bismuth atom trains (arrows) of the $(BiO)_2$ layers are not distributed equally along the b axis, for example, the spacing is small in the vicinity of the symbol B (minimum of about 2.4 Å) while it is large in the vicinity of the symbol D (maximum of about 3.0 Å), periodically fluctuating with a mean spacing of about 2.7 Å. We called the B and D portions the "Bi concentrated zone" and "Bi diluted zone," respectively. In addition, a closer inspection of the electron microscopic image reveals that the distance between the two (BiO) planes in the c-axis direction is slightly larger in region B than in region D. In other words, when the distance decreases in the b-axis direction, it expands in the c-axis direction (region B), while, conversely, when it expands in the b-axis direction it shrinks in the c-axis direction (region D). In other words, each (BiO) plane is subjected to a modulation in the b-axis direction for longitudinal waves and a modulation in the c-axis direction for transversa waves. The modulation period estimated from the spacing between the satellite reflections is 4.8 b~26 Å. The actual measurement of the spacing between the Bi concentrated zones of the electron microscopic image shows the sandwiching of nine sheets (24.3 Å) or 10 sheets (27 Å) of the lattice fringes in the longitudinal direction (with mean spacing of b/2~2.7 Å). It can be understood that the 26 Å spacing that corresponds to an average of 9.6 sheets is represented in the satellite reflections. A model diagram of the modulated structure, assuming a period of 5 b~27 Å, is shown in Figure 14.[28] This model was drawn based on a computer simulation of the high resolution electron microscopic image in which a partial replacement of positive ions, in addition to the displacement of the atoms, was assumed. For example, the Bi sites on the bismuth diluted zone have been partially replaced by Sr, while the Sr sites above and below the bismuth concentrated zone have been partially replaced by Bi. As in the above, the outline of the modulated structure became clear as a result of the observation of the high resolution electron microscopic image,

but analysis of the oxygen sites has been impossible. Recently, Yamamoto, et al.,[29] carried out the (Liedbert) analysis of the powder neutron diffraction of phase 2212, and performed a precision analysis of the modulated structure, including the oxygen sites. According to the results, excessive amounts of oxygen enter the interlattice positions so that the distance between Bi atoms is said to be somewhat increased. On the other hand, it is said that the replacement of the Bi sites by other elements is almost nil, giving results that differ from those obtained by the electron microscopic image.

(b) Modulated Structures of 2223 and 2201 Phases

As mentioned in the above, although the phase 2223 (as long as there is no Pb addition) includes a large number of intergrowth defects, its modulated structure is relatively similar to that of the phase 2212. Namely, the modulation period in the b-axis direction is approximately Bs = 26 Å, while the positions of the bismuth concentrated zones of the $(BiO)_2$ layers that are adjacent vertically interchange by Bs/2. In contrast, by observation of the electron microscopic image, it has been seen that the 2201 phase, although its modulation period is also about 26 Å, does not have the Bs/2 value, but instead a value of Bs/4~Bs/5 for the interchanging of the upper and lower bismuth concentrated zones. Because of this, the modulated structure is described as monoclinic, differing greatly from the orthorhombic system for the 2212 phase.[27] In addition, it is said that in the 2201 phase the ratio of Bi to Sr varies continuously and, correspondingly, the modulation period also changes. Moreover, it is known that the Bi-Sr-Cu-O system contains three kinds of nonsuperconducting phases, in addition to the 2201 superconducting phase, each having an extremely interesting superstructure.

(c) Effect of Addition of Lead

It was mentioned above that the high temperature phase (2223) can be stabilized by the addition of Pb, but the situation of the modulated structure changes along with the replacement of the Bi sites by Pb. This was first reported by Ikeda, et al.,[30] who noted the way in which the satellite reflections of the b^*-c^* electron beam diffraction pattern differ from those of the Pb-free 2212 phase, as shown in Figure 15 [not reproduced]. Namely, the points of the first order satellite reflections are observed at the due sides of the point of the fundamental reflection. The modulation period anticipated from the spacing between the satellite reflections is 40~50 Å, which is fairly large compared with that of the Pb-free case. Further, an inspection of the corresponding high resolution electron microscopic image shows that the displacement of the individual atoms is small, and that the upper and the lower $(BiO)_2$ layers are subjected to modulation at approximately the same position, which differs greatly from the anti-phase relationship by b/2 regarding the modulated positions of the Pb-free case.[31] As for the prolongation of the modulation period as a result of Pb addition, the idea that the interlattice oxygen atom concentration which is responsible for bringing about the modulation in the $(BiO)_2$ layer, is reduced by the replacement of Bi^{3+} with Pb^{2+} and leads to a slow modulation seems to be generally supported. In this case, the modulation period is thought to vary continuously to some extent with the amount of Pb added. In reality, however, it changes discontinuously

from type I to type II, which needs further clarification in the future. We are anticipating a precise analysis of neutron diffraction, etc., for the case of the Pb addition. The effect of Pb addition is also being investigated for the 2212 phase and the 2201 phase, but it is known that the modulated structure itself disappears when the added amount exceeds a certain limit. For example, in the 2201 phase, no satellite reflection is observed when the lead replacement is greater than 30 percent, but, instead, new diffraction points arise at 110, 001, 003, etc., (Figure 16)[23] [not reproduced]. This suggests that although long-period modulation disappeared, a short-period superstructure remains, and represents a future problem.

(d) Co, Fe, and Mn Oxides Having Modulated Structures[33]

Tarascon, et al., reported that it is possible to isomorphously replace the copper atoms of the bismuth system superconductors by other transition metal elements, and almost all of them possess modulated structures. Although these compounds are not superconductors for the purpose of investigating the essential points of the modulated structure, they may be said to be extremely interesting objects. Figure 17 (upper part) [not reproduced] shows an electron beam diffraction image and a high resolution electron microscopic image of $Bi_2Sr_2CoO_y$ in which there are perovskite layers with one cobalt layer.[34] From the former it can be seen that the modulation period in the b-axis direction is about four times that of the fundamental lattice (about 27 Å), having an orthorhombic system similar to that of the 2212 (Cu) phase. In this case, the period and symmetry of the modulated structure change when Cu is replaced With Co. On the other hand, $Bi_2Sr_3Fe_2O_y$, which has perovskite layers with two layers of iron, has also been synthesized, and its modulation period is 4.5 times the fundamental period. $Bi_2Ca_2FeO_y$ with one iron layer has a low modulation period of 3.5 times the fundamental period, and has an orthorhombic system which is the same as that of the corresponding 2201 phase of copper[35] (Figure 17 (lower part) [not reproduced]). In this case, the modulation period tends to become reduced when Cu^{2+} is replaced by Co^{3+} or Fe^{3+}. It is generally understood that, differing from the case when Pb is added, the concentration of the inter-lattice oxygens of the $(BiO)_2$ layer is increased, enhancing the degree of modulation.

3.4 Surface and Interface Structures

(a) Undulatory Cleavage Plane

The coupling of the two (BiO) planes of the $(BiO)_2$ layer is extremely weak, as mentioned above. From this, it has generally been anticipated that this super-conductor will have a cleavage at the center of the two (BiO) planes. If such is the case, interest has been expressed in whether the atomic displacement accompanying the modulated structure of a bulk material will also appear in the outermost surface of the (BiO) plane. Kirk, et al., observed the cleavage (001) plane by scanning tunnel microscope (STM), and showed that the surface layer is a (BiO) plane and also that it has a periodic unevenness along the b axis.[36] In contrast, we observed the surface by the so-called profile method employing a transmission microscope.[37] This is a method for detecting the unevenness on the atomic level by obliquely projecting the surface layer from

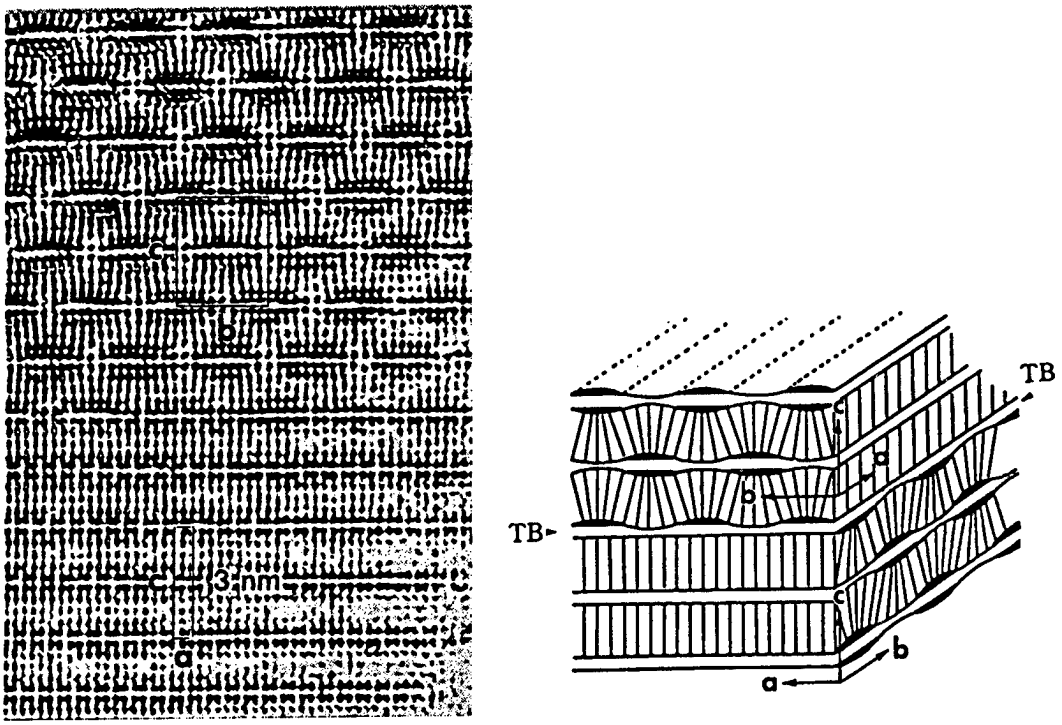

Figure 19. HRTEM Image (Left Part) of the 90° Rotary Twinning of Phase 2212 and Its Schematic Diagram (Right Part)[38]

an appropriate direction. Figure 18 [not reproduced] shows the results obtained by projecting the crystal particles of the 2212 phase having a sharp (001) plane as a crystal end in the a-axis direction, showing that the crystal end consists of an individual (BiO) plane. Further, a variation in contrast is seen in the end (BiO) plane in which the height of the portion (B), with stronger contrast, is slightly smaller than that of the portion (D), with weaker contrast. Moreover, the period of modulation is about 26 Å, which coincides roughly with the modulation period of a bulk body. From these observations, it can be seen that the surface (BiO) layer resulting from the cleavage of a bismuth system superconductor keeps the atomic displacements accompanying the modulation structure of a bulk body approximately as they are. As a result, it has been confirmed that this represents an undulation in the vertical direction, with a period of about 26 Å. A similar undulatory surface has also been observed in the phase 2201 to which Pb has been added.[32]

(b) Rotary Twinning Structure (Twisted Boundary)

The "twinning structure," in which the directions of the a and b axes are interchanged by 90°, has also been observed in bismuth system superconductors.[38] However, it differs from $Ba_2YCu_3O_y$ in that the twinning boundary is the {001} structure rather than the {110} structure. An example of the observation of twins by an electron microscope is shown in Figure 17 [not reproduced]. In contrast to the modulated structure that can clearly be observed in the upper side of the boundary surface indicated by arrows, at first glance modulation seems to be absent on the lower side. This is due to the fact that, in the

lower region, the direction of projection coincides with the b axis, namely, the direction of modulation. In contrast, the upper side of the image is believed to be an electron microscopic image projected in the a-axis direction. The most interesting thing in this electron microscopic image is that the twin interface indicated by the arrows comes at the exact center of the two (BiO) planes. In other words, the upper and lower (BiO) planes are receiving modulation in directions that differ by 90° (Figure 19). This is thought to be due to the extremely weak coupling between the two (BiO) planes. As a result of transmission electron microscope (TEM) observation of the cross section of the bismuth system superconductors obtained by joining the c planes at various angles, Ishida, et al., found that the twisted surface comes at the center of the two (BiO) planes.[39]

References

1. Bednorz, J.G. and Muller, K.A., Z. PHYS., Vol B64, 1986, p 189.

2. Tokura, Y., et al., NATURE, Vol 337, 1989, p 345.

3. Matsui, Y., JPN. J. CRYSTALLOG., Vol 29, 1987, p 374.

4. Ibid., SURFACE SCIENCE, Vol 9, 1988, p 500.

5. Ibid., JPN. J. CRYSTALLOG., Vol 31, 1989, p 8.

6. Matsui, Y., et al., JEOL NEWS, Vol 26E, 1988, p 16.

7. Matsui, Y., THE HITACHI SCIENTIFIC INSTRUMENT NEWS, Vol 32, 1989, p 3015.

8. Izumi, F., et al., JPN. J. APPL. PHYS., Vol 26, 1987, p L649.

9. Matsui, Y., et al., Ibid., p 2021.

10. Cava, R.J., et al., PHYS. REV., Vol B36, 1987, p 5719.

11. Matsui, Y., et al., JPN. J. APPL. PHYS., Vol 26, 1987, p L1693.

12. Ibid., J. ELECTRON MICROSC., Vol 36, 1987, p 246.

13. Tomita, M., et al., JPN. J. APPL. PHYS., Vol 27, 1988, p L636.

14. Kogure, T., PHYSICA C, Vol 157, 1988, p 159.

15. Matsui, Y., et al., JPN. J. APPL. PHYS., Vol 27, 1988, p L350.

16. Miyatake, T., et al., NATURE, Vol 341, 1989, p 41.

17. Akimitsu, J., et al., JPN. J. APPL. PHYS., Vol 26, 1987, p L2080.

18. Michel, C., et al., Z. PHYS., Vol B68, 1987, p 421.

19. Maeda, H., et al., JPN. J. APPL. PHYS., Vol 27, 1988, p L208.

20. Tarascon, J.M., et al., PHYS. REV., B37, 1988, p 9382.

21. Shimazu, S., et al., Research report of Institute for Inorganic Research, 1980, p 23.

22. Adachi, H., et al., JPN. J. APPL. PHYS., Vol 27, 1988, p L1883.

23. Matsui, Y., et al., Ibid., p L1241.

24. Takano, M., et al., Ibid., p L1041.

25. Matsui, Y., et al., Ibid., p L361.

26. Ibid., p L372.

27. Ibid., p L1873.

28. Horiuchi, S., et al., Ibid., p L1172.

29. Yamamoto, A., et al., PHYS. REV. B, (submitted).

30. Ikeda, S., et al., JPN. J. APPL. PHYS., Vol 27, 1988, p L2040.

31. Hirotsu, Y., et al., Ibid., Vol 28, 1989, p L1783.

32. Matsui, Y., et al., Ibid., Vol 29, 1990, p L273.

33. Tarascon, J.M., et al., PHY. REV., Vol B39, 1989, p 11587.

34. Matsui, Y., et al., JPN. J. APPL. PHYS., Vol 28, 1989, p L1991.

35. Shoda, K., et al., Ibid., Vol 29, 1990, p L287.

36. Kirk, M.D., et al., SCIENCE, Vol 242, 1988, p 1673.

37. Matsui, Y., et al., JPN. J. APPL. PHYS., Vol 28, 1989, p L946.

38. Ibid., Vol 27, 1988, p L827.

39. Takahashi, H., et al., 46th Meeting of Japanese Society of Electron Microscopy, preprints, 1990, p 172.

Electron Structure of High Temperature Superconductor

916C1001C Tokyo HYOMEN KAGAKU SEMINA in Japanese 27-29 Jun 90 pp 27-41

[Article by Hideo Ihara, Electrotechnical Laboratory]

[Text] **1. Introduction**

The most serious imminent obstacle in the study of high temperature oxide superconductors is the elucidation of the superconductivity mechanism. The fundamental matter that has to be made clear in elucidating the mechanism is the electronic structures that comprise the stages of the superconductivity phenomenon. Since the carriers of the superconductivity phenomenon are the electrons (or the holes) themselves, it is necessary to ascertain the states (wave functions, energies, electronic state densities, etc.) of the original electrons that serve as the parents of the superconducting electrons. Now, as to the electronic states, there are two theories, namely, 1) that they are ordinary electronic states (Fermi liquid) of the metals which form the Fermi surfaces that are common to conventional superconductors and 2) differing from the Fermi liquid theory, they are doped states (non-Fermi liquid) of the Mott insulators in which spins play an important role.[1]. The difference between the two theories demonstrates the difference between placing emphasis on the fluctuations of the electric charge and placing emphasis on the fluctuations of the spin in the superconductivity mechanism model. Recently, 3) a phenomenological theory, called the marginal Fermi liquid model, which emphasizes the fluctuations of both the spin and the charge, a theory which seems to be on the borderline of the above two theories, has been proposed.[2]

Experimentally, a Mott insulator resulting from Coulomb repulsion has been definitely realized in a region in which the carrier concentration in the nonsuperconducting phase of a copper oxide is low. However, from the recent measurements through the photoelectron spectroscopy, light absorption, positron annihilation and the de Haas-van Alfven effect, it has been made clear that a metallic band appears and a Fermi surface is formed in regions in which the carrier concentration is increased and superconductivity is exhibited. On the other hand, phenomena which cannot be explained solely in terms of the typical Fermi liquid theory are being observed in experiments involving nuclear magnetic resonator (NMR), Raman scattering, tunnel spectroscopy, neutron scattering, etc.

Before going into more detailed descriptions of the problem, a discussion of the general theory of the electron is in order. Generally, if an electron is localized at a position in a crystal, its kinetic energy (t) becomes high as a result of the uncertainty principle ($\Delta \times \Delta p \sim h$). Thus, the electron tries to reduce the kinetic energy (momentum) by becoming nonlocalized. Therefore, if there exist conditions by which the atomic orbits overlap, facilitating electron motion, metallic coupling is generated and a band which traverses the Fermi liquid (E_F) is formed, making it possible for the electron to be stabilized in proportion to the amount of reduction of kinetic energy. When a band is formed, for temperatures below a certain value (T_F), electrons which are fermions are accommodated in a state (k, E(k)) in pairs (neglecting the spins) in accordance with the Fermi-Dirac statistics, and are degenerated thermodynamically. A many-body system of fermions that are in a high density liquid state as a result of degeneration is called a Fermi liquid. In forming a Fermi liquid, the interaction between the particles, the temperature of the system, and the particle density are important. The electrons (or the holes) in a Fermi liquid state form a Fermi surface and the crystal becomes metallic.

On the other hand, when the electrons try to move around, the case occurs in which two electrons overlap in one atomic site. As in the CuO_2 plane, the $Cu3d^9$ state is formed and, when one electron is assigned for each of the crystal's Cu sites, the energy U of the repulsion of the two electrons at the Cu site acts conspicuously, satisfying $U > t$ and obstructing the electron motion, making the crystal an insulator. The insulator formed as a result of the electron correlation due to Coulomb repulsion between the electrons is called a Mott insulator, and this state is realized in La_2CuO_4 and $YBa_2Cu_3O_6$.

That the Coulomb repulsion energy (electron correlation energy) U_{dd} of the d electrons at the Cu sites in a CuO system is large (~8 eV) is due to the fact that the d orbitals of Cu are on the side of the inner shell, as shown in Figure 1, and that the d orbit has an intrinsically small spread of the wave function compared with the s or p orbitals, making it easy to localize, etc. However, even when U_{dd} is large, when the holes are doped so that the state obtained is not one in which all of the Cu sites are necessarily allocated to one electron (in which case a d^8 state exists in part) or, conversely, when electrons are doped so that some Cu sites exist where two electrons are allocated (in which case there exists a d^{10} state in part), if a metallic band is formed, carriers can move without being directly hampered by the Coulomb repulsion. Accordingly, if carriers can be introduced by doping, it is natural to form a metallic bonding band in the vicinity of the Fermi level so as to lower the kinetic energy by the nonlocalization of the carriers. Since, in this case, it is difficult to form a band passable by the electrons by overlapping the orbital of the Cu3d electrons, use is to be made of an appropriate hybrid orbital with the O2p orbital. From the energy levels and the wave function spreads, it is assumed that the combination of the Cu3d and the O2p orbital is suitable for forming such a metallic bond. With such changes in the properties of the wave functions of the carriers themselves, it is believed that the electron correlation effect of the d electrons will not appear directly as it did in the metallic Cu or Ni, but will approach a metallic state (Fermi liquid) where the band theory is a good approximation.

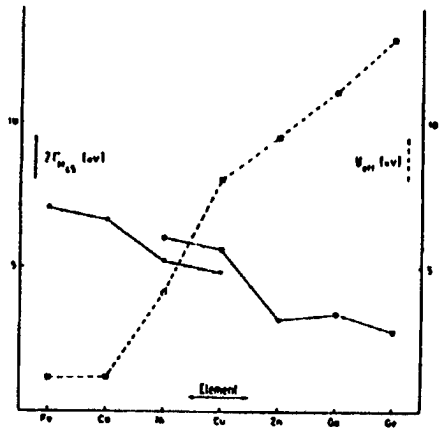

U_{eff} (squares on dashed line) and $2\Gamma_{M_{45}}$ (circles on solid lines) vs atomic number for Fe, Co, Ni, Cu, Zn, Ga, and Ge in eV.

Figure 1.

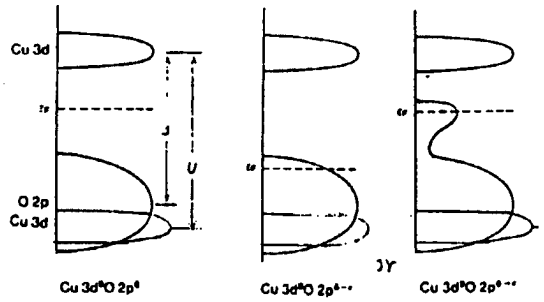

Figure 2. Schematic Diagram for Electronic State Density for a System With Strong Electron Correlation
Represents a charge transfer-type system.

It is thought that the formation of a metallic band by carrier doping in a copper oxide is quite similar to the transition from the formation of impurity levels in a semiconductor to a degenerate semiconductor by a high concentration doping of the carriers. the only differences are that since U's action is strong, it is not clear whether the one-body approximation band theory is applicable to this region and the presence of the spin is not negligible.

Therefore, the electronic structure research of oxide superconductors may be summarized by the following points:

(1) The state of change in the host crystal from the electronic structure of the insulating phase to the electronic structure of the superconducting phase.

(2) To which atomic sites the carriers are introduced.

(3) Whether or not the electronic structure of the superconducting phase is a Fermi liquid.

(4) The electronic structure (energy level, wave function, and electronic state density) in the vicinity of the Fermi liquid (E_F).

(5) Which aspect of the electronic structure determines the superconductivity.

(6) How the presence of the spin is related to the electronic structure and superconductivity.

As means of research for elucidating the above-mentioned points, photoelectron spectroscopy, X-ray absorption, electron beam energy loss spectroscopy, optical reflection and absorption, NMR, neutron scattering, tunneling spectroscopy, etc., are being studied experimentally, while the band calculation and calculations of the cluster and impurity models are being carried out theoretically. In the following, research on the atomic orbital, wave function, energy level, band structure, and electronic state density as they concern the electronic structure of oxide superconductors will be

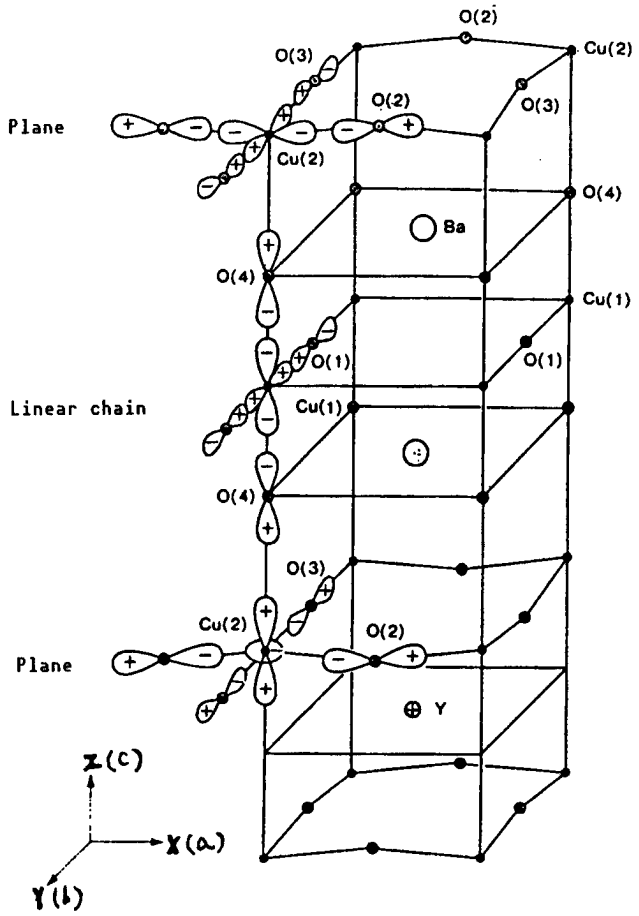

Figure 3. Atomic Orbital of $YBa_2Cu_3O_7$ (A. Kotani (Ref. 5))

surveyed by dividing the subject into the Fermi liquid theory and the non-Fermi liquid theory.

2. Fermi Liquid Theory

Atomic Orbital and Doping Sites of the Holes

The components of high temperature superconductors include octahedral CuO_6, pyramidal CuO_5, and planar CuO_4. The characteristic common to these is that they have a two-dimensional CuO_2 plane. In this CuO system with no carrier, its electronic state doped is $Cu^{2+}(3d^9)$–$O^{2-}(2p^6)$, forming an insulator. The reason for this is that the electron correlation energy U of Cu3d is large (6~7 eV) and the energy level of the 3d state is split, creating an energy gap as shown in Figure 2.

The O2p level is lower than E_F within the Cu3d gap and forms a hybrid orbital with $3d^L$ (the lower Hubbard band of 3d). The mean energy Δ (the charge transfer energy) required for moving the O2p electron to $Cu3d^H$ (the upper Hubbard band of 3d) is about 2~4 eV, which is less than U. A material having an electronic

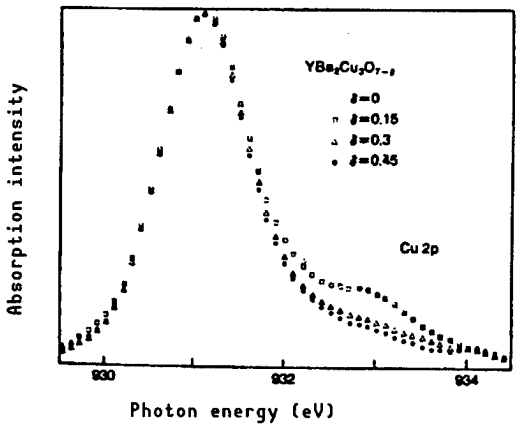

Figure 4. Cu2p X-Ray Absorption Spectra for Polycrystalline Sample of $YBa_2Cu_3O_{7-\delta}$ (A. Kotani (Ref. 5))

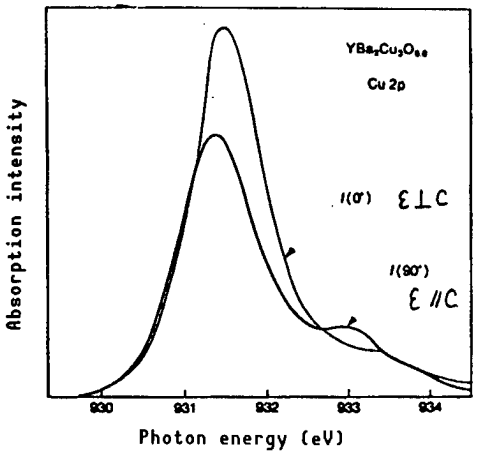

Figure 5. Polarization Dependence of Cu2p X-Ray Absorption Spectra for $YBa_2Cu_3O_{6.8}$ Single Crystal Sample (A. Kotani (Ref. 5))

structure for which $U > \Delta$ holes is called a charge transfer-type insulator. In such a charge transfer-type system, holes enter the O2p state when they are doped. However, since O2p and Cu3d are commonly bonded, holes also enter the 3d state. In a pyramidal component, when carriers are introduced, they enter the two-dimensional plane in the beginning, contributing to electric conduction. When carriers are further introduced, they enter the vertex oxygen sites. However, when different clusters of CuO_n coexist, the situation is somewhat different. In order to see this in more detail, let us consider the YBCO and the BiSrCaCuO systems. The compound $YBa_2Cu_3O_7$ has two kinds of Cu sites, Cu(1) and Cu(2), and four kinds of O sites, O(1) to O(4), as shown in Figure 3. The orbitals that contribute to the bonding are O2px on the planes. The combinations of the bonded orbitals of the various Cu3d and O2p orbitals are as follows:

(a) Orbitals on ab plane:	O(2) $2p_x$, $2p_y$ O(3)	Cu(2)$3dx^2-y^2$
(b) Orbitals in c-axis direction	O(4) $2p_z$	Cu(1)$3dz^2-y^2$
(pyramid vertex)		Cu(2)$3d3z^2-r^2$
(c) Orbitals of CuO chain:	O(1)$2p_y$	Cu(1)$3dz^2-y^2$

In a polycrystalline sample of $YBa_2Cu_3O_{7-\delta}$, the X-ray absorption spectra (XAS) of Cu2p (Figure 4) shows an increase in the satellite peak at 932.5 eV with the increase in oxygen concentration, confirming that the Cu3d orbital related to this transition ($2p^63d^9-2p^53d^{10}$) affects the introduction of the holes.

The symmetry of the wave function of the hole can be determined from the polarization dependence of the XAS of a $YBa_2Cu_3O_{6.8}$ single crystal. The polarization characteristic of the XAS for Cu2p (Figure 5) seems to show a

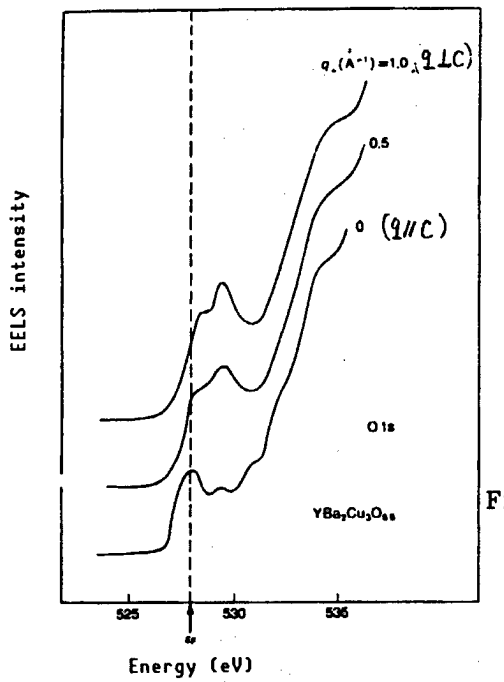

Figure 6(a) Momentum Dependence of Electron Energy Loss Spectra of 0.1s for a $YBa_2Cu_3O_{6.8}$ Single Crystal Thin Film (A. Kotani)[5]

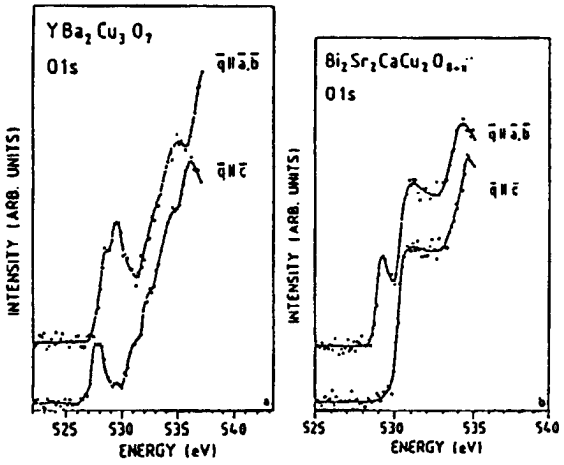

Figure 6(b) EELS curves at the O1s edge from single crystals of: (a) $YBa_2Cu_3O_7$ and (b) $Bi_2SrCaCu_2O_8$ for different orientations of the momentum transfer q. The enhanced signal for q in the a-b plane conclusively shows that the O2p holes have primarily x,y character.

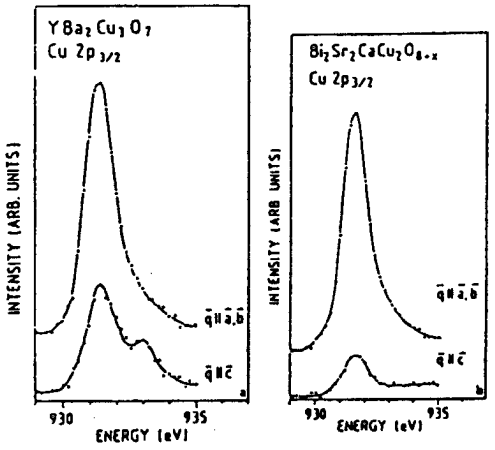

Figure 7(a) EELS Spectra at the $Cu2p_{3/2}$ Threshold for Single Crystals of (a) $YBa_2Cu_3O_7$ and (b) $Bi_2Sr_2CaCu_2O_8$ for Different Orientations of the Momentum Transfer q (From Nucker, et al. (38))[3]

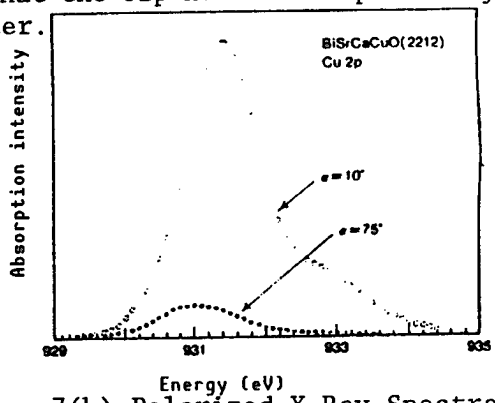

Figure 7(b) Polarized X-Ray Spectra of Cu2p for a BiSrCaCuO (2212) Sample (A. Kotani)[5]

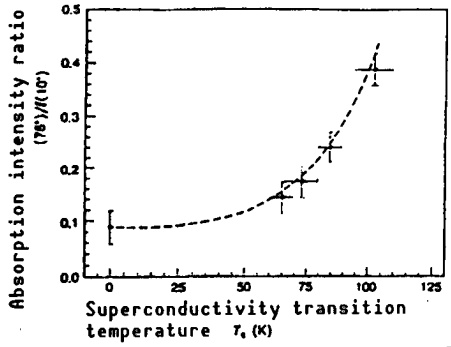

Figure 7(c) Relationship Between Intensity Ratio of Polarized X-ray Absorption I(75°)/I(10°) of Cu2p and Superconductivity Transition Temperature T_c for Various BiSrCaCuO System Samples (A. Kotani)[5]

large change in the satellite peak at 932.5 eV. Since this peak corresponds to the allowed transition for E_c, it can be interpreted that Cu(1)$3dz^2-y^2$ and Cu(2)$3d3z^2-r^2$, representing the orbitals in the c-axis direction, and the O(4)$2p_z$ orbital that forms hybrid orbitals with them, contribute to the hole doping. According to a more detailed analysis, it is shown that the satellite peak corresponds to the contribution by Cu(1), its spectral shape is approximately the same as that of Cu(1) and Cu(2), and that holes are doped there. In addition, the results of the electron beam energy loss spectra (EELS) of the O1s of a $YBa_2Cu_3O_{6.8}$ single crystal thin film (Figure 6) shows that absorption occurs for both cases of $q_\perp(A^{-1}) = 0$ (q // c) and $q_\perp(A^{-1}) = 1$ (1 $\perp$ c), while for q // c a transition of the $O2p_z$ hole occurs in the vicinity of E_F. As in the above, in the YBCO system, the doped holes first enter the O sites of the CuO linear chains and at the pyramid vertices, then the O sites of the CuO planes.

In the BiSrCaCuO system, the holes exist only in O2px, $2p_y$ in the CuO planes and not in $O2p_z$ due to the fact that, as opposed to the YBCO system, it does not contain one-dimensional chains of CuO. This fact is shown in the polarized XAS data of O1s (Figure 7). On the other hand, the polarized X-ray absorption intensity ratio I(75°)/I(10°) of the XPS of Cu2p shows a strong correlation with the T_c (Figure 7(c)). This shows that the hole concentration of the Cu$3dx^2-y^2$ component increases with respect to the concentration of the Cu$3d3z^2-r^2$ component as the T_c becomes higher. However, it is not possible to explain by means of the tetragonally symmetric CuO_4 cluster alone, which lacks the $3d3z^2-r^2$ component, that the absorption of I(75°) is due to the transition to the Cu$3d3z^2-r^2$ hole orbital. In order to explain this, the theory has been proposed that a hybrid orbital is created between dx^2-y^2 and $d3z^2-r^2$ due to rhombic distortion of the CuO_4 planes or as a result of a band dispersion due to crystal symmetry. The distortion theory suggests that the rhombic distortion is larger for higher T_cs.

Electron Spectroscopy

The significant contributions of photoelectron spectroscopy are the distinct observation of the Fermi edge, the observation of the relatively high electronic state density there, and the observation of the energy dispersion curve that depends on the wave number vector. In addition, the evaluation of the electron correlation energy U, the charge transfer energy Δ between Cu and O, and the bandwidth (kinetic energy) t of the hybrid orbitals between Cu3d and O2p by X-ray photoelectron spectroscopy are also important.

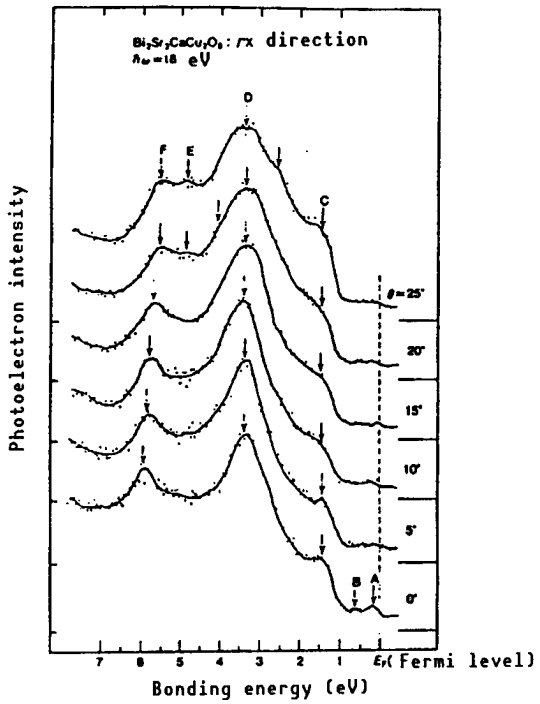

Figure 8(a) Angular Resolved Photo-Electron Spectra in the Vicinity of the Fermi Level for $Bi_2Sr_2CaCu_2O_8$ Single Crystal (T. Takahashi, et al.)[1]

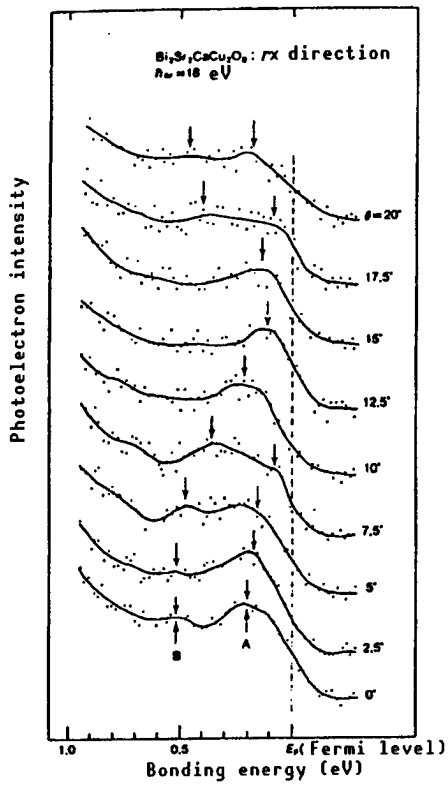

Figure 8(b) Angular Resolved Photo-Electron Spectra of $Bi_2Sr_2CaCu_2O_8$ Single Crystal Excitation light $\hbar\omega$ = 18 eV. Measurement is made in the ΓX direction of the Brillouin zone. θ is the angle of photoelectron emission from the crystal surface.

The observation of the high electronic state density at the Fermi edge, the observation of the energy dispersion curve that crosses the Fermi liquid, and the observation of the Fermi edge of unoccupied electronic states by inverse photoelectron spectroscopy through electron spectroscopy are considered to be powerful evidence for the Fermi liquid model. Figures 8 and 9 show the angular dependence of the spectra obtained by photoelectron spectroscopy for the superconducting phases of $Bi_2Sr_2CaCu_2O_8$ by Takahashi, et al., and the YBCO system by Sakisaka, et al., and give the dispersion curves of the energy levels against the wave number vector.[1] The results show the formation of a metallic band structure that crosses the Fermi level.

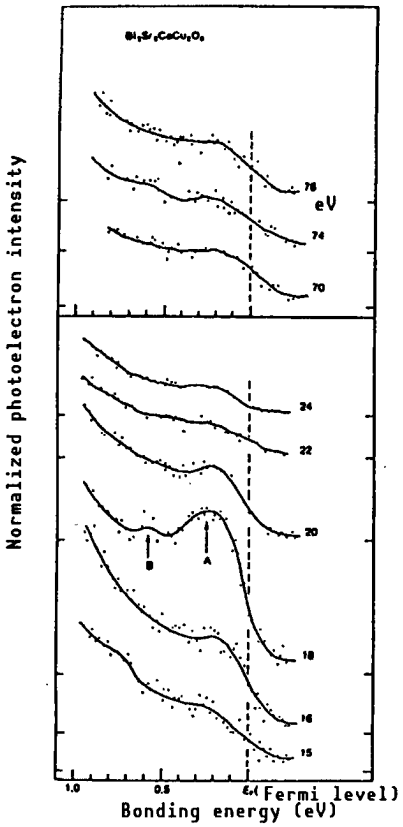

Figure 8(c) Photoelectron Spectra (Resonant Photoelectron Spectroscopy) in the Vicinity of the Fermi Level Measured by Varying the Energy of the Excitation Light

Note that band A displays a resonant increase at the energy ($\hbar\omega$ = 18 eV) of the 2s inner shell excitation of oxygen.

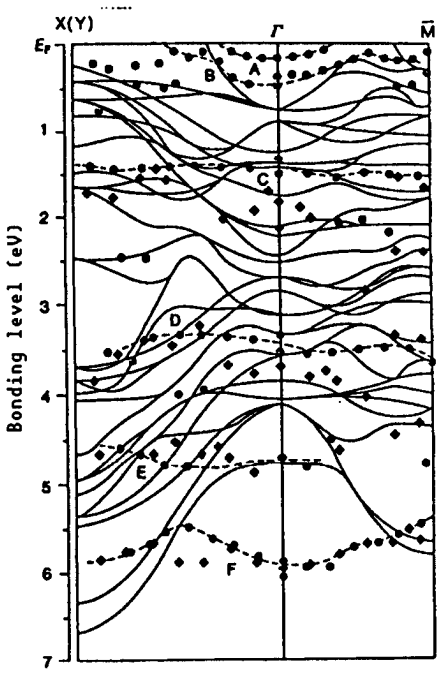

Figure 8(d) Band Structure of $Bi_2Sr_2CaCu_2O_8$ Determined by Angular Resolved Photoelectron Spectroscopy

- • represents data obtained for excitation light with $\hbar\omega$ = 18 eV.
- ♦ represents measurement with $\hbar\omega$ = 40 eV. A to F correspond to the respective bands in Figures 2 and 3. For comparison, the results of band calculations are shown.

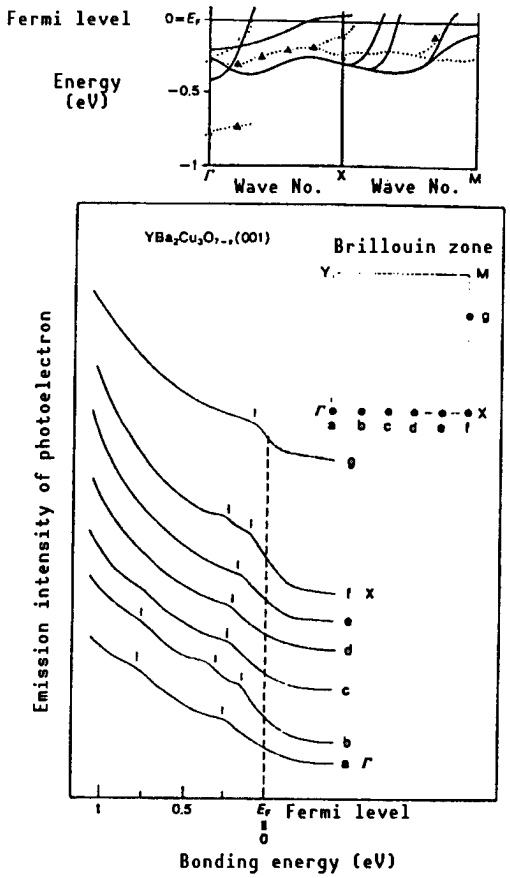

Figure 9. Angular Resolved Photoelectron Spectra of $YBa_2Cu_2O_{7-x}$ (001) Near the Fermi Level Measured by Varying the Emission Angle in the Γ–X and X–M Directions

Excitation light has an energy h_ν = 40 eV. The symbols a to g next to the spectra correspond to the points a to g in the Brillouin zone. The result of the band calculations are shown for comparison (from Y. Sakisaka (Ref. 1)).

In the $Bi_2Sr_2CaCu_2O_8$ system, that the band formed within the charge transfer gap has a strong O2p characteristic is confirmed also by an experiment involving resonant photoelectron spectroscopy. Further, from the angular dependence of XAS of O1s by the use of the c plane of a $Bi_2Sr_2CaCu_2O_8$ single crystal, it has become clear that this band is formed mainly by the $O2p_x$, $2p_y$ orbitals within the ab plane.

Figure 10 shows the UPS spectra measurements of a $YBa_2Cu_3Ca_{1-x}O_{6.9}$ system crystal cleaved at 20 K obtained by Arko, et al.[3] The rise of the spectra at the Fermi edge is steep and large, and it may be said that the agreement of the measured results and the results of the band calculation is good, with an error of about 0.5 eV. To tell the truth, before these data were obtained, the results of electron spectroscopic measurement of the YBCO system showed a weak spectral intensity at the Fermi edge due to the deposition of oxygen and barium on

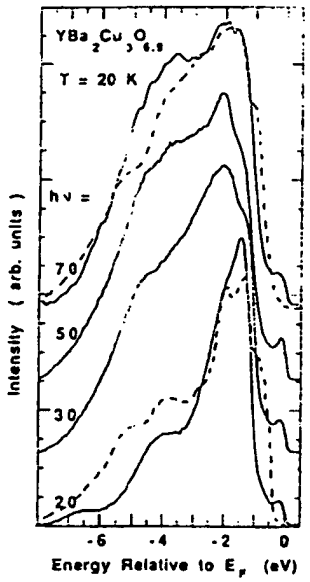

Figure 10. Comparison of Experimental Spectra (Solid Curves) From $YBa_2Cu_3O_{6.9}$ With Calculated Spectra for $YBa_2Cu_3O_7$ (Dashed Curves) (From Arko, et al., Ref. 3)

the surface, displaying a large discrepancy from the results of the band calculation, which has been dominant in supporting the idea of the breakdown of the band theory in this crystal. The breakdown of the band theory was decisive in that, in contrast to the fact that the correlation energy between the Cu3d electrons in an insulating phase is large, localizing the 3d electrons at each atomic site and giving an insulator-like structure, the band theory leads to the formation of a metallic band structure. For this reason, tendency to take it for granted that the band theory will also break down in the superconducting phase has been strong.

Another contribution of photoelectron spectroscopy is that it is useful in evaluating the correlation energy U_{dd}, the charge transfer energy Δ between Cu3d and O2p, and the spread t of the hybrid band between Cu3d and O2p. These parameters are useful in identifying the nature of copper oxides as material systems:

$$U_{dd} = E_{kin} - E_6(2p) - 2E_6(3d^9) \quad \sim 7 \text{ eV}$$

$$\Delta = E(d^{10}\underline{L}) - E(d^9) \quad \sim 3 \text{ eV}$$

$$t = \langle d^9 \, |H| \, d^{10}\underline{L} \rangle \quad \sim 1 \text{ eV}$$

In the above, E_{kin} is the kinetic energy of the Auger peak $L_3N_{45}N_{45}$, and $d^{10}\underline{L}$ represents the $Cu3d^{10}$–$O2p^5$ electronic configuration obtained as a result of moving a hole from $Cu3d^9$ to the ligand O2p.

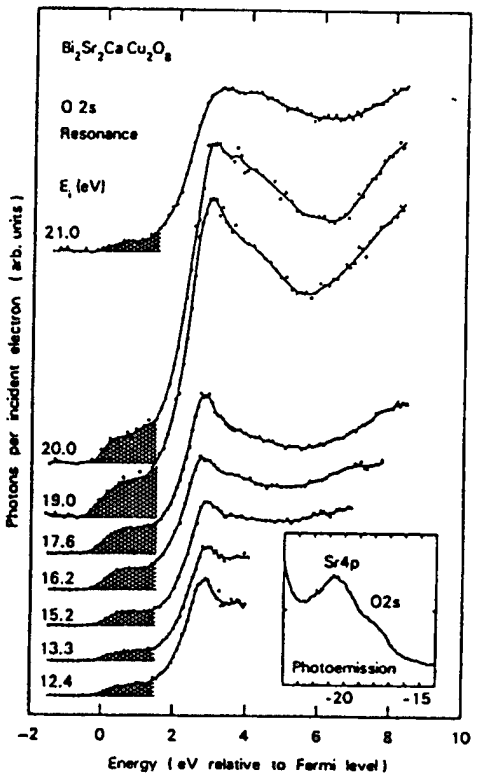

Figure 11. Inverse Photoemission Spectra From $Bi_2Sr_2CaCu_2Ox$ Showing a Resonance Just Above the Fermi Level for an Initial Energy About 19.5 eV Above the Fermi Level (From Drube, et al. (Ref. 3))

In addition, the observation of the Fermi edge of the unoccupied electronic states by means of inverse photoelectron spectroscopy (Figure 11) is also powerful evidence for the Fermi liquid model theory.

The absorption coefficient α (Figure 12) of an $La_{2-x}Sr_xCuO_4$ single crystal thin film has been obtained by Suzuki, et al., from the reflectance and transmittance of infrared rays.[1] Since α represents the electronic state of bonding $N'(E)N(E-\hbar\omega)$, α will be representing the electronic state density of the valence band on the lower side of E_F provided that the energy dependence of N(E) for the upper Hubbard band can be assumed to be small. For the undoped condition of x = 0, a 2 eV-wide absorption band appears that corresponds to an insulating gap. When the number of holes is increased by Sr doping, a new absorption peak appears at 1.5 eV which rises with the amount of Sr doped. These results can be interpreted as saying that a new energy band is growing in the charge transfer-type gap, as shown in Figure 13. This band's characteristics are mainly those of the 2p state of oxygen, and the that fact it crosses E_F is also confirmed by the EELS measurement. In addition, the fact that this band is not merely a localized impurity level, but is forming a band and is contributing to the formation of the Fermi surface is known also from the metal-like temperature change of the resistance in the region $x > 0.1$.

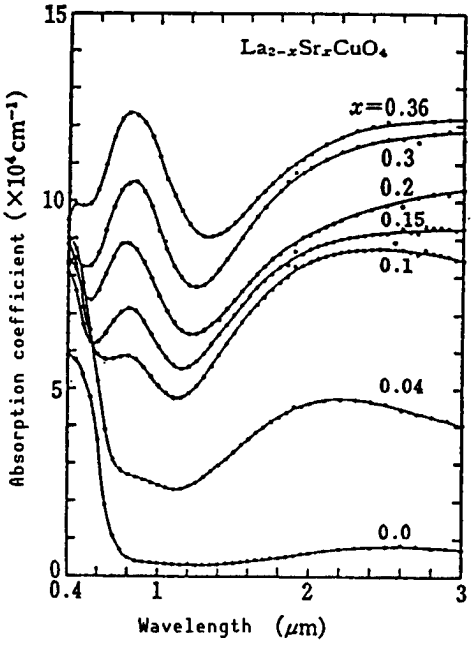

Figure 12. Absorption Coefficient of $(LA_{1-x}Sr_x)_2CuO_4$ (M. Suzuki, et al., Ref. 1))

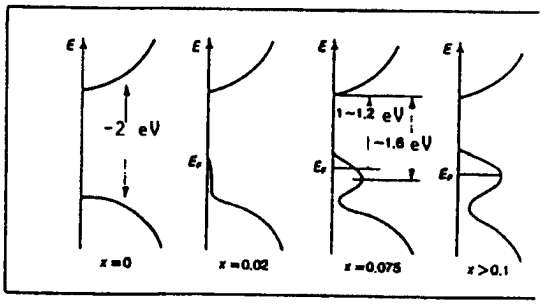

Figure 13. Conceptual Diagram for the State Density of $(La_{1-x}Sr_x)_2CuO_4$ (M. Suzuki, et al., Ref 1))

As to the formation of this band, there is one theory that it is due to the many-body effect and another theory that it can be described in terms of the one-electron theory-like band theory. Within the one-electron theory there are two ideas as to how this metal-like band is formed in the vicinity of the Fermi liquid. One of them is a rigid band model in which the shape of the band remains unchanged and the Fermi liquid shifts as the carrier concentration becomes large. In the other theory, a new energy level is formed by the increase in the carrier concentration, and it grows to a band that forms a Fermi band. The domination of the latter idea can be confirmed by the change in the wavelength dependence on x of the optical absorption coefficient of the $La_{2-x}Sr_xCu_2O_4$ system and by the concentration dependence of the XAS spectra of oxygen in $Bi_2Sr_2Ca_{1-x}Y_xCu_2O_8$.

Despite such measurement results by photoelectron spectroscopy and light absorption, there are some who are skeptical about the Fermi liquid model. Direct evidence for a Fermi liquid is obtained through observation of the Fermi surface. Representative techniques for this purpose include the de Haas-van Alfven (dHvA) effect and the positron annihilation method. The measurement of the dHvA effect has been considered difficult for samples with many vacant lattices and a short electron mean free path, as well as for samples with large Hc_2 and a magnetic field that is difficult to penetrate. However, Muller, et al., of the Los Alamos Laboratory announced before the meeting of the recent American Physics Society that they had observed vibrations of magnetization, which were considered to be due to the dHvA effect, for a YBCO sample at a magnetic field above 70 T and at a temperature of 4.2 K.[6]

Evidence that this is due to the dHvA effect is that it exhibits a phenomenon [$X = \exp(-kT/\hbar\omega)$] characteristic of the dHvA effect in that the amplitude X increases for lower temperatures. They have determined the cross sectional area and the effective mass of two Fermi surfaces with two frequencies. The results are as follows:

(1) The areas of the Fermi surfaces are 0.27 and 0.11 a.u.

(2) The effective masses are 4.6 m_0 and 2.9 m_0.

(3) The area of the Brillouin zone is $2.7 \times 10^{16} cm^{-2}$.

(4) The dHvA frequency is $\omega_H = 2.8 \times 10^4$ T ($\omega_H = eH/m^*c$).

If these data are not in error, then it is undoubtedly a Fermi liquid.

In researching the positron annihilation method, Tanikawa, et al., observed a two-dimensional hole surface on an $La_{1.8}Sr_{0.2}CuO_4$ single crystal.[1] Permitting an E_F shift of about 0.5 eV, the results can be made to correspond qualitatively with the results of the band calculation. However, since a similar hole surface is also observed on an Sr-undoped La_2CuO_4 sample, there remains some doubt about the experimental results.

Band Theory

At one time a paper appeared which gave the impression that the band theory had been completely broken down based on the photoelectron spectroscopic spectra obtained by the use of samples with unclean surfaces. However, there was a report recently on the results of research on the superconducting phase with a clean surface which supports the band theory to a large extent. The grounds for which the band theory is not applicable are: 1) an electronic state density is not observed at the Fermi edge; 2) the overall electronic state density and the spectral shape do not agree; and 3) a satellite peak that shows the localization of Cu3d electron appears in the vicinity of 10 eV. However, as we have already seen, the results of photoelectron spectroscopy obtained from samples with clean surfaces cleaved at 20 K show that evidence 1) and 3) have no grounds. In addition, although the appearance of the satellite peak in 3) is an experimentally correct one, this is an excited state similar to the multiply-split peaks of $2p^5 3d^9$ that appear in the Cu2p peak as a result of excitation by X-ray or light. Accordingly, it is a peak that is not required for the results of band calculations indicating the ground state.

As in the above, the denial of the band calculation results by the photoelectron spectroscopic experiments in the early days has nearly been overturned and the recent results are that, at least in the superconducting phase, the photoelectron spectroscopic experiments agree with the band calculations within an error of about 0.5 eV. Errors of this order sometimes occur during the ordinary calculations of the metallic bands. However, since the agreement in the insulating phase leaves no doubt, the future task is how to handle the electron correlation.

Although many results of band calculations have been published, no results have yet been obtained which can exactly explain the electronic structure in which a band gap occurs in the insulating phase. It should be mentioned that a band gap can be made to appear by introducing the electron correlation artificially by ignoring the wave function of Cu3s,, 3p or by taking antiferromagnetism into consideration, but none of these corresponds to taking the electron correlation straightforwardly. On the other hand, the band structure in the superconducting phase can be explained fairly nicely by the band calculation results.

Problems of Observation

In studying the electronic structure of oxide superconductors, it is sometimes necessary to differentiate whether the data is a piece of information regarding the superconductor itself of whether it is data that included a piece of information concerning the observation process of the superconductor. In particular, care must be exercised since the superconductivity phenomenon is one with an energy level that is less than 100 meV, while many of the observation means that are related to the electronic structure use excitation energy greater than that value. For example, since the satellite peaks of Cu2p or Cu3d by XPS or UPS are due to energy levels that are generated as a result of excitation with light, there are portions in which the electronic state density (band structure) calculated for the ground state does not necessarily correspond to the spectrum of photoelectric spectroscopy. Such a situation can also happen with other means of observation, so it is important to examine the perfection of the samples and the influence of the excitation effect in establishing an anomalous phenomenon.

3. Non-Fermi Liquid or Anomalous Fermi Liquid Theory

As to the experimental results which are said to be the grounds for a non-Fermi liquid, definitive evidence does not seem to exist. There are so-called "anomalous normally conducting states" which differ from the conventional typical Fermi liquid,[1] and it is conceivable that they may be explainable by extending the conventional ideas about Fermi liquids. However, it is necessary to take up the so-called bases of the non-Fermi liquid.

The temperature change in the nuclear spin lattice relaxation rate $1/T_1$ of a superconductor, as observed by nuclear magnetic resonator (NMR), peaks directly beneath the T_c for a BCS-type superconductor, but it does not appear in a high temperature superconductor. The reason for this is that the electronic state density remains in the energy gap. This represents a deviation from the BCS theory, which is based on the Fermi liquid, and it may be considered as evidence for a non-Fermi liquid. It also deviates from the Korringa relation (T_1T = const.), which is expected for an ordinary metal when T_c is exceeded, and the deviation becomes more conspicuous with an increase in the T_c. This can also be considered as representing a deviation from the typical Fermi liquid.

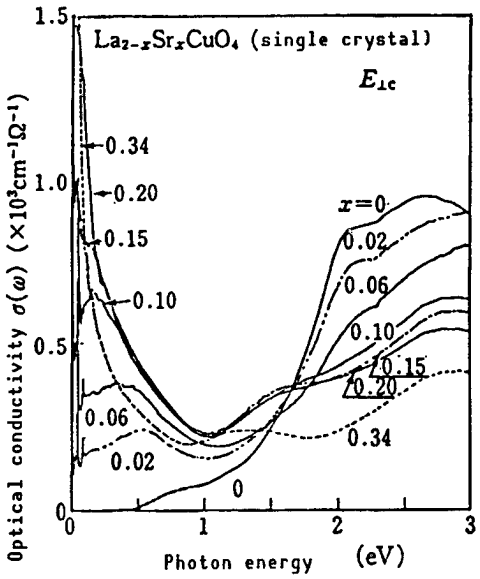

Figure 14. Optical Conductivity Spectra Obtained by the Kramers-Kronig Transformation From the Light Reflection From the c Plane of $La_{2-x}Sr_xCuO_4$ Single Crystal (S. Taijima, et al., Ref. 4)

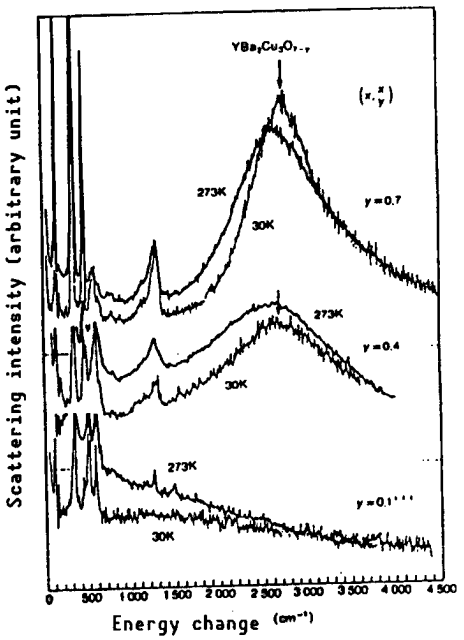

Figure 15. Oxygen Concentration Dependence of Raman Spectra The arrow indicates the peak of 2-magnon scattering (S. Sugai, et al., (Ref. 1))

Above we said that the result of light absorption (Figure 12) is one piece of evidence for the Fermi liquid. However, based on the results (Figure 14) of optical conductivity (corresponding to the light absorption), it is sometimes interpreted as a non-Fermi liquid. A system with a large ratio of Sr (x= 0.34) to La_2CuO_4 shows a Drude-type spectrum ($\sigma(0) \rightarrow \infty$) due to the conduction electrons of a typical Fermi liquid. Although its electrical conductivity exhibits properties that are similar to those of typical metals, it is a nonsuperconducting state. When the doping quantity of Sr is successively reduced, the Drude-type absorption is correspondingly reduced, a new absorption peak appears in the low energy region, and the peak gradually shifts from 0~0.5 eV. Superconductivity appears in the intermediate region. This absorption peak is not due to the overlapping of impurity levels within the charge transfer-type band gap, but it is interpreted as being due to the fluctuations of the $Cu3d^9$ spin. At the extremities where the metallicity and spin ordering are respectively complete, superconductivity disappears, while in the intermediate region where the two characteristics approach each other, superconductivity appears. Therefore, by looking at it from a different angle, it may be interpreted as being an entirely opposite Fermi liquid.

The result of Raman scattering is shown in Figure 15. In the superconducting region (y = 0.1~0.4) it differs from bending metals (x = 0.34) and the remains of the 2-magnon excitation spectra are observed in the high energy region

(~3,000 cm^{-1}). The 2-magnon excitation spectrum is something not seen in the typical Fermi liquid. The magnon spectral intensity shifts to the low energy side while decreasing accompanying the reduction in the doping amount of the holes. This is considered to be due to the working of the ferromagnetic interaction between Cu atoms by the introduction of the holes to oxygen, which destroys the antiferromagnetic order that existed in the beginning. In addition, in the superconducting state, since the intensity of the Raman scattering remains even below the gap energy, gradually decreasing toward the energy's zero value, it is anticipated that a considerable amount of the electronic state density remains within the gap.

The fact that the electronic state density remains within the energy gap of a superconducting state, has also been measured in the combined-type tunneling spectra and in the scanning-type tunneling spectra,[1,4] which differ in this respect from the BCS-type. These may be interpreted as representing deviations from the simple BCS-type superconducting state. However, the claim of people who believe in the non-Fermi liquid theory is that if it is the superconductivity of a typical Fermi liquid, the state density should not remain within the gap. However, when a BCS-type superconductor is subjected to a perturbation which is not invariant to the time reversal, e.g., when a magnetic impurity is introduced, it is recognized that it becomes a gapless superconductor. Further, in a metal that exhibits ferromagnetism or antiferromagnetism, and in a paramagnetic metal which is in a state close to that of the metal just described, a deviation from the Korringa NMR relationship is observed due to the strong electron correlation.

When a conspicuous spin effect appears in a Fermi liquid, an explanation of what represents a deviation from the typical Fermi liquid (whether it is an extension of the Fermi liquid model or the Fermi liquid breaks down) will be a future task.

When La_2CuO_4 is doped with Sr, it has been observed that although the two-dimensional antiferromagnetic state is destroyed, a new three-dimensional spin order is formed in the superconducting phase by means of neutron scattering. Since this component, with its slow spin fluctuations ($E < 0.5$ meV), grows more at lower temperatures and forms a three-dimensional magnetic order, it is anticipated that it may have something to do with the manifestation of superconductivity. However, no direct evidence that relates the spin fluctuations to the superconducting phenomenon has yet been found.

In conclusion we will present the marginal Fermi liquid model. The basis of this model has not yet been established theoretically, but it is very promising phenomenologically. The starting point of this model exists, with the Raman spectrum as a reference, in that the spectrum of the charge density fluctuations with the wave number q and the frequency ω is given in terms of the electronic state density N(0) and the temperature T by

$$P(q,\omega) \sim -N(0)\ (\omega/T) \quad : \quad |\omega| < T$$

$$-N(0)\ \mathrm{sgn}\ (\omega) \quad : \quad T < |\omega| < \omega_c$$

The magnitude of these fluctuations at T ~ 100 K have an intensity which is greater by two orders of magnitude than the fluctuations (T ~ 10^4 K) of the ordinary Fermi liquid. By introducing such an assumption, the deviation anomaly of the nuclear magnetic relaxation rate $1/T_1$, optical electric conductivity $\sigma(\omega)$, temperature dependence of the electric resistance R(T)~T, and conductance of the combined tunneling spectroscopy, etc., begins to be explainable. In this model, the fluctuations of the phonon and the charge act as an attraction to the superconductivity mechanism, while the fluctuations of the spin act as a repulsion. An estimate of the superconducting parameters from the characteristics of the normal conductive state of the $YBaCu_3O_7$ system gives T_c = 75~110 K, $2\Delta/KT_c$ = 7.9~7.7, etc., making it provisionally successful as a phenomenological theory.

4. Conclusion

The results of the measurements of electron spectroscopy (UPS, XPS, IPS, EELS), X-ray absorption, and light absorption commonly point to the formation of a metallic band in the superconducting phase consisting mainly of the O2p orbitals that cross the Fermi level, forming a Fermi liquid. The band calculation is basically effective, but since there is an error of about 0.5 eV in the superconducting phase, the view that is necessary to accurately take into account the electron correlation is gaining support. Although a number of people continue to point out the powerlessness of the band calculations of one-body approximations, this seems to have been resolved by the improvement of the band theory.

On the other hand, as empirical grounds for claiming a non-Fermi liquid or a deviation from the Fermi liquid, one may enumerate the deviation of NMR from the Colinha rule (T_1T = const.), the observation of a spin liquid by neutron scattering, observation of scattering in the high energy region in Raman scattering, and the observation of state density within the energy gap in tunneling spectroscopy, etc. However, these experimental results cannot be considered as grounds for proving that an electronic system is totally different from the Fermi liquid. Rather, it seems natural to think of it as a kind of magnetic metal which is a Fermi degenerated electron system and has a strong electron correlation, for which the spin fluctuations cannot be ignored. Thus, the following image of the electronic structure can be painted at the present time.

Due to a strong Coulomb repulsion, the Cu3d electrons remain localized and contribute to the spin fluctuations even when holes (or electrons) are doped. The O2p orbitals form a metallic band between oxygen and contribute to the conductivity by accommodating the holes (or electrons). Further, the Cu3d and the O2p orbitals form a hybrid band which is part metallic, and contribute to the charge fluctuations between Cu and O because of the minimal amount of charge transfer energy. This model differs from the simplified band theory and the Hubbard model which deals only with the degree of freedom of the d electrons. The image of the electronic structure that has been obtained regarding copper oxide superconductor includes the dual characteristics of wandering and localization as well as an advantage due to its pd hybridization.

For an explanation of the superconductivity mechanism, a theory seems to be required that will incorporate the charge and spin fluctuations, as well as the contribution of some of the phonons.

References

1. Edited by the Parity Magazine Editorial Board, "High Temperature Superconductivity [2]," Maruzen Publishing Co., Parity Supplementary Series, No 6, 1989.

2. Varma, C.M., et al., PHYS. REV. LETT., Vol 63, 1989, p 1996; Kuroda, Y., PARITY, Vol 5 No 3, 1990, p 40.

3. Lindberg, P.A.P., et al., SURFACE SCIENCE REPORTS, Vol 11, 1990, p 1.

4. Kishio, K., et al., APPL. PHYS. (JPN.), Vol 59, 1990, p 554.

5. Kotani, A., PARITY, Vol 3 No 11, 1988, p 36, or ref. 1, 1990, p 80, and PARITY, Vol 5 No 5, 1990, p 36.

6. NIKKEI SUPERCONDUCTIVITY, 16 April 1990, p 3.

Property Design of High Temperature Superconductor

916C1001D Tokyo HYOMEN KAGAKU SEMINA in Japanese 27-29 Jun 90 pp 43-51

[Article by Yoshinori Tokura, Faculty of Science, The University of Tokyo]

[Text] **1. Introduction**

In the current article, the basic strategy for the design of high temperature superconductor properties will be described using the "block layer" concept that will be explained later. The viewpoint of this approach is to classify the copper oxide superconductors, with the Cu-O network as the center, and to seek ways to make carrier doping possible in response to the N- and P-type characteristics. In the following, this idea will be described with the most basic cases as examples. Many concrete examples and recent developments using the above-mentioned strategy will be presented in detail at the seminar.

2. The Block Layer Concept

Every high temperature superconductor has a "CuO_2 plane" as its structural unit. What is meant by the "CuO_2 plane" is a plane formed by squares of CuO_4 having four oxygen atoms coordinated around a Cu atom, with their vertices joined as shown in Figure 1. All of the high temperature superconductors discovered so far have structures in which the CuO_2 planes and atomic layers (X and Y in Figure 1 which are called "block layers") are superposed, one after another. Moreover, each CuO_2 plane is in an isolated state, separated by the block layers, as opposed to the usual cubic perovskite structure.

Now, what constitutes the block layers? The basic policy here is to extract general-purpose block layers from the copper oxide superconductors known so far, and to design new high temperature superconductors by reconstructing these block layers. To begin, let us consider the two most basic superconductors—$La_{2-x}Sr_xCuO_4$ and $Nd_{2-x}Ce_xCuO_4$.

As shown in Figure 2, the La system has La_2O_2 layers with the NaCl (rock salt) structure that sandwich the CuO_2 planes, while the Nd system has Nd_2O_2 layers with the CaF_2 (fluorite) type structure. The La_2O_2 layer and the Nd_2O_2 layer correspond to the block layers indicated in Figure 1. (These will be referred to as the L layer and G layer, respectively.)

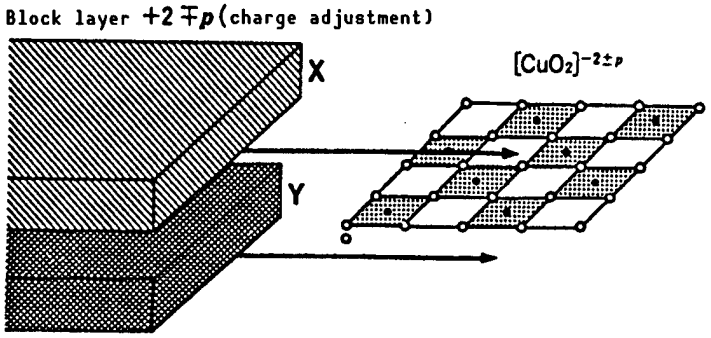

Figure 1. Block Layer Concept

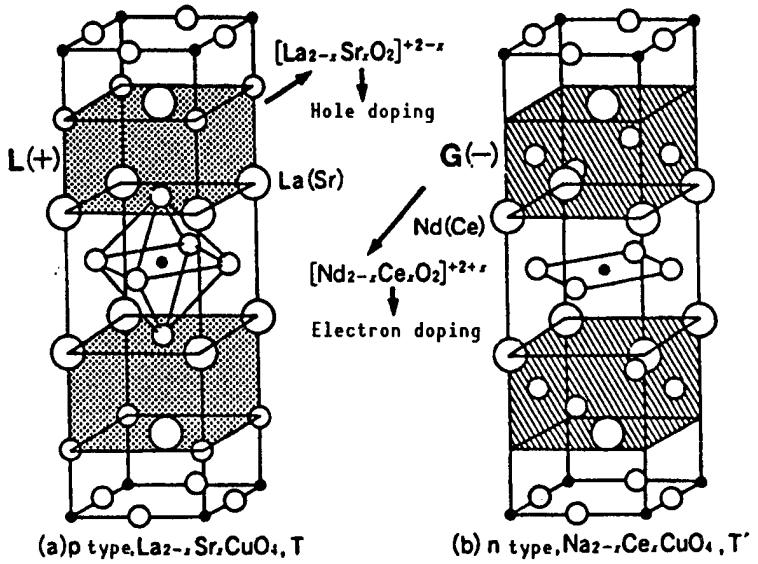

Figure 2. Carrier Doping in (a) $La_{2-x}Sr_xCuO_4$ and (b) $Nd_{2-x}Ce_xCuO_4$

In an L layer, an O atom in a plane is situated as a vertex oxygen atom directly above (or beneath) a Cu atom in a CuO_2 plane. On the other hand, in a G layer, the O oxygen lattice in a plane is at a position obtained by translating the oxygen lattice in a CuO_2 plane as is, so that it does not serve as a vertex oxygen.

For the manifestation of metallic conductivity or superconductivity, carrier doping to the CuO_2 planes is indispensable. With respect to this point, the two layer structures L = La_2O_2 and G = Nd_2O_2 are contrastive. First, let us rewrite La_2CuO_4, which is the base material, as $(La_2O_2)^{2+}(CuO_2)^{2-}$—a block layer and a CuO_2 layer.

In the base material, elements are considered to form the ions La^{3+}, Cu^{2+}, and O^{2-}. By replacing La^{3+} with Sr^{2+}, since the charge of the block layer L is reduced to $(La_{2-x}Sr_xO_2)^{+2-x}$, a positive charge corresponding to Px flows into the

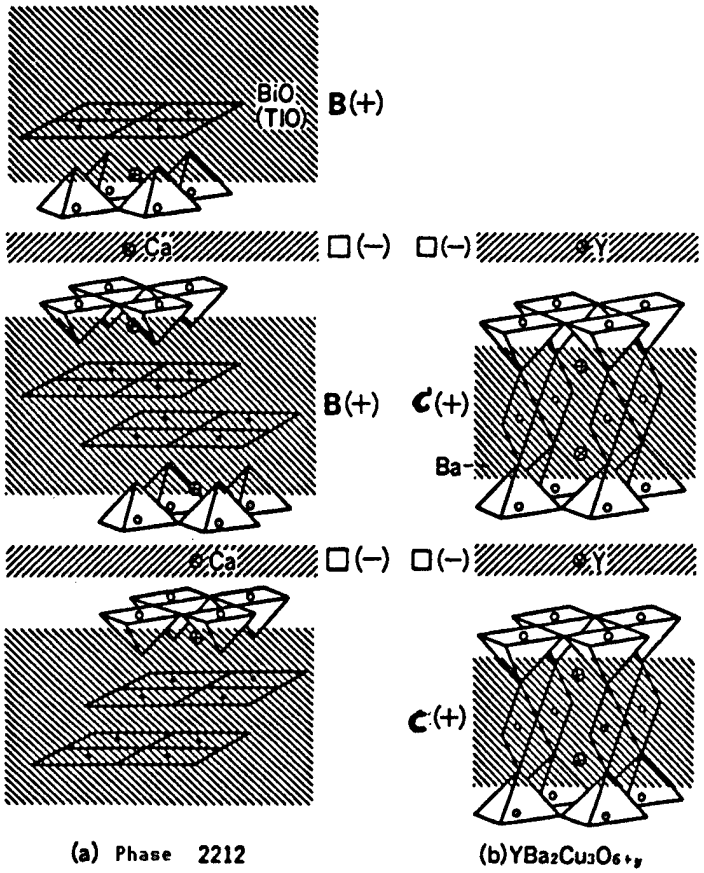

Figure 3. Block Layers in (a) Phase 2212 $Bi_2Sr_2CaCu_2O_{8+y}$, $Tl_2Ba_2CaCu_2O_{8+y}$ and (b) $YBa_2Cu_3O_{6+y}$

CuO_2 plane in order to cancel the change in the charge, forming $(CuO_2)^{-2+x}$. This is hole doping due to Sr replacement. (Here, we assumed that the holes were within the CuO_2 plane. In reality, however, there may be a contribution from the vertex oxygen within the La_2O_2 layer.)

Exactly opposite, in the electron conduction-type compound $Nd_{2-x}Ce_xCuO_4$, when the original G = (Nd_2O_2) layer is partly replaced by Ce^{4+}, the charge is increased in the form of $(Nd_{2-x}Ce_xO_2)^{+2+x}$. Accordingly, a negative charge corresponding to x flows into the CuO_2 plane to form $(CuO_2)^{-2-x}$, that is, electron doping takes place.

As in the above, the block layer plays the role of controlling the carrier concentration in the CuO_2 plane by adjusting the amount of charge in its own layer. Further, as its attribute, cases can be cited of its supplying a vertex oxygen atom to the CuO_2 plane directly above or below (for example, the L layer) and of its not supplying this atom (for example, the G layer). The former and the latter will be called the + type and − type block layers, respectively.

3. Extraction of the Block Layer

Now, what kind of block layers can be extracted when the same viewpoint is applied to the Bi or Y systems, which have higher critical temperatures (T_cs)?

Figure 3(a) presents the $Bi_2Sr_2CaCu_2O_{8+y}$ structure, called phase 2212, which shows a T_c of 80~100 K. Phase 2212 exhibits a structure in which the pyramid type CuO_2 planes face each other, sandwiching the Ca□ layers (□ denotes an oxygen deficiency). When this structure is viewed from the standpoint of the alternate lamination of the CuO_2 plane and the block layer in the above, it may be said that two kinds of block layers, $(SrO)(BiO)_2(SrO)$ or $(BaO)(TlO)_2(BaO)$ (B layer) and Ca□ (□ layer), and the CuO_2 plane are laminated alternately. (The thicknesses of the block layers differ considerably, but since both prevent the interconnection of the CuO_2 planes, it should not be of much concern.)

The B layers supply the vertex oxygen atoms to the CuO_2 planes. Since, however, the layers have an oxygen deficiency to begin with, there is no way to supply the vertex oxygen. According to the notation mentioned above, this situation will be described as (B,□). In phase 2221, i.e., the (B,□) structure, each block layer basically has a charge of +2 (which is standard for a block layer). However, the role of charge adjustment is principally played by the B layer and, in particular, when B^{+2-2y} is formed due to the presence of the excess oxygen in the BiO layer, it looks as if holes are supplied to the pyramid-type CuO_2 plane.

Next, how should we analyze the case of the Y-Ba-Cu-O system superconductors? Since YBa_2CuO_{6+y}, shown in Figure 3(b) (in the figure, y = 1) has the pyramid-type CuO_2 plane as its basic component, by studying the block layers that sandwich the CuO_2 planes, it can be seen that they consist of the (Y□) layer and the (BaO)(CuOy)(BaO) layer.

Since the former has basically the same structure as the (Ca□) layer shown in Figure 3(a), it is represented again in terms of □, while the latter, showing the chain structure that is characteristic of the Y system, will be called a block layer C. The C layer includes the Cu-O network in itself, but since it is unlikely to be playing an essential role in high h superconductivity, it may be considered to be a block layer utilized merely for the charge adjustment. Accordingly, the Y system superconductor (the so-called 123 structure) shown in Figure 3(b) may be represented as the two block structure (C,□) in accordance with the notations currently being employed. Here, it should be noted that the block layer C includes vertex oxygen (+ type), while □ does not supply vertex oxygen (-type).

The (y-1) sample with high oxygen content possesses the composition of $YBa_2Cu_3O_7$, making it capable of supplying a sufficient quantity of holes to the pyramid type CuO_2 plane without particularly depending upon the element replacement. However, one need only initially consider the block layer C with y = 0 (namely, (BaO)Cu(BaO)), provided that "charge adjustment of the block layer," concept is adopted.

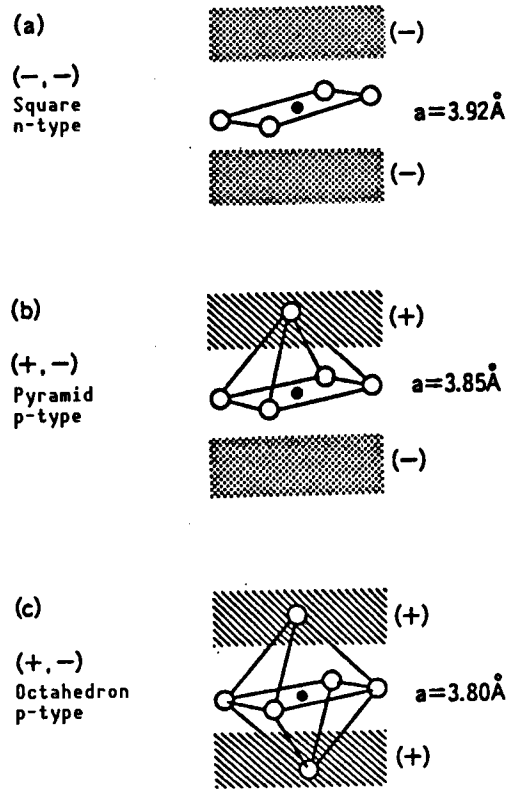

Figure 4. Formation of Three Kinds of Cu–O Networks According to Combinations of the + Type and − Type Block Layers

Since the Cu atom within the block layer has double coordination and a valence of unity, and the insulator with y = 0, $YBa_2Cu_3O_6$, has the charge distribution of (C^{+1}, $\square^{+3}$), with an average charge of +2, it will balance with two sheets of $(CuO_2)^{-2}$. Consequently, when y exceeds 0, it becomes C^{+1-q}, and holes are injected in the form of $(CuO_2)^{-2+q/2}$. (However, since the value of q depends on the shape and the degree of order of the CuO chain in the layer C, it is not possible to assume that q = 2y.)

4. Reconstruction of the Block Layers

Next, let us consider the reconstruction of candidate materials for high temperature superconductors by the use of the various block layers. In the above, we established the + or − attribute depending on whether it supplies or does not supply the vertex oxygen. Because of this, there are three kinds of combinations, (−,−), (+,−), and (+,+), of the block layers above and below a CuO_2 plane, as shown in Figure 4. The corresponding Cu–O networks that include the CuO_2 plane are the (a) square-type, (b) pyramid-type, and (c) octahedral-type. According to the empirical rule, it is known that (a) is of the N-type, while (b) and (c) are of P-type. Accordingly, the N-type ((−,−)) and P-type ((+,−)), and ((+,+)) are determined by the combinations of + and −.

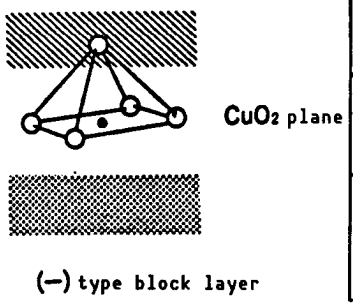

(−) type / (+) type	[3.2Å] □= Ca □ Y □ (−)	[6.0Å] G=(LnO)₂ (−) (Ln=Pr–Gd)
[6.5Å] L=(LaO)₂·(SrO)₂ (+)	(?) $La_2CaCu_2O_6$	T* (1989) $(La, Sr)LnCuO_4$
[8.1Å] C=CuO(BaO)₂ (+)	(1987) $YBa_2Cu_3O_7$	(1989) $(Ln, Ce)_2(Ln, Ba)_2Cu_3O_9$
[12.0Å] B=(BiO)₂(SrO)₂ / (TlO)₂(BaO)₂ (+)	(1988) Bi-2212 Tl-2212	(1989) Bi-2222 Tl-2222

Figure 5. Design of Two Block Structure Having Pyramidal-Type CuO_2 Plane

In addition, empirically speaking, the lattice constant a (= b; tetragonal system) in the direction of the CuO_2 plane is approximately determined as 3.95±0.003 Å for the tetragonal type, 3.860±0.02 Å for the pyramidal type and 3.80±0.02 Å for the octahedral type, corresponding to the Cu–O networks.

First, let us consider the two-block structure (X,Y). To each instance of X and Y, the + or − sign, or the index α or β is attached. Here, the α and β indexes are used to discriminate the case (α), in which the upper and lower CuO_2 planes of a block layer are arranged "in phase" in the c-axis direction so as to have Cu–Cu correspondence, and the case (β), in which the upper and lower CuO_2 planes are shifted by a/2 + b/2 (a and b are the unit cell vectors on the CuO_2 plane). For example, the block layer C is an α type, while the layers L, G, and B are β types.

For example, phase 2212 in Figure 3(a), being (B+β, □−α), is of the pyramidal type, and the c axis is given as twice the thickness of the repetitive unit that contains two sheets of the CuO_2 plane. In this same way, the designation of the combination of the block layers should instantly clarify the fundamental structure, lattice constant, discrimination of the P-type or N-type and the carrier introduction method (method of doping corresponding to the characteristics of the block layer).

A specific example will be shown below. First, let us design a P-type superconductor (candidate material) with a two block structure having a pyramidal type CuO_2 plane. For this purpose, a combination of (+,−) block layers is appropriate. Therefore, let us form a matrix of possible combinations using the block layers described in the above (Figure 5). L(β), C(α), and B(β) are taken as the + layer, while □(α) and G(β) are taken as the − layer. Even for these combinations, six kinds of structures are conceivable, all of which had been synthesized by November 1989. In particular, it should be emphasized that the two block structures of (L,G) and (B,G) were synthesized for the first time based on the design policy described above.

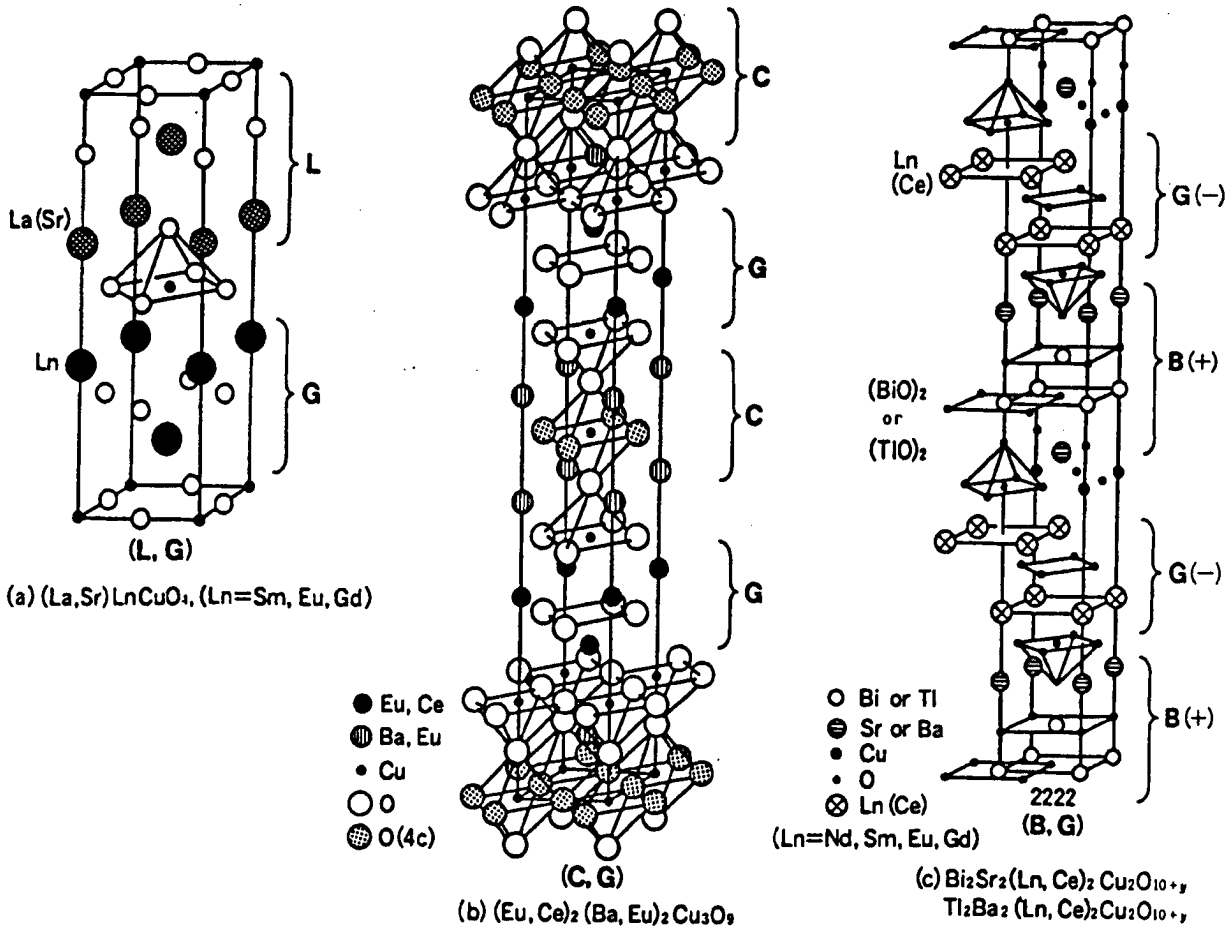

Figure 6. Structures of (a) T^* Phase, (b) Eu–Ba–Ce–Cu–O Phase and (c) 2222 Phase

First, let us take □ as the − layer, and study its combinations with the + layers. As was mentioned in reference to Figure 3, (C,□) corresponds to $YBa_2Cu_3O_{6+y}$ and (B,□) corresponds to $Bi_2Sr_2CaCu_2O_{8+y}$ or $Tl_2Ba_2CaCu_2O_{8+y}$, which are superconductors of the 90 K class that were discovered in the beginning of 1987 and 1988, respectively.

Another example of the (L,□) structure has the composition of $La_2CaCu_2O_6$ (or $(La_2SrCu_2O_6)$ in which two pyramidal-type CuO_2 planes face each other. Curiously enough, although it exhibits metallic conductivity it does not demonstrate superconductivity until extremely low temperatures are reached and, in that sense, it represents a material which is very important for basic research.

On the other hand, the three kinds of structures corresponding to the case of taking the block layer G (fluorite type structure) as the − layer possess T_cs of 25~45 K, and were discovered within the past year. Figure 6 shows the (L,G), (C,G), and (B,G) structures. The two block (L,G) structure (Figure 6(a)) is the so-called T^* phase, and is composed of $LaLnCuO_4$ (Ln = Sm, Eu, Gd, Tb, etc.).

In practice, stabilizing the structure only requires that the charge in the L layer be decreased and the charge in the G layer be increased, i.e., in a manner like $(La_{1-x}Sr_x)(Gd_{1-y}Ce_y)CuO_4$. However, since this is a (+,−) combination, has a pyramidal type CuO_2 plane, and is of the P type, it has to have a hole doped structure, making it necessary to satisfy the condition $x > y$. The T^* phase was first discovered by Akimitsu (Aoyama Gakuin University) and Muromachi (Institute for Inorganic Materials, MITI) in the form of (Na,Sr)(Nd, Ce)CuO_4. In this case, Nd is used in place of La. However, the use of La permits many T^* phase structures to be synthesized without the use of Ce.

Now, the (C,G) structure shown in Figure 6(b)is one discovered recently by Sawa, Akimitsu, and others (Aoyama Gakuin University), and has the composition of $(Eu,Ce)_2(Eu,Ba)_2Cu_3O_{8+y}$. In this case, too, Eu (or Nd) exists in both the C and G layers, but it is anticipated that Eu(Nd) in the C layer may be changed to La, while Eu(Nd) in the G layer may be changed to another rare-earth ion with a smaller ionic radius. In fact, there have been many reports of products substituting for the above type. However, the C layer in this case is a solid solution system of La (or Nd or Eu) and Ba, so that the CuO_y chain in the C layer is in a disordered state. It is known that in the samples for which the oxygen content has been sufficiently raised to the y=1 state, the T_c is about 40 K.

5. Synthesis of the Phase 2222

In Figure 6(c), a new Bi or Tl system copper oxide, designed and synthesized in accordance with the method shown in Figure 4, is presented. It exhibits the (B,G) structure. This structure was discovered recently by a joint research team from the University of Tokyo, the University of Tsukuba, and IBM (Almaden), and its properties have been investigated in detail. The new structure has two sheets of pyramidal-type CuO_2 planes between $(BiO)_2$ or $(TlO)_2$. Its composition may generally be represented as $Bi_2Sr_2(Ln_{1-x}Ce_x)_2Cu_2O_{10+y}$ or $Tl_2Ba_2(Ln_{1-x}Ce_x)Cu_2O_{10+y}$ (Ln stands for a rare-earth element) (phase 2222). In particular, in the Bi-2222 phase, 11 elements can replace Ln, i.e., Y, Pr, Nd, Sm, Eu, Gd, Dy, Tb, Ho, Tm, and Yb.

In the Bi system, $y = 0.24$ or so, and it is necessary to carry out the Ce replacement of $x = 0.03$~0.25 in order to stabilize the G layer. However, since it has pyramidal-type CuO_2 planes, it is a hole conductivity type (p type with $y > x$), and exhibits a maximum T_c of about 40 K. A new structural characteristic is that it has the (β,β) combination in the (B,G) structure, and the CuO_2 plane overlap changes whenever the B and G layers cross, eventually returning to the original position by the two block layers. Accordingly, differing from phase 2212 (Figure 3(a)) or phase 2223 (Figure 7(a)) of the same Bi or Tl system, the length of the c axis is equal to the thickness of the repetitive unit. However, since the nearest two CuO_2 planes that are sandwiched by the $(BiO)_2$ or $(TlO)_2$ layers have a G layer of the − type, they are characterized by "phase" shifts.

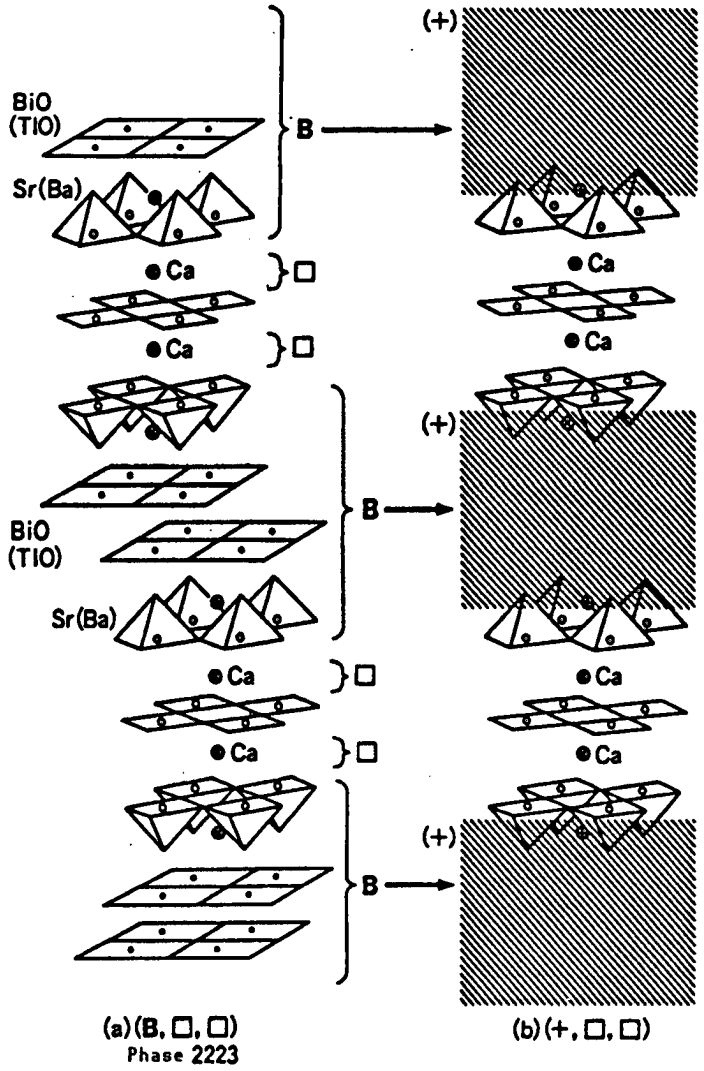

Figure 7. High T_c Structures

6. Possibility of Discovering New Structures

Will it be possible to discover even more new superconductors by using the block layer concept described above? To answer this question, two approaches can be taken, i.e., 1) examining the combinations of three or more block layers, and 2) examining the combinations of new block layers by developing new block layers.

As an example of the three block structure in 1), one may mention phase 2223 of Bi or Tl (Figure 7(a)). According to the notation here, the structure will be represented as a three block structure (B,□,□). For entirely unknown reasons, a network of these two sheets of pyramidal-type CuO_2 planes and the sheet of square-type CuO_2 plane sandwiched between them seems to be indispensable for obtaining a high T_c (>120 K). Such a network will generally be

realized by the structure (+,□,□) (+ denoting a + type block layer) (Figure 7(b)). Since there are many structures in addition to the B layer (namely, [(BaO)$(TlO)_2$(BaO)]) that can be used for the + layer, the possibility of synthesizing superconductors with structure and composition other than that of phase 2223 and having a comparable (120 K class) T_c exists.

One method of constructing multiblock layer structures involves literally laminating blocks (with the CuO_2 planes attached), one on top of the other. Such a block layer epitaxy method may be established in the near future in the field of copper oxide superconductors as well. In that case, not only the high T_c structures mentioned above, but also two or more kinds of CuO_2 planes (the P type or N type, or both) may be realized, or P–N junctions which would be able to gradually eliminate the lattice constant mismatch within a CuO_2 plane may be produced.

Another key for designing new structures is the development of new block layers. There are currently many known block layers in addition to those shown in Figure 5. Among them should be some that will be usable as general-purpose block layers in the future. In addition, if some new high temperature superconductors happen to be found "accidentally," then it will become instantly possible to design and synthesize new structures, one after another, by means of a "matrix," as shown in Figure 5, provided that it is possible to lead out block layers and their attributes like those described above. The latest examples of the above design policy will be given [at the planned seminar].

Current Status of, Outlook for PVD

916C1001E Tokyo HYOMEN KAGAKU SEMINA in Japanese 27-29 Jun 90 pp 53-67

[Article by Hideomi Koinuma and Mamoru Yoshimoto, Institute for Industrial Materials, Tokyo Institute of Technology]

[Text] **1. Introduction**

The most widely employed method for producing high temperature superconductors is the physical vapor deposition (PVD) process in which physical energy is injected into single or multiple solid materials which are vaporized and then rearranged in a substrate as thin films. In general, this method differs fundamentally from the chemical vapor deposition (CVD) process, which uses volatile precursors in high energy states as the materials, in that the films produced and the material solids are in chemically equivalent states. Since it has fewer limitations regarding the surface of the raw materials, its general utility is high, and there are many variations due to the reaction apparatus, the kind of injected energy (heat, electrons, ions, light, etc.), the method of its application, etc. The representative methods include vacuum evaporation and sputtering, from which are derived such methods as molecular beam epitaxy (MBE), ion plating, ion cluster beam (ICB), etc., and currently new improved methods are being devised.

In this article, after reviewing the current status of the technologies for manufacturing high temperature superconductors by PVD, the authors take up several key technologies that may control the future development to present examples of research and examine the problems involved.

2. Methods of Film Formation and Process Conditions

Since oxide superconductors contain more constituents and complicated crystalline structures than ordinary metals or semiconductors, the manufacture of superconductors starts with the preparation of the constituents, the selection of the methods of the crystal structure formation (layered perovskite) of the superconductive phases, and the search for reaction conditions. In particular, the oxygen content within a film changes with the environment, not only while these superconductors are being manufactured, but also during the post treatment process (annealing), which significantly affects the physical properties

of the superconductor obtained. Assuming that the metallic constituents are appropriately controlled, the formation of the superconducting phases depends primarily on the temperature and pressure (partial pressure of oxygen). High temperatures accelerate the diffusion of the metallic components, and are advantageous for the construction of the crystal structures.

On the other hand, since the equilibrium oxygen content in a film drops at high temperatures, it leads in a hole conductive-type oxide with a reduction in the carrier (hole) concentration. In addition, since it is a method of depositing films on a foreign material, i.e., a substrate, it is necessary, in a high temperature process, to pay attention to the generation of cracks due to physical (difference in the coefficients of thermal expansion) and chemical (mutual diffusion) interactions and to the progress of deterioration due to the reaction of the solid phase to the interface. Needless to say, the interface reaction is undesirable for fabrication, including laminating a thin film structure into a device.

Let us classify the superconducting manufacturing processes by focusing attention on the temperature and pressure.

(1) Low Temperature Film Formation (Amorphous or Incomplete Crystal)

High temperature annealing	→	Crystallization (generally crystalline, but sometimes solid phase epitaxy)
Low temperature (≤500°C) oxygen annealing	→	Oxygen content adjustment: Superconductivity

(2) High Temperature (>Crystallization Temperature) Film Formation (Incomplete Crystal)

High temperature annealing	→	Crystallization, grain growth
Low temperature oxygen annealing	→	Oxygen content adjustment: Superconductivity

(3) Film Formation (Crystallization)

Low temperature oxygen annealing	→	Oxygen content adjustment: Superconductivity

(4) Film Formation (Crystallization)

Cooling	→	Superconductivity

The reports in the past have mostly been about (1) or (2), but the as-grown processes (3) and (4) are also becoming possible as a result of the advancement of the manufacturing techniques. In manufacturing laminated devices, it is preferable to use in situ processes (4) in which the crystallization and

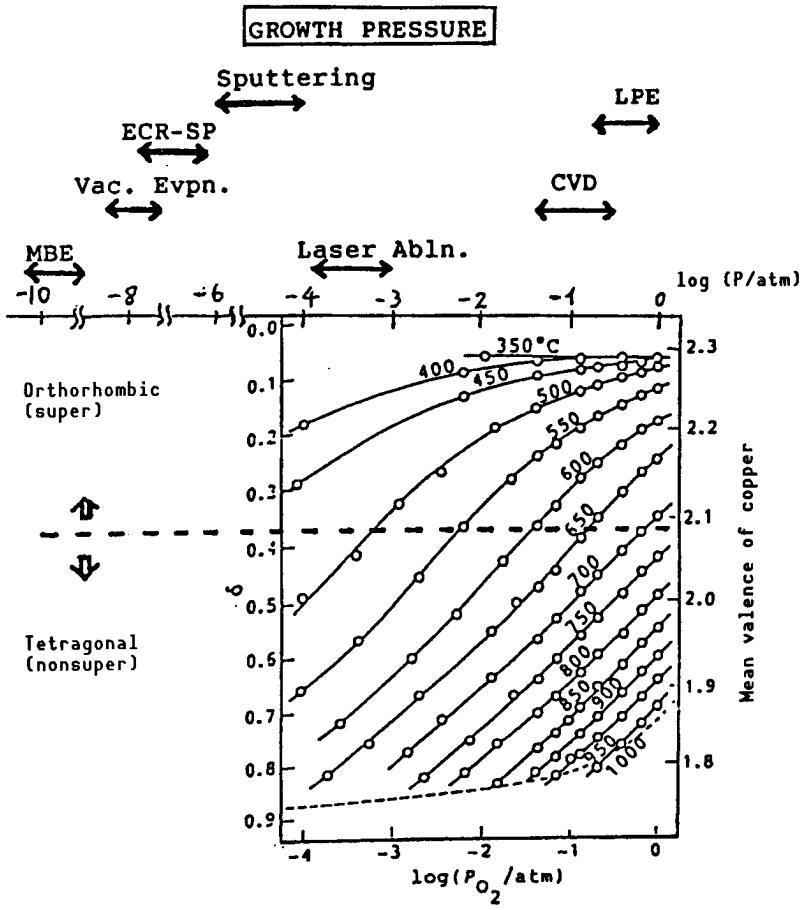

Figure 1. Relationship Between Oxygen Deficiency, Mean Copper Valence and Oxygen Pressure in $YBa_2Cu_3O_{7-\delta}$ Film Formation Process[1]

oxygen content adjustment can be secured simultaneously at the time of film formation.

Except for the electron carrier (n-type) Nd-Ce-Cu-O (NCCO) system, almost all of the high temperature superconductors discovered so far demonstrate the optimum characteristics of the equilibrium oxygen content at a relatively high oxygen partial pressure and low temperature (<500°C). Accordingly, methods of forming films under a low temperature and high oxygen partial pressure as possible within the range of formation of the crystal structures will be adopted as in situ (as-grown) thin film processes, advantageous for the construction of the devices. Figure 1 compares the pressure region at the time of reaction of the representative thin film formation methods with the equilibrium oxygen content of the $YBa_2Cu_3O_{7-\delta}$ (YBCO) system.[1] The CVD or laser ablation method under a relatively high pressure will be advantageous, in principle, for the in situ film formation. However, since a plasma exists in the sputtering method and, in the vacuum evaporation method, a dc or rf plasma is used concurrently in the activated evaporation, active oxygen, such as atomic oxygen, is generated within the reaction system, and there is a possibility of producing oxygen activity which exceeds the apparent pressure.

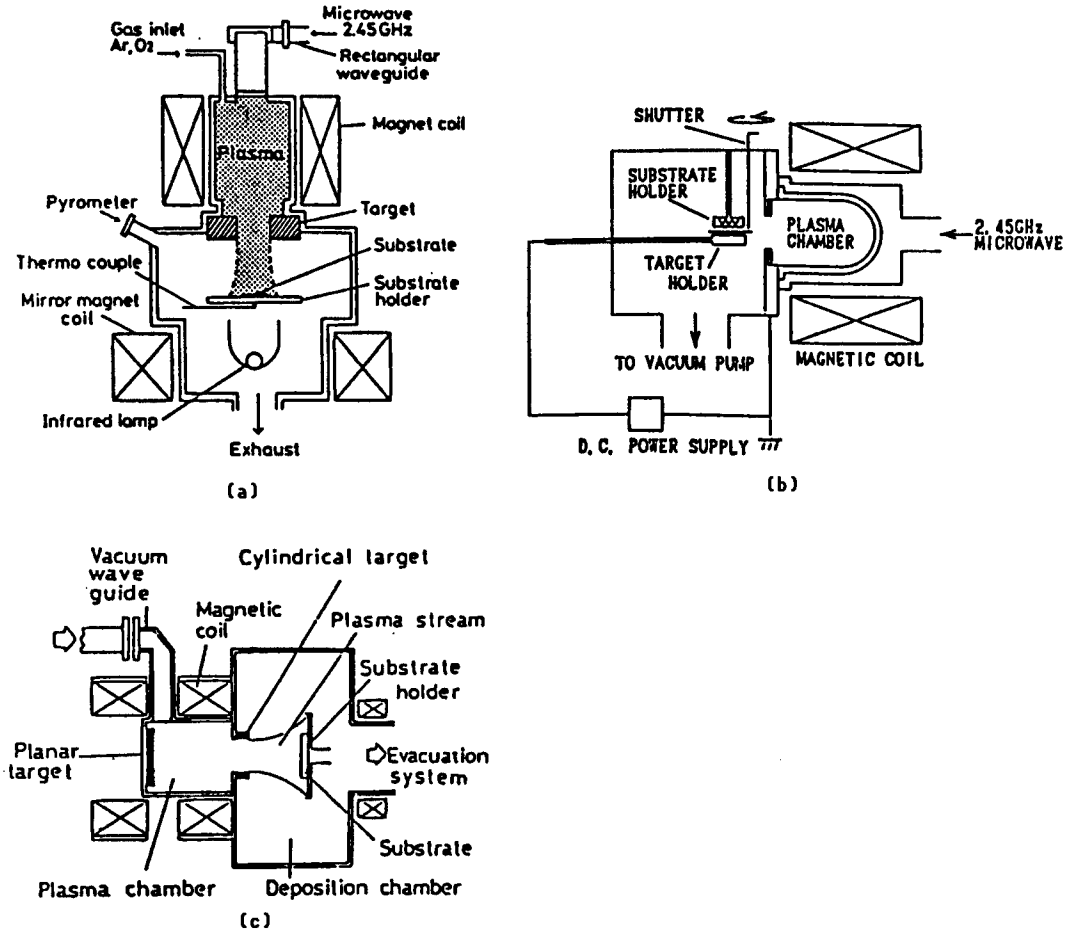

Figure 2. ECR Plasma Sputtering Systems[4]
(a) Tohoku University
(b) Osaka University
(c) NTT

3. Current Status of PVD as Seen From the Methods

Many reports and reviews have already been published regarding the (reactive) sputtering and the (activated) evaporation methods. Only those film making methods which are novel in methodology and those with a relatively small number of research examples will be discussed.

3.1 Methods Based on Sputtering

Since a method that uses two sheets of opposing targets does not place a substrate on an electrode, no direct irradiation damage arises due to plasma, and the manufacture of high quality films can be expected. The ac (50 Hz) sputtering which initially manufacture the LSCO, YBCO, and BSCCO system thin films is an example.[2] Copper rods are inserted from both faces into a quartz tube, and a superconducting pellet is fixed on the tips to be attached with a silver paste. Although it is a simple method involving the application of high

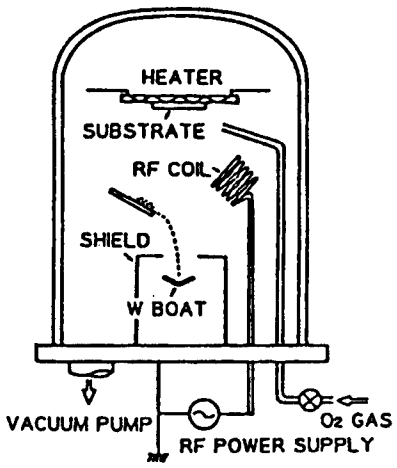

Figure 3. Flash Evaporation System[5]
(The rf coil generates an oxygen plasma.)

voltage under reduced pressure from a neon sign transformer to generate a plasma, it has advantages in that pellets can be made by the experimenter himself and that the application of light or a magnetic field from the outside is facilitated, etc. Further, it is possible to manufacture films that have different compositions for different positions of the substrate by changing the compositions of the target sheets. Xi, et al., (KFK) obtained films exhibiting superconductivity, even for extremely thin films of 20 Å, by the epitaxial growth of YBCO using an opposing target type rf magnetron sputtering system.[3]

An ECR sputtering method which uses an ECR plasma not only for the activation of oxygen, but also for the sputtering of the target, has been devised. Sketches of the systems used by Tohoku University, Osaka University, and Nippon Telegraph and Telephone (NTT) are shown in Figure 2.

3.2 Methods Based on Evaporation

Examples of these methods include the flash evaporation method (Figure 3),[5] ion cluster beam (ICB) method,[6] and molecular beam epitaxy (MBE). Laser ablation intrinsically belongs to this group, but it will be summarized in the next section. In ICB, vapor phase chemical species that are clustered (an aggregate of several dozen to several hundred atoms) at the time of evaporation from a crucible are irradiated with an electron beam to be ionized, and it is advertised that high quality films are obtainable by controlling the kinetic energy in the direction of the substrate with a bias.

It is reported that even at the low temperature of 60°C an X-ray diffraction pattern of phase 123 of YBCO is generated, as shown in Figure 4. Film formation by MBE has been reported by many research organizations, including Stanford University, the University of Tokyo, and Sanyo Electric Co. Most of them use the constituent metal as the evaporation source, with an added device to introduce the molecular oxygen or active oxygen to the vicinity of the

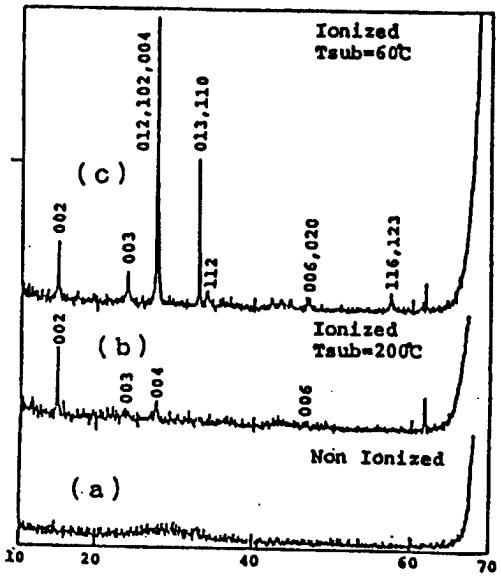

Figure 4. X-Ray Diffraction Pattern of YBCO Thin Film Obtained by ICB Method[6] {Substrate: Si(100)}
(a) Ionization not accelerated (substrate at 200°C)
(b) Ionization accelerated (1 kV) (substrate at 200°C)
(c) Ionization accelerated (1 kV) (substrate at 60°C)

substrate. In addition, there are many cases in which an "in the site" observation of the growth surface by reflected high-energy electron diffraction (RHEED) is carried out. Although a superhigh vacuum is not advantageous for the in situ growth of oxide films, it will be promoted increasingly in the future as an orthodox technique for use in the manufacture of multilayered films by layer-by-layer growth. In addition, a gas source MBE (metallo-organic molecular beam epitaxy (MOMBE)) is also being tested.[7]

3.3 Laser Ablation[8]

The process of irradiating a solid substance with laser beams to vaporize it and deposit a thin film was started by Smith, et al., in 1965, utilizing the ruby laser.[9] It is only recently that it has also become a method suited for the manufacture of dielectric ceramics and compound semiconductor thin films.[10] This method has the following characteristics, and research is being actively engaged in at various laboratories following the precursor groups at Bellcose, the State University of New York, Osaka University, etc., as a process suitable for use in the manufacture of multi system oxide films.

(1) It facilitates making a substance into a thin film, even if it has a high melting point, as long as it can absorb laser beams.

(2) Since the energy is brought in as laser beams, there is no need to install a resistor heater or a filament for electron beam emission in the case of electron beam evaporation, and the contamination can be minimized.

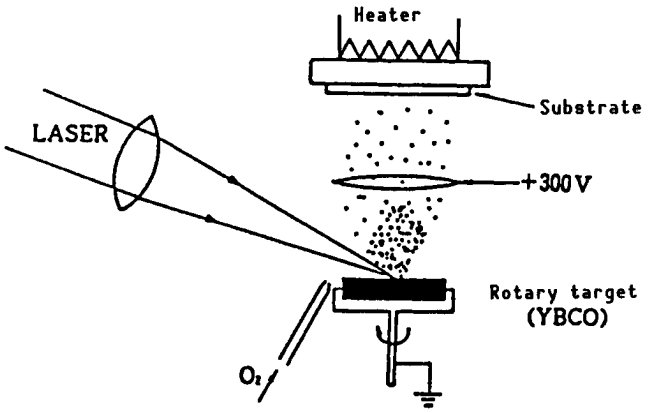

Figure 5. Laser Ablation Film Formation System Using dc Plasma

(3) The high vacuum needed for vacuum evaporation or sputtering is not required. Because of this, it is possible to increase the oxygen partial pressure within the reaction system, improving the oxygen content in the film.

(4) By the use of a short wavelength pulsed laser that has a high power peak, it is possible to instantaneously decompose and peel only the extreme surface layer part, so that the deviation of the composition of the constituents can be made to occur less frequently.

An example of the reaction system is shown in Figure 5. A plasma is induced by installing an rf coil or a dc bias electrode, and a high T_c as-grown film is obtained at a substrate temperature of less than 500°C.[11] However, a considerable distribution of the film thickness seems to exist, and there is a report that, with an increasing deviation of the composition, the deposition rate decreases as the direction deviates from the perpendicular direction to the target surface.[12] For the purposes of reaction control and a mechanism estimate, an analysis of the emission spectra of the plasma plume generated in the laser irradiation point and a measurement of the vapor phase mass spectra have been started. However, it will be necessary to accumulate more data before developing a systematic discussion.

The laser beams used include those from excimer lasers (193 and 248 nm, etc.), Nd-YAG lasers (335 nm, etc.), CO_2 layers (> 1 μm), etc. The results of previous records indicate that a short wavelength excimer laser is appropriate for the manufacture of high quality films. Recent topics of interest include the manufacture of low temperature as-grown superconductor films by splitting the laser beam and the irradiation of light on the growth plane[13] (Figure 6), and research aimed at improving the weakness of the laser method in which it is difficult to manufacture homogeneous and large area films by wide range beam scanning.[14] Laser ablation is a kind of etching process, and it should be applied and developed as part of the fine machining technology related to device fabrication.[8,15]

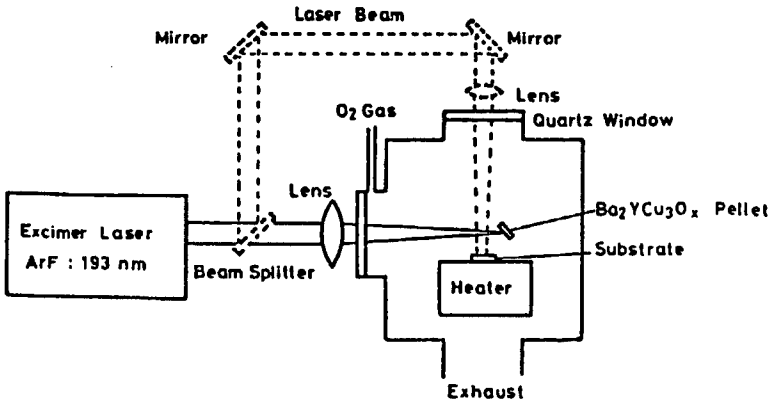

Figure 6. Sketch of a Laser Ablation System[13]
(The substrate can also be irradiated with a laser.)

4. Current Status of PVD From Materials Viewpoint

We will now summarize systems other than the YBCO and Tl-Ba-Ca-Cu-O systems.

4.1 Bi-Sr-Ca-Cu-O (BSCCO) System

Phase 2223 low temperature film formation that produces a high T_c (~110 K), as collected by Ogawa, is shown in Table 6[16] [not included in this text]. In addition, the manufacture of Pb-doped BSCCO films by ECR plasma sputtering has been reported. When T_{sub} = 570 and 590°C, $T_{c.zero}$ = 58 and 64 K, respectively, for as-grown films. In the past, the T_c of the Bi-Sr-Cu-O system ($Bi_2Sr_2CuO_x$; phase 2201) that did not include Ca had been said to be 20 K at the most. Recently, it has been discovered that a Bi-Sr-Cu-O film deposited on MgO at T_{sub} = 630~650°C by magnetron sputtering and annealed for 30 minutes at 750°C in oxygen has a $T_{c.onset}$ of about 80 K.[16] X-ray diffraction shows the presence of phase 2212, and it suggests that the structure in which oxygen-deficient Ca sites are replaced by Sr is fixed as a stable phase in the thin film process.

4.2 Nd-Ce-Cu-O (NCCO) System

The manufacture of thin films of this material has been reported by Hitachi Central Research Laboratory, Matsushita Central Research Laboratory, Chemistry Institute of Kyoto University, Bell Labs, Tokyo Institute of Technology, etc. A summary is shown in Table 7 [missing from text]. This film, which is an electron carrier (n-type) superconductor, is often rendered superconductive by annealing a film, forming the T' (Nd_2CuO_4)-type-crystal structure at high temperatures in a reducing atmosphere. It is said that in situ superconductive films are manufactured by the activated evaporation method. However, in this case, a process is involved in which Nd, Ce, or Cu metal is deposited while oxygen is blown to the vicinity of $SrTiO_3$ (100) substrate that is heated to 800°C, and the supply of oxygen is then halted and cooled under a reduced pressure of 10^{-6} Torr. The generation of a superconducting film under reducing conditions is advantageous for high vacuum processes such as MBE, and it is

also appropriate for in situ device fabrication by the formation of junctions with semiconductors or metals. The coherence length has been reported to be 7 Å in the c-axis direction and 96 Å in the a direction in the ab (CuO_2) plane, exhibiting the tendency to be somewhat larger than other hole conduction type oxide superconductors. The discovery of n-type superconductors with T_cs higher than the temperature of liquid nitrogen, corresponding to the YBCO, Bi or Tl systems, is being awaited.

The electron spectroscopic data, optical properties, magnetic characteristics, etc., are being actively investigated by a group at Matsushita Central Research Laboratory.[17] In addition, the balance of oxygen (nonstoichiometry) of the $(Nd_{1-x}, Ce_x)_2CuO_{4-\delta}$ system has been measured by the thermal capacity analysis of the bulk sintered body.[18] It is considerably smaller than that of the BSCCO system, not to speak of that of YBCO, and it is said that $\delta \sim 0.001$.

4.3 (Ba,M)BiO_3 System (M = K: BKBO or M = Rb)

Enomoto, et al., evaporated Ba, K, and Bi metal from the K cell in the presence of an ECR oxygen plasma ($\sim 10^{-2}$Pa), and deposited it as an as-grown superconducting film on MgO (100) and $SrTiO_3$ (100) substrates at 500°C.[19] In contrast to the fact that, with the bulk sintering process, it is difficult to obtain a solid solution perovskite phase for $Ba_{1-x}K_xBiO_3$ with $x > 0.4$, a solid solution with $0 < x < 0.8$ was possible in a film. Superconductivity is generated in the range of $x = 0.2 \sim 0.5$, and both the lattice constant and T_c (~30 K) were greatest in the vicinity of $x = 0.5$

The (Rb,Ba)BiO_3 film is grown epitaxially on $SrTiO_3$ (100) or (110) and MgO (100) substrates by MBE, in which oxygen atoms activated by rf plasma are introduced. Films with a $T_{c.onset}$ of ~27 K were obtained for $T_{sub} \leq 350$°C.[20]

5. Key Technologies for Film Fabrication

5.1 Oxygen Activation and Nonstoichiometry

Almost all of the high quality oxide thin films are manufactured by film formation processes involving reduced pressure, that is, under low oxygen partial pressure. If the substrate temperature is set at a high value, the equilibrium $M_n \rightleftharpoons M_{n-\delta}+O_2$ or $2p'+O_O^x \rightleftharpoons V_O'' + O_2$ shifts toward the right, generating an oxygen deficiency V_O'' and reducing the hole concentration. Most of the oxide superconductors, including YBCO, are of the hole carrier type, which means that the optimum hole concentration value to produce the maximum T_c cannot be secured under the film formation conditions. In addition to the method of elevating the effective oxygen partial pressure on the film surface by oxygen flashing in the vicinity of the substrate and by differential pumping, various means are being used to activate oxygen in a form other than the molecular (O_2) form and to introduce a sufficient quantity of oxygen into the film, even under high vacuum and high temperatures. Basically, the oxygen radical (atomic oxygen) and ions (O^+, O_2^+, etc.) are considered to be effective, and the following methods for generating these species are being tested.

(a) Oxygen Plasma

An oxygen plasma is generated by rf or microwaves, and is introduced into the reaction system (near the substrate). For example, Aida, et al., introduced an ECR oxygen plasma to the vicinity of the substrate while forming a YBCO film by vacuum evaporation.[21] They obtained an as-grown film with T_c = 83 K even for a substrate temperature of 450°C. With activated evaporation or laser ablation, there are many cases in which a dc or rf plasma is generated within the reaction system.

(b) Ozone

An as-grown YBCO film with high T_c (82 K) (at the substrate temperature of 700°C) is obtained by vaporizing liquefied (pure) ozone and supplying it to the vicinity of the substrate.[22] The introduction of pure ozone is also said to supply a sufficient quantity of oxygen during YBCO film formation by MBE at the high vacuum of 10^{-6} Torr. However, since liquefied ozone, as an ozone source, is highly explosive, sufficient care needs to be exercised.

(c) Oxygen Ion Beam and Reaction System Bias Effect

Since an ECR oxygen plasma can become a source for generating oxygen ions, it may be used to irradiate a substrate by applying an appropriate acceleration voltage. It is reported that the application of a positive bias during film formation by the cluster ion beam method or the application of a positive bias to an Si substrate having a ZrO_2 buffer layer by the rf magnetron sputtering method[23] is effective for manufacturing as-grown YBCO film.

(d) Solid Oxygen Source

It is already known that it is possible to manufacture oxide films, such as Al_2O_3, SiO_2, MgO, and Al_2MgO_4, by evaporating Sb_2O_3 and by oxidizing metallic vapors on the substrate surface.[24] The Sb component is evaporated and removed in the atomic form or as SbO. The application of such a solid source of oxygen is expected to be used for film formation in high vacuum, such as gas source MBE.

(e) O_2 (+ N_2O)/UV

It is believed that oxygen decomposes and generates atomic oxygen when it is irradiated with a low pressure mercury lamp or with an excimer laser which generates ultraviolet rays with wavelengths of less than 190 nm. It is known that N_2O can be decomposed with an even longer wavelength. When the O_2/UV treatment is given to a Bi-Sr-Ca-Cu-O (2122) film, clearly a reduction of T_c and an increase of the hole concentration, indicating an increase of the oxygen content, is observed.[25] On the other hand, the N_2O/UV treatment does not seem to be directly connected to the increase of oxygen content, although it is effective for reducing the crystallization temperature during film formation. Is the difference in reactivity due to the difference in the excited states of oxygen?

(f) NO_2

It has been reported that a Bi-Sr-Cu-O (2201) film was grown by the MBE method and employing NO_2 at the low temperature of 300°C, producing a high vacuum of the order of 10^{-7} Torr.[26] Activation by decomposition, such as $NO_2 \rightarrow NO+O$, is conceivable, but it may also be necessary to consider the involvement of surface reactions.

5.2 Ultrathin Film

The manufacture of thin films that exhibit superconductivity for a thickness of less than 100 Å has been reported on the YBCO film by Venkatesan, et al., (Bellcore),[27] Terajima, et al., (Chemistry Institute, Kyoto University),[28] Xi, et al., (KRK),[3] Triscone, et al., (University of Geneve),[29] , etc. The methods employed include laser evaporation, hollow cathode type magnetron sputtering, activated evaporation, and dc magnetron sputtering, respectively.

Terajima, et al., concluded from X-ray diffraction pattern analysis that a 100 Å-thick YBCO film deposited on an $SrTiO_3$ (100) substrate is not an orthorhombic system. From the fact that this film shows a $T_{c.zero}$ of 80 K, they determined that the lattice distortion of the orthorhombic system is not an indispensable requirement for the YBCO system. Xi, et al., fabricated a film exhibiting zero resistance, even for a film thickness of 20 Å, on an $SrTiO_3$ (100) substrate at a temperature of 800°C, and annealed it for one hour in oxygen at 950-1,000°C. By analyzing the electric conductivity near T_c, they estimated a three-dimensional conductivity mechanism, even for ultrathin films. The value of J_c was 3.5 x $10^5 A/cm^2$ (at 4.2 K) for a film 50 Å thick. On MgO film with large lattice mismatch, a thickness of 60 Å is required for superconductivity manifestation.

5.3 Surface Reaction Process

The formation of a high temperature superconducting film or a heterojunction is a process which attempts to deposit a film with high crystallinity on a foreign matter, termed a substrate, or by an underlying layer. The in situ observation and control of the grown surface are desired. Although this technology has aspects common to semiconductor superlattices and can be used for reference, it may be said that it is more complex and difficult because many components are involved, as is the control of quantities of volatile oxygen. Studies on reaction tracking by means of RHEED, transmission electron microscope (TEM) observation of the cross sections, changes in the resistivity accompanying the growth of the film, analysis of the surface atomic states by X-ray photoelectron photoscopy (XPS) and IR spectra, etc., have been conducted.

In Figure 7, the dependence of the lattice spacing on the film thickness, as determined by the RHEED pattern during the growth process of a YBCO film, is shown as obtained by Bando, et al. (Chemistry Institute, Kyoto University).[30] The distortion starts to disappear from the neighborhood of the c-axis length (12 Å) of YBCO, and makes the transition to a two-layer lattice which nearly corresponds to the bulk YBCO. Kobayashi, et al. (Faculty of Engineering, Osaka

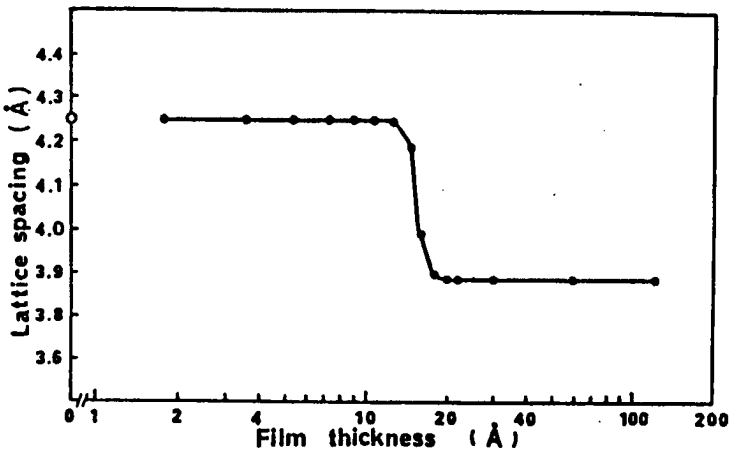

Figure 7. Relation Between Film Thickness and Lattice Spacing of a YBCO Thin Film on an MgO Substrate[30]

University), used RHEED and TEM to analyze the MgO film deposition process on a YBCO film by sputtering.[31] They observed that the orientability of the film changes delicately with the temperature of the underlying layer. They report that in an attempt to form a double heteroepitaxy of YBCO/MgO/YBCO, an island-like growth occurs when the thickness of the MgO film is made as thin as 20 Å, and it was not possible to form a satisfactory SIS tunneling junction. On the other hand, from the TEM image, the SNS junction of YBCO/PrBCO/YBCO, which has a basically identical crystal structure, was found to be forming a homogeneous interface.[32]

Research to analyze the surface reaction on the monomolecular layer level is drawing attraction as the basic process to be used in the construction of new ceramic superstructures by atomic layer epitaxy. Kawai, et al. (Tokyo Institute of Technology) analyzed the monomolecular MBE evaporation of Bi metal on silicon and the oxidation behavior by oxygen by means of XPS,[33] and the CVD reaction process of $Cu(DPM)_2$ on silicon, the surface of which is covered with hydroxide by means of IR spectroscopy.[34]

One confirmation of ideal epitaxy in which growth of from one to several atomic layer units is repeated on a clean surface will be through the observation of RHEED vibrations. A few results suggesting these RHEED vibrations, which have been regarded as being difficult to observe during the growth of ceramic layers, are now appearing. Schlom, et al., of Stanford University successfully grew a $Bi_2Sr_2Ca_{n-1}Cu_nO_x$ ($n = 1\sim5$) film by MBE by using Bi, Sr, Ca, and Cu as the source under an ozone atmosphere of the order of 10^{-4} Torr.[35] They observed changes in the RHEED intensity accompanying shuttering corresponding to each atomic layer. Bando, et al., at the Chemistry Institute, Kyoto University, detected the RHEED vibrations during the growth processes of YBCO and related oxides by the activated evaporation method.[36] They also found that its frequency period corresponds to the growth of a minimum structural unit that holds charge neutrality. Recently, Koinuma, et al. (Tokyo Institute of Technology) observed RHEED intensity vibrations corresponding to a two-dimensional

layered structure during the manufacture of an epitaxial CEO_2 thin film on an Si substrate by superhigh vacuum laser ablation.[37]

5.4 Structure and Stability of Interface

The interfaces of the heterojunctions and tunnel junctions, the growth surface of atomic layer epitaxy, etc., as the junctions of different kinds of materials, may be said to represent a thermodynamically unstable phase. A quantitative evaluation of the reactivity or stability of the interfaces should be a powerful piece of information for setting the manufacturing conditions for the junction devices and laminated films.

Nakajima, et al. (Research Institute for Metals, Tohoku University), measured the Rutherford backward scattering (RBS) spectra before and after heat treating sputter-deposited YBCO films on various kinds of substrates (MgO, sapphire, quartz, and Si).[38] The depth from the interfaces before and after the heat treatment and the concentration C(x,t) of each constituent are found, and are then substituted into a diffusion equation for a pair of semi-infinite solid bodies, modified as in the following: $\text{erfc}^{-1}(2C/Co) = x/[2(Dt)^{1-X}]$. In this equation, C is the concentration at depth x when heat treatment under predetermined conditions is executed for length of time t, $C_0 = C\ (o,0)$ and D is the diffusion coefficient. By plotting the left side computed for the experimental values of C and Co against the depth x, D can be determined from the slope of the plot obtained. By using Arrhenius plotting to plot the D values, obtained for various heat treatment temperatures T against 1/5, the frequency factor D_0 and activation energy Q for the diffusion can be determined: $D = D_0\ (-Q/RT)$. Of the metallic constituents in YBCO, Cu was most easily diffusible, while MgO was most stable as the substrate.

Bakunin, et al. (Ura University, Academy of Sciences, Soviet Union), obtained an effective diffusion coefficient in a way similar to the above by using Auger electron spectroscopy (AES) to analyze the depth of the YBCO film sputter-deposited on $SrTiO_3$ and YSZ substrates.[39]

6. Layer-by-Layer Deposition and New Materials

The manufacturing technology of high temperature superconductive thin films has reached the level at which high crystallinity and T_c for as-grown superthin films of less than 100 Å can be obtained. However, in the formation of films on ceramics whose lattice constants deviate significantly or on semiconductors, such as Si and GaAs, a general technology for obtaining satisfactory heteroepitaxy has not yet been established. Considering the short coherence length, and severe requirements for the flatness and homogeneity of the surfaces and interfaces, the eventual development of thin film technology that will supersede semiconductor superlattices (oxygen control under high vacuum, etc.) is demanded. Here, an example of an approach to the search for new superconductors by manufacturing new superlattices through laminating the atomic layers within the layered perovskite lattice by artificially controlling the atomic layers is presented.

The laminated films have been obtained by controlling the lattice number (film thickness), i.e., by keeping the lattices of the known superconductors as they are. High temperature superconductors represent one kind of ceramic superlattice in that the layered structures with long cycles manifest a macroscopic quantum effect called superconductivity. In particular, in the Bi and Tl system superconductors, the tendency for T_c to become elevated with an increase in the number n of sheets of CuO_2 layers from 1~2 has been observed. If crystals having a higher order of layers can be manufactured by utilizing the artificial superlattice manufacturing technology, it can be expected that superconductors with higher T_c or room temperature superconductors will be realized.

In the formation of ceramic thin films utilized for insulators, dielectrics, transparent conductive films, etc., for semiconductor devices, use is made of vapor growth methods, such as vacuum evaporation including MBE, sputtering, CVD, etc. In manufacturing superlattices, it is customary to prepare multiple evaporation sources and targets for sputtering, and to deposit films sequentially. The current status of various methods of the atomic layer film formation of superconducting ceramic laminated thin films is summarized in Table 5 [missing from text]. Adachi, et al., carried out film formation according to a reactive sputtering method that uses four-component metallic targets of Bi, SrCu, CaCu, and SrCu by varying the amount of evaporation of the Ca-Cu-O layer in the Bi-Sr-Ca-Cu-O system, and by controlling the atomic layer of the various superconducting thin films, with CuO_2 layers of n = 2, 3, and 4.[40] The film with n = 4 was not obtained as a single phase in bulk, so its T_c was not clearly found. When the CuO_2 layers in a laminated film were increased to four sheets, the X-ray diffraction pattern showed a nearly single phase $Bi_2Sr_2Ca_3Cu_4O_x$ structure, but, not only did its T_c not rise, instead it was found that it dropped to 90 K. Although it is regrettable that the T_c did not increase, this attempt showed that ceramic lamination technology has the potential for bringing about important knowledge in the study of properties of matter as well, including the superconductivity mechanism.

Subsequently, various attempts to form layer structures with artificially designed atomic layer configuration within one lattice have been reported in succession, centering around the Bi system, by means of such methods as beam sputtering, laser ablation, plasma controlled sputtering, multicomponent activated evaporation, and MBE. Recently, research has been reported in which RHEED is employed for surface observation to detect the vibration patterns of the growth within a superhigh vacuum chamber, which is analogous to the growth process of semiconductor superlattices. It is no longer merely a dream that technologies will be realized that will manufacture new materials by epitaxially growing one to several atomic layers of a ceramic that will contain oxygen, which is unstable and difficult to control. The following is a brief presentation of the research on the epitaxial growth of the Bi system by MBE carried out by Schlom, et al. (Stanford University).

Schlom's group pursued the development of a technology which would epitaxially grow in situ by controlling atomic layers of the oxide layers of Bi, Sr, Ca, and Cu by employing a multicomponent MBE system, as shown in Figure 8.[35] First, the effect of pure ozone as a source of active oxygens was studied, showing

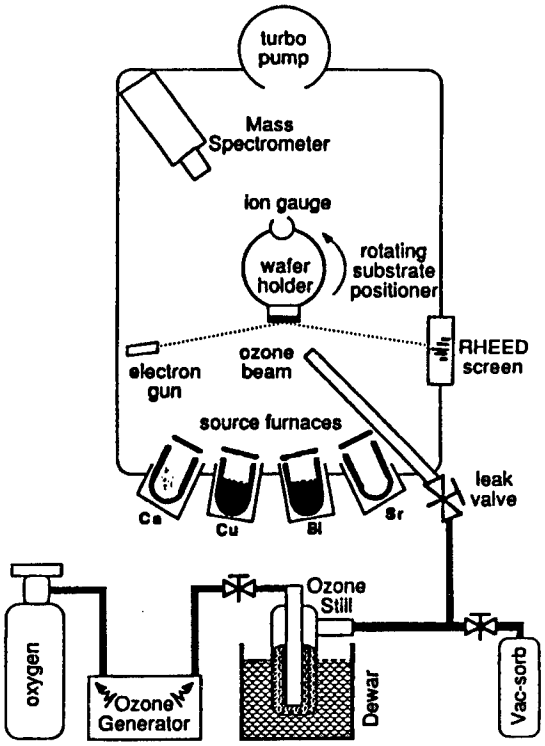

Figure 8. Layer-by-Layer Deposition System of $Bi_2Sr_2Ca_{n-1}Cu_nO_x$ Thin Film by MBE

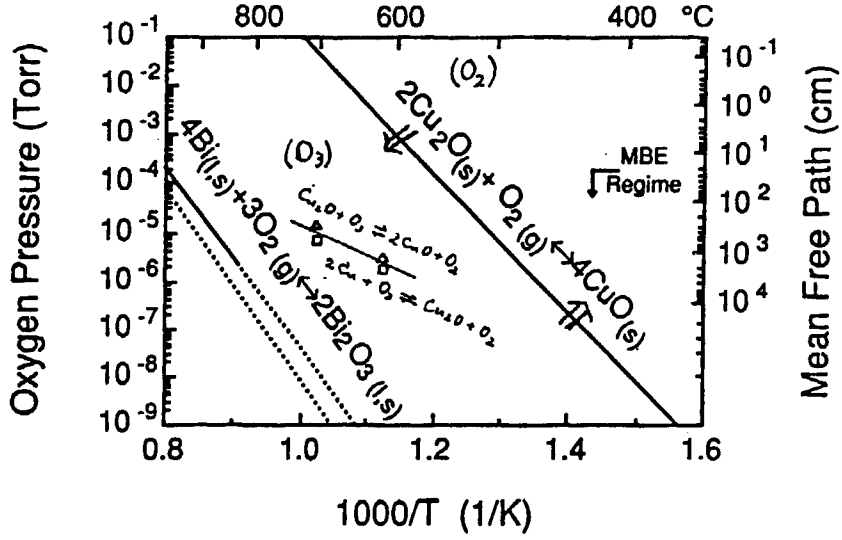

Figure 9. Equations for Equilibrium States Related to Oxidation Reactions of Cu and Bi Compounds

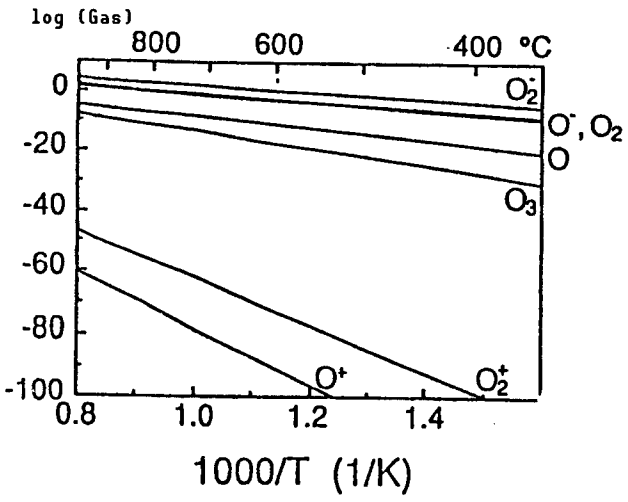

Figure 10. State Equation for Oxidation Equilibrium of Cu by Various Active Oxygen Gases[35]

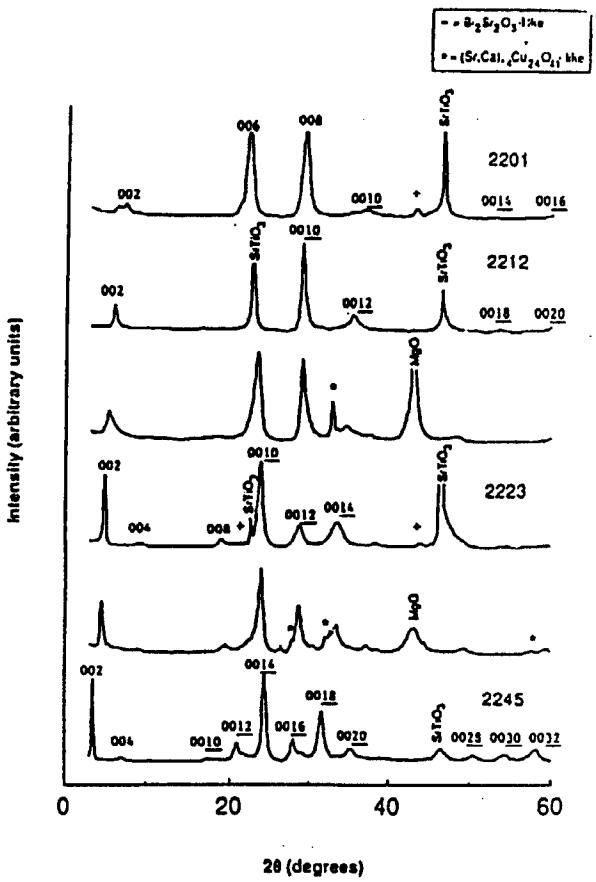

Figure 11. X-Ray Diffraction Patterns of (n = 1,2,3, and 5) Films of $Bi_2Sr_2Ca_{n-1}Cu_nO_x$ Thin Films Manufactured by the Layer-by-Layer MBE Method[35]

that even in the MBE region ($P < 2 \times 10^{-4}$ Torr and mean free path < 20 cm) evaporated metals (especially Cu) could be fully oxidized. As shown in Figure 9, ozone is capable of producing CuO at temperatures above 600°C and under pressures below 10^{-6} Torr. The safety was reportedly improved by devising materials for pipings, adsorption to silica gel, etc.

In Figure 10, the calculated values for the equilibrium state diagrams of $Cu_2O + O_2 \rightleftharpoons CuO$ for various kinds of active oxygen are given. It is shown that ozone's oxidizing force is superior to that of atomic oxygen. By making reference to Fujita, et al.'s[39] results of RHEED observation with respect to the manufacture of Bi system multilayered films by ion beam sputtering, first one atomic layer of SrO was deposited on a substrate and, by repeating the deposition O_2 of each layer of CuO, CaO, and BiO_x, in this order, using a computer to control the thickness, they manufactured $Bi_2Sr_2Ca_{n-1}Cu_nO_x$ (n = 1,2,3, and 5). The as-grown films, at substrate temperatures of 550~600°C, showed nearly single phase design structures, as shown in Figure 11. In addition, the oscillation of reflection intensity accompanying the shuttering

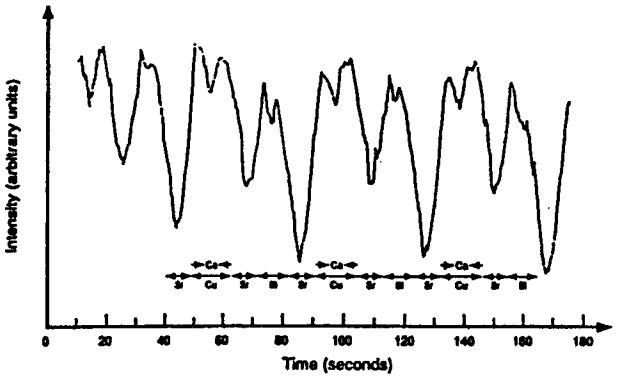

Figure 12. Changes With Time of Reflection Intensity as Seen in in situ RHEED Observation of the Layer-by-Layer Grown Surface of $Bi_2Sr_2Ca_{n-1}Cu_nO_x$ Thin Film by MBE

was observed by RHEED observation of the growth surface, as shown in Figure 12. Further, Koinuma, et al. (Tokyo Institute of Technology), examined the reactions on the substrate surface and crystallization by in situ RHEED in situ XPS measurements in conjunction with the epitaxial growth of ceramic thin films by laser ablation within an ultrahigh vacuum ($\leq 10^{-7}$ Torr) chamber.[42] It is expected that the accumulation of data related to the surface processes will be useful in designing ceramic superstructures.

References

1. Fueki, "Chemistry of Oxide Superconductors," edited by Fueki and Kitazawa, Kodansha, 1988, p 1.

2. Koinuma, H., et al., JOURNAL OF APPLIED PHYSICS, Vol 62, 1987, p 1524; JAPANESE JOURNAL OF APPLIED PHYSICS, Vol 26, 1987, p L738; Ibid., Vol 27, 1988, p 376.

3. Xi, X.X., et al., APPLIED PHYSICS LETTERS, Vol 54, 1989, p 2367.

4. Masumoto, H., et al., Ibid., Vol 55, 1989, p 498; Nishimori, Y., et al., JAPANESE JOURNAL OF APPLIED PHYSICS, Vol 28, 1989, p L1220; Matsuura, T., et al., MOL. CRYST. LIG. CRYST., in press; Yasuda, Y., et al., APPLIED PHYSICS LETTERS, Vol 55, 1989, p 307.

5. Yasuda, Y., et al., APPLIED PHYSICS LETTERS, Vol 55, 1989, p 307.

6. Kanedo, NSMF NEWS, No 17, 1989, p 1.

7. Endo, K., et al., Proc. ISS '89, in press.

8. Koinuma and Takeuchi, JOYSTICK, Nov 89, p 52.

9. Smith, H.M., et al., APPL. OPT., Vol 4, 1965, p 147.

10. Cheng, J.T., et al., CRC CRITICAL REV. IN STATE AND MAT. SCI., Vol 15 No 1, 1988, p 63.

11. Witanachchi, S., et al., APPLIED PHYSICS LETTERS, Vol 53, 1988, p 234.

12. Venkatesan, T., et al., Ibid., Vol 52, 1988, p 1193.

13. Otsubo, S., et al., JAPANESE JOURNAL OF APPLIED PHYSICS, Vol 28, 1989, p 2211.

14. Greer, J.A., et al., MRS '89 Fall Meeting, M7, 1989, p 189.

15. Koinuma, SOLID-STATE PHYSICS, Vol 23, 1988, p 125.

16. Adachi, H., et al., to be published in JAPANESE JOURNAL OF APPLIED PHYSICS, Vol 29 No 1, 1990.

17. Hiroshi, K., et al., PHYSICA C, Vol 160, 1989, p 273; S. Hatta, et al., JAPANESE JOURNAL OF APPLIED PHYSICS, Vol 28.

18. Fueki, Report on Results of Grant for Special Region of Science "Chemistry of New Superconductors," 1989.

19. Enomoto, Y., et al., JAPANESE JOURNAL OF APPLIED PHYSICS, Vol 28, 1989, p L1335.

20. Hellman, E.S., et al., MRS '89 Fall, M5-2, 1989.

21. Aida, T., et al., JAPANESE JOURNAL OF APPLIED PHYSICS, Vol 28, 1989, p L635.

22. Berklay, D.D., et al., APPLIED PHYSICS LETTERS, Vol 53, 1988, p 1973.

23. Myoren, H., et al., JAPANESE JOURNAL OF APPLIED PHYSICS, Vol 28, 1989, p 351.

24. Stall, R.A., J. VAC. SOC. TECH., Vol B1, 1983, p 135.

25. Takeuchi, K., et al., JAPANESE JOURNAL OF APPLIED PHYSICS, Vol 29 No 1, 1990, p L70.

26. Watanabe, S., et al., Ibid., to be submitted.

27. Venkatesan, T., et al., APPLIED PHYSICS LETTERS, Vol 54, 1989, p 581.

28. Terashima, T., et al., Proc. 2nd Int'l. Symp. on Superconductivity (ISS'89), in press.

29. Triscone, J.M., et al., PHYS. REV. LETT., Vol 64, 1990, p 804.

30. Terashima, T., et al., JAPANESE JOURNAL OF APPLIED PHYSICS, Vol 28, 1989, p L987.

31. Sakuta, K., et al., Proc. ISS'89, in press.

32. Schbert, J., et al., Proc. HTC-USTRON'89, Poland, in press, 1989.

33. Hanada, T., et al., to be published in VACUUM.

34. Sekine, R., et al., to be published in APPLIED PHYSICS LETTERS.

35. Schlom, D.G., et al., J. CRYST. GROWTH, in press.

36. Terajima, '90 Spring Meeting, Japan Chemical Society, invited lecture.

37. Koinuma, H., et al., to be submitted.

38. Nakajima, H., et al., APPLIED PHYSICS LETTERS, Vol 53, 1989, p 1437.

39. Bakunin, O.M., et al., Ibid., Vol 55, 1989, p 78.

40. Adachi, H., et al., JAPANESE JOURNAL OF APPLIED PHYSICS, Vol 27, 1988, p L1883.

41. Fujita, J., et al., JOURNAL APPLIED PHYSICS LETTERS, Vol 64, 1988, p 1292.

42. Yoshimoto, M., et al., JAPANESE JOURNAL OF APPLIED PHYSICS, in press.

Current Status of, Outlook for CVD

916C1001F Tokyo HYOMEN KAGAKU SEMINA in Japanese 27-29 Jun 90 pp 69-82

[Article by Ken Ihara, Atsugi Research Laboratory, Fujitsu Ltd.]

[Text] **1. Introduction**

The chemical vapor deposition (CVD) process can readily control crystal compositions by controlling the concentration of a reaction gas placed in the growth atmosphere. This process also eliminates the necessity for annealing after film formation. The use of single crystal substrates, may be able to produce single crystal films of good quality. The CVD process can also be applied to uniform and large areas, and is suitable for the mass production of films. The CVD process can be classified into:

- The halide CVD process which uses halogen compounds (frequently used for semiconductor preparation) as source materials and;

- The metallo-organic chemical vapor deposition (MOCVD) process which uses organic metals (research on which is being promoted in the compound semiconductor field) as source materials.

The purity of halogenated metals can easily be improved. Halogenated metals can be obtained at low prices, easily handled, and maintained in a comparatively stable state up to high temperatures. The halide CVD process, therefore, makes it possible to precisely control crystal compositions, thereby making it easy to obtain highly pure thin film crystals. The halogenated metals currently available are solids at room temperature and atmospheric pressure, and their steam pressure is low. Therefore, to generate gases of the necessary concentration in the growth atmosphere, source materials must be maintained at higher temperatures. This, however, results in higher growth temperatures.

The MOCVD process uses organic compounds with complicated structures as source materials, thereby making it difficult to improve the purity of source materials, and thus problems are involved when improving the purity of the thin films formed. Organic substances are also used to form oxides. These cause films to be susceptible to contamination by carbon.

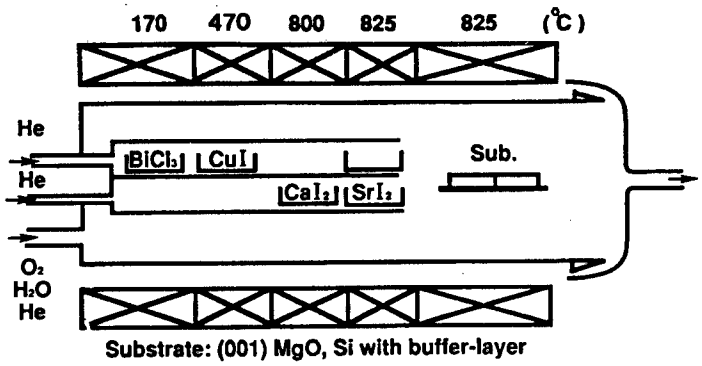

Figure 1. Atmospheric Halide CVD Equipment for Growing High-Temperature Bismuth Superconductor Crystals

However, since organic metals that can be easily decomposed at low temperatures are used as source materials, crystals are likely to grow at low temperatures. Thus, the MOCVD process is very attractive to those engaged in the development of new materials.

Meanwhile, as is well known, substrate crystals of good quality are necessary if high quality superconductive thin film crystals are to be obtained. Oxide crystals such as $SrTiO_3$,MgO, and ZrO_2 (YSZ) are currently being used as substrate crystals. The development of substrate crystals (e.g., Si and heteroepitaxially structured substrate crystals using Si) for application to electronic devices has been initiated. In this paper, the author describes the current status of and outlook for the CVD process (with emphasis laid on the halide CVD process) with respect to crystal growth technology and crystal properties, and the technology for the heterojunction of raw materials and substrate crystals with semiconductors.

2. Thin Film Crystal Growth Technology

2.1 Atmospheric Halide CVD Process

Bismuth-based superconductive crystals[1] possess the high critical temperature of 110 K and are comparatively stable structure crystals. Their atoms may be replaced by using a layered structure. Thus, they represent an attractive kind of crystal. The author's group started developing the bismuth-based superconductive crystal thin film vapor phase growth process quite a long time ago, and have successfully developed an atmospheric halide CVD process [2-7] that uses metal halogen compounds and oxygen gas as raw materials.

Figure 1 shows a schematic drawing of the atmospheric halide CVD equipment used to grow high-temperature bismuth superconductor thin film crystals. This crystal growing equipment is composed of a quartz reaction tube, quartz source chamber, horizontal five-zone resistance furnace, and gas flow rate control unit.

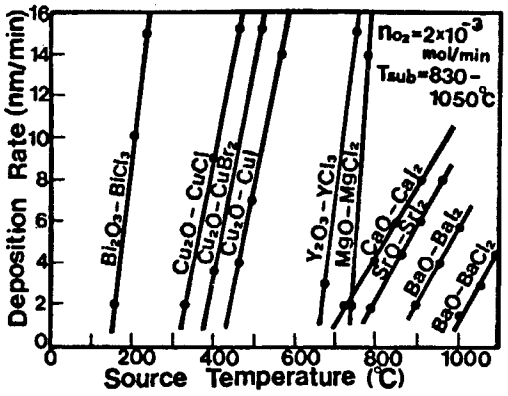

Figure 2. Relationship Between Film Deposition Rate of Metal Oxides Comprising the Chemical Composition of Oxide Superconductive Crystals and Various Halide Source Temperatures

$BiCl_3$, CuI, CaI_2, and SrI_2 were used as halide source materials and were heated in the source chamber to control the respective team pressures. The source temperatures were individually controlled as follows:

- $BiCl_3$ = 150~170°C
- CuI = 450~470°C
- CaI_2 = 780~830°C
- SrI_2 = 800~850°C

Oxygen gas was used as the oxidizing agent and its flow rate was controlled to 0.5~5 ℓ/min using a mass flow meter. H_2O steam (which can be obtained by bubbling He gas in H_2O) was used as the oxidation accelerating agent. The H_2O concentration was controlled to several hundred ppm with respect to the total amount of He carrier gas flowing into the reaction tube. He gas was used as the carrier gas and was introduced into the source chamber and reaction tube, respectively, at a rate of 10~20 ℓ/min. The surface of a (100) MgO single crystal substrate (30 x 30 mm^2) prepared by the annealing process was treated using an HCl(90) and H_2O_2(10) mixed liquid, and the surface treated MgO single crystal substrate was then heated to 800~850°C in the reaction tube.

The structure's reaction tube system prevents the inflow of oxygen gas into the source chamber. Therefore, halide sources and their gaseous substances are placed in a nonreacted state. Halide source gases transported to the deposition region, oxygen gas, and H_2O gas are intermixed, thus initiating deposition reactions. As a result, the concentration of reacted gases in the deposition region, that is, the composition of depositing crystals, can be controlled precisely.

Figure 2 shows the relationship between the film deposition rate of simple substance metal oxides that comprise the chemical composition of high-temperature oxide superconductive crystals and the available halide source temperatures.

The halide source temperatures required to obtain the practical deposition rates (more than several nm/min) necessary for bismuth-based superconductive crystal deposition are as follows:

- $BiCl_3$ = 150~220°C
- CuI = 450~550°C
- $CuBr_2$ = 380~500°C
- CuCl = 330~450°C
- CaI_2 = 750~900°C
- SrI_2 = 800~950°C

On the other hand, growing yttrium-based superconductive crystals requires quite high source temperatures, as shown below:

- YCl_3 = 680~750°C
- BaI_2 = 900~1,000°C
- $BaCl_2$ = 1,000~1,100°C

The deposition temperature also becomes 950°C or higher. These conditions, however, cause solid-phase reactions to substrate crystals to take place intensely, thereby making it difficult to obtain good-quality superconductive crystals. For thallium-based crystal depositions, a Ba halide source is used. When the Tl oxide steam pressure is high and the crystal deposition temperature is also high, difficulties in controlling the composition of the Tl element arise. For this reason, coupled with the detrimental property of the Tl element, in many cases the Ba halide source is not appropriate for use in the CVD process.

Figure 3 [not reproduced] shows an optical surface photograph (a) and a scanning electron microscope (SEM) photograph (B) of typical bismuth-based as-grown crystals which were vapor phase grown on a (100) MgO crystal substrate.

Abnormally grown convex portions (hillocks) that frequently appear on the epitaxially grown crystal surface of semiconductors, were present on the deposited crystal surface. However, comparatively smooth crystals with a film thickness of about 0.1 μm and a degree of irregularity of about 10~30 nm were obtained. With respect to the epitaxy relationship with the substrate crystal, observations using transmission electron microscope (TEM) and a polarization microscope confirmed that large crystals with a growth domain size of 100 μm to 1 mm were nearly fit and deposited in the (100) and (110) directions. In order to develop electronic devices, it is necessary to reduce the hillock density, improve fine irregularities (irregularity on semiconductor crystal surface: less than several nm) on crystal surfaces, and develop a complete epitaxial technology. The crystal deposition conditions are as follows:

- Deposition temperature = 775°C
- $BiCl_3$ = 165°C
- CuI = 460°C
- CaI_2 = 825°C
- SrI_2 = 850°C
- Oxygen gas concentration vs. He carrier gas = 11 percent
- H_2O concentration = 300 ppm
- Deposition rate = about 1 nm/min.

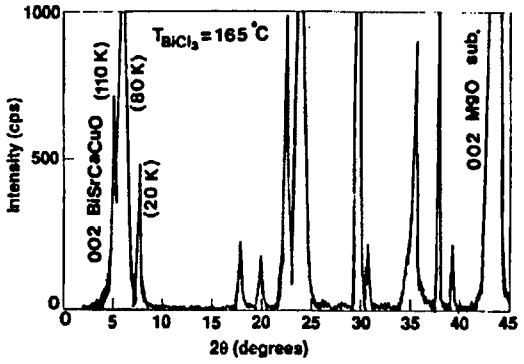

Figure 4. X-Ray Diffraction Pattern on Bismuth-Based Crystals Obtained at a $BiCl_3$ Source Temperature of 165°C

Figure 4 shows the results of X-ray diffraction measurement of as-grown crystals deposited at a deposition temperature of 775°C and a $BiCl_3$ source temperature of 165°C, respectively.

The figure shows that the diffraction pattern of the crystal phase referred to as the "80 K phase" is apparently strong. In addition, weak diffraction patterns of the "110 K" and "20 K" crystal phases can be observed. The figure shows that these types of crystal phases are intermixed.

Figure 5 [not reproduced] shows a TEM photograph of the section of crystals deposited at 850°C, taken by a high resolution transmission electron microscope (acceleration voltage: 200 kV). The same diffraction patterns can be observed in these crystals. In other words, the photograph showed that crystal phases such as the 80 K phase (inscription 2), 110 K phase (inscription 3), and 20 K phase (inscription 4) have grown in layered structures. In particular, the interface between bismuth-based crystals and MgO substrate crystals is sharp. No deteriorated layers or precipitates arising from the reactions of these two types of crystals can be observed, and a satisfactory heterointerface has been formed. It is expected that the deposition of ultra thin films of high quality and a superconductor/insulator/ superconductor heterojunction with MgO crystals can be achieved.

Figure 6 shows the results of X-ray measurement of as-grown crystals deposited at a $BiCl_3$ source temperature of 160°C. Compared with the crystals shown in Figure 4, the diffraction strength of the 110 K phase is visibly high, while the diffraction strength of the 80 K and 20 K phases has become quite weak.

Figure 7 shows the temperature dependence of the electrical resistance of these two types of grown crystals. Curve A shows crystals (specimen) deposited at a $BiCl_3$ source temperature of 165°C. A change in resistance can be observed around 110 K. The tail, however, is large, and the critical temperature is 81 K. Curve B shows crystals (specimen) deposited at a $BiCl_3$ source temperature of 160°C and shows a sharp temperature change; its critical temperature is 95 K.

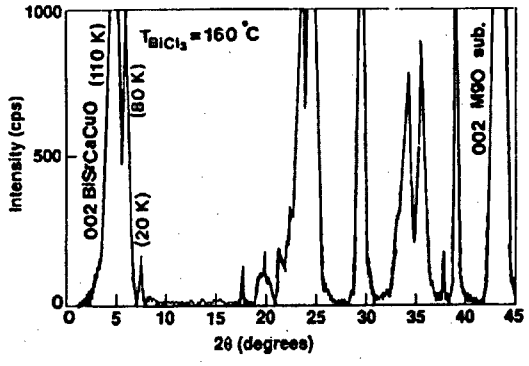

Figure 6. X-Ray Diffraction Pattern of Bismuth-Based Crystals Obtained at a $BiCl_3$ Source Temperature of 160°C

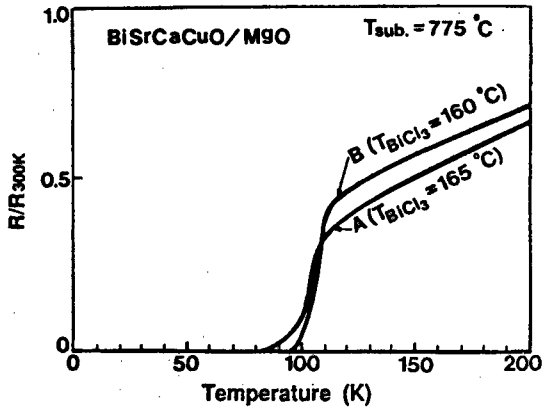

Figure 7. Temperature Dependence of Bismuth-Based Crystal Electric Resistance
A ($BiCl_3$ temperature = 165°C)
B ($BiCl_3$ temperature = 160°C)

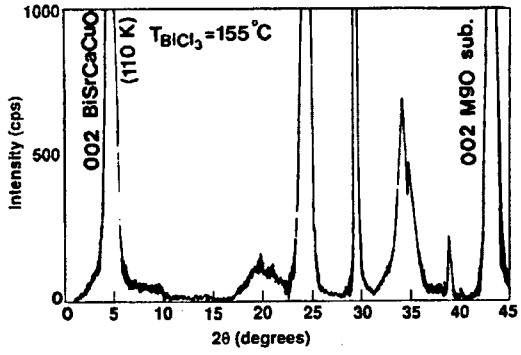

Figure 8. X-Ray Diffraction Pattern of Bismuth-Based Crystals Obtained at a $BiCl_3$ Source Temperature of 155°C

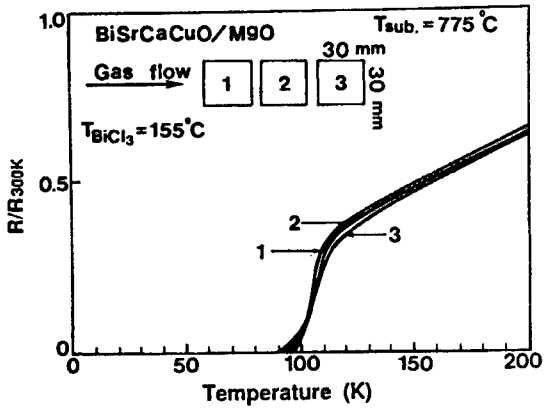

Figure 9. Temperature Dependence of Electrical Resistance of Bismuth-Based Crystals Simultaneously Deposited on Three MgO Crystal Substrates

Figure 8 shows the results of X-ray diffraction measurement of as-grown crystals deposited at a $BiCl_3$ source temperature of 155°C. Compared with the crystals shown in Figure 6, the 110 K phase diffraction strength has increased. Diffraction patterns cannot be observed for the 80 K and 20 K phases.

Thus, the optimization of crystal composition values, in particular, Bi atom composition values, makes it possible to change the 110 K phase to a single phase in an as-grown state (without high-temperature long-time annealing) by doping Pb atoms. The X-ray diffraction pattern of Bi-based crystals obtained at a $BiCl_3$ source temperature of 150°C shows that the 80 K phase is again intermixed. In addition, the diffraction strength has weakened, i.e., by about one-half to two-thirds, and the crystal quality has noticeably worsened.

Figure 9 shows the temperature dependence of the electrical resistance of Bi-based crystals simultaneously deposited using three MgO crystal substrates (30 mm x 30 mm each) at a $BiCl_3$ source temperature of 155°C. Their critical temperatures are comparatively uniform, i.e., 97 K, 93 K, and 89 K from the upstream side. These crystals were patterned to a size of 10 x 20 μm by photolithography. Then, the critical current densities were measured by the electrification method. The distribution of these densities inside the wafer is shown in Figure 10. A maximum critical current density of 8 x $10^5 A/cm^2$ (at 10 K) was obtained. The scattering of critical current densities in the wafer is larger than that of critical temperatures. It is necessary to develop a technology for growing highly uniform crystals with a high critical temperature and density.

2.2 Vacuum Halide CVD Process

The vacuum halide CVD process (reaction tube internal pressure: 0.1~10 Torr), employing characteristics of the atmospheric halide CVD process, is expected to be able to deposit crystals of higher homogeneous quality. This process has the following features:

(1) It provides an independent source cell inside the vacuum chamber, thereby improving the source gas concentration controllability.

(2) The mean free path of reaction gas molecules, such as source gases, becomes large, and the composition controllability is much improved. Thus, it is possible to uniformly deposit crystals on a crystal substrate with a large area.

(3) The reaction gas concentration can be maintained at a lower level, compared with the atmosphere process. This makes it possible to lower crystal deposition temperatures, such as the entire reaction system holding temperature and substrate crystal temperature.

Although the vacuum halide CVD process has the above attractive features, it has disadvantages such as complicated equipment structure and high equipment cost.

Figure 11 shows a schematic diagram of the vacuum halide CVD equipment recently developed by the author's group.

Independent cells serving as halide source materials, such as $BiCl_3$, CuI, CaI_2, and SrI_2, are provided inside a vacuum chamber. Halide source gases are transported by He carrier gas to the crystal substrate. The susceptor used to heat the substrate rotates, thus serving to enhance the uniformity of the films. O_2 gas (oxidizing agent) can be changed to a plasma using high frequencies. Figure 12 shows the distribution (inside the substrate crystal surface) of the film growth rate of simple substance metal oxides whose chemical compositions are turned into those of Bi-based crystals using this equipment. A sapphire crystal, 75 mm in diameter, is used as the crystal substrate. All compositions can be controlled at a deposition rate of about 5±1 A/min. It is expected that highly uniform and high-quality crystals can be deposited, compared with the atmospheric CVD process.

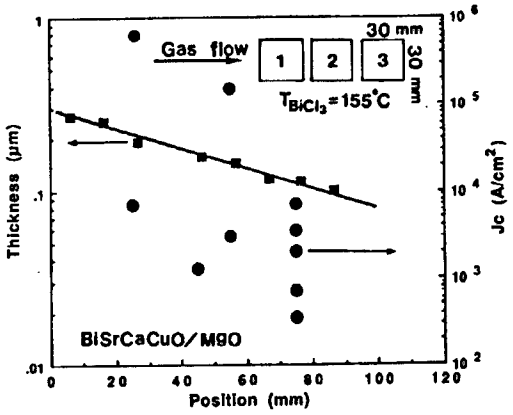

Figure 10. Distribution (Inside Wafer) of Critical Current Density of Bismuth-Based Crystals Simultaneously Grown on Three MgO Crystal Substrates

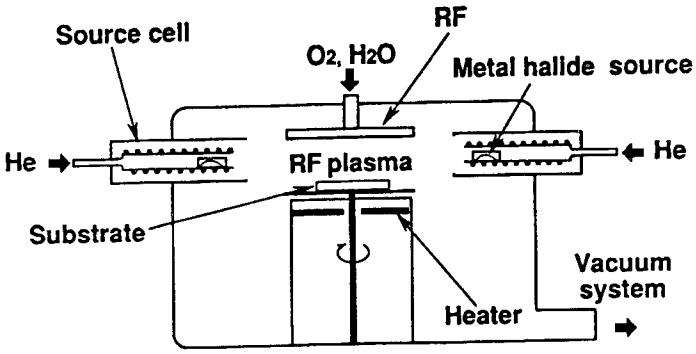

Figure 11. Vacuum Halide CVD Equipment

Figure 13 shows the temperature dependence of the electrical resistance of Bi-based crystals deposited on MgO and sapphire crystal substrates. Crystals deposited under the following conditions showed satisfactory surface conditions, i.e., 70 nm in film thickness and less than 5 nm in irregularity.

- Deposition temperature = 610~670°C
- Deposition rate = about 0.3 nm/min

The critical temperature of the crystals deposited ranged from 46~70 K.

Figure 14 shows the temperature dependence of a typical critical current density of Bi crystals. The critical current density is high, i.e., $7 \times 10^6 A/cm^2$ (at 20 K). This confirms that the improvement in the controllability of crystal compositions is serving to achieve a high critical current density.

M. Ottosson,[9] et al., recently developed a Y-based crystal deposition technology using the YCl_3-BaI_2-$CuCl$-O_2-based vacuum CVD process. The deposition temperature ranges from 870~910°C and the deposition rate is 5 nm/min. Although the deposition temperature is quite high, as-grown Y-based crystals

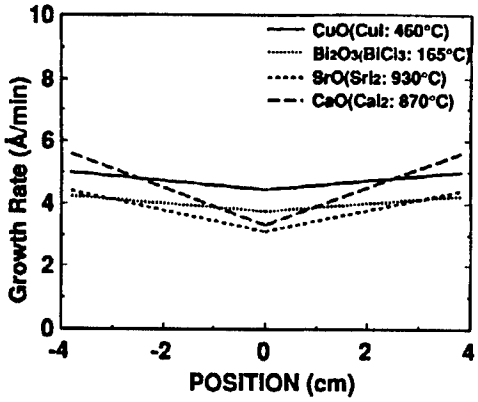

Figure 12. Distribution (Inside wafer surface) of Film Growth Rate of Metal Oxides Comprising Each Composition of Bismuth-Based Crystals

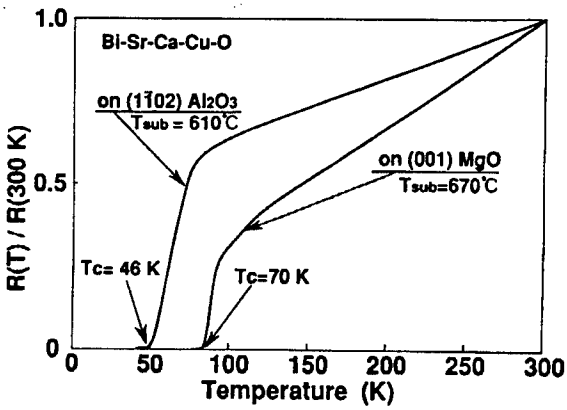

Figure 13. Temperature Dependence of Electrical Resistance of Bismuth Crystals Grown on MgO Substrate and Sapphire Substrate Crystal

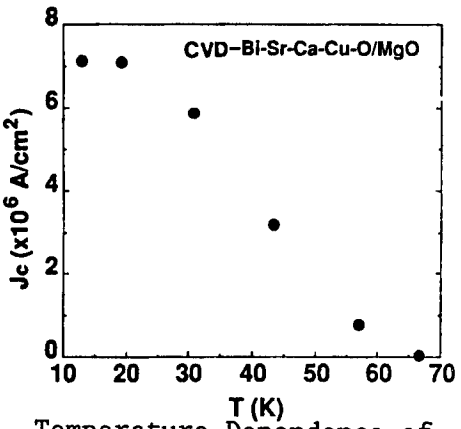

Figure 14. Temperature Dependence of Critical Current Density of Bismuth-Based Crystals Grown on MgO Crystal Substrate

of 40 K in critical temperature were obtained. The SEM observation of the crystal surface showed satisfactory results. The features of the halide-based CVD process were fully exhibited.

2.3 MOCVD Technology

The MOCVD growth process[10-11] is a chemical vapor-phase growing process using organic metal compounds and oxygen gas as raw materials. As a rule, it possesses the same features as those of the halide-based CVD growth process. High hopes are being placed on this process as a technology that may achieve crystal growth at low temperatures and high speed. However, little research on raw materials that consist of organic compounds containing rare metal elements and copper has been conducted, and these raw materials have not yet been obtained. However, various types of beta diketone metal complexes, etc., have been developed recently and, consequently, crystal growth has been started mainly for the yttrium system, as well as the bismuth system.

Source materials such as $Y(Cu_{11}H_{29}O_2)_3$, $Ba(C_{11}H_{29}O_2)_2$, and $Cu(C_{11}H_{29}O_2)_2$, which are beta diketone metal complexes used mainly as CVD raw materials for yttrium-based superconducting crystals, are solid at room temperature. These materials are heated to 100~300°C to obtain the steam pressure necessary for crystal growth. Bismuth-based superconducting crystals demonstrate similar trends. Currently available MOCVD source materials are characterized by their large molecular weight, as shown by the above molecular formula, and an excessive number of constituent atoms versus one metal atom. It is necessary, therefore, to develop easily usable, stable, inexpensive MOCVD source materials, provided with sufficient steam pressure at room temperature.

Described below are the deposition conditions and crystal characteristics already reported for the yttrium-based superconducting crystal deposition technology.

- Source temperature:

  - $Y(C_{11}H_{29}O_2)_3$ = 130~140°C
  - $Ba(C_{11}H_{29}O_2)_2$ = 240~260°C
  - $Cu(C_{11}H_{29}O_2)_2$ = 120~140°C

- Deposition temperature : 800~850°C
- Ar carrier gas flow rate : 100 cc/min
- Oxygen gas flow rate: : 100 cc/min
- Reaction tube : horizontal and vertical types
- Reaction tube internal pressure: decompressed to 10 Torr or less
- Substrate crystal : MgO, $SrTiO_3$, sapphire
- Heating of substrate crystal: rf induction heating and resistance heating
- Yttrium-based superconducting crystal characteristics are:

  T_c = 65~85 K
  J_c = ~10^6A/cm^2

Under a high magnetic field, satisfactory characteristics, i.e., J_c = 6.5 x 10^4A/cm^2 (at 27 T, 77 K) were obtained. It is hoped that the technology for growing crystals with higher critical temperatures and good uniform surface conditions will be developed.

3. Crystal Substrates for Crystal Deposition

The following can be cited as important characteristics required for crystal substrates used to deposit oxide superconducting thin films:

1) Solid-phase reactivity to deposited crystals
2) Lattice matching
3) Crystal quality
4) Thermal expansion coefficient, thermal conductivity dielectric constant
5) Processability, area, etc.

These characteristics play vital roles in obtaining high-quality crystals and applying thin films to electronics. In addition to these characteristics, the crystal substrates must be prepared at low cost. However, crystals used to prepare yttrium- and bismuth-based superconducting crystal deposition substrates that are capable of satisfying all the said characteristics have not yet been developed.

The author's group studied the solid-phase chemical reactions between simple oxidized substances, such as CaO, Cu_2O, SrO, and Bi_2O_3, chemical compositions of bismuth-based superconducting crystals, and various types of available crystal substrates. The results are shown in Figure 15.

Substrate	CaO	Cu_2O	SrO	Bi_2O_3
YSZ	o	o	o	o
MgO	o	o	o	o
$SrTiO_3$	o	o	o	o
Al_2O_3	o	o	x	x
$MgAl_2O_3$	o	o	x	x
GGG	o	o	x	x
$LiTaO_3$	o	o	x	x
$LiNbO_3$	x	x	x	x
Si	x	x	x	x
SiO_2	x	x	x	x
Si_3N_4	x	x	x	x
SiC	x	x	x	x

$T_{sub.}$ = 850°C
time = 60 min

o: No reactions observed
x: Reactions observed

Figure 15. Solid-Phase Reactivity of Metal Oxides (Individual chemical compositions of bismuth-based superconducting crystals) to Substrate Crystals

These simple substance oxides were put on the respective substrate crystals and were annealed in the carrier gas at 850°C for 60 minutes. Then, the existence of solid-phase chemical reactions was studied using an optical microscope. A circle was marked on the substances on which no reactions were observed, while a cross was marked on the substances on which reactions were observed. No reactions were observed on the YSZ, MgO, on $SrTiO_3$ substrate crystals, which, therefore, can be used as substrate crystals for growing bismuth-based superconducting crystals.

Substrate crystals other than YSZ, MgO, and $SrTiO_3$ were observed to react to any chemical composition (oxide). Therefore, they cannot be used to grow bismuth-based superconducting crystals. These results are thought to be applicable to yttrium-based superconducting crystals. Of course, as the processing temperature decreases, the rate of reaction is reduced. Therefore, the successful lowering of superconducting crystal deposition temperatures

serves to increase the types of substrate crystals that can be used. It also allows lattice matching and other characteristics to be selected, thus facilitating the application to electrons.

As was mentioned above, no solid-phase chemical reactions were observed between single substance oxides (chemical compositions of bismuth superconducting crystals) and three types of substrate crystals—YSZ, MgO, and $SrTiO_3$. On the MgO and $SrTiO_3$ substrates, bismuth-based superconducting crystals were successfully deposited by using the halide-based CVD growth process. On the YSZ substrate, insulator crystals grew under the same conditions. This may be because multicrystal substrates were used and the bonds of the surface atoms did not effectively serve to grow crystals, thereby preventing the progress of crystallization. On the other hand, this may have resulted from the surface catalyst effects being small and divergences having occurred in the composition values.

Figure 16 shows the lattice surface distance between yttrium-based and bismuth-based oxide superconducting crystals and typical substrate crystals. Of the substrate crystals, those with large size and satisfactory crystallinity are not currently being marketed, except for silicon and sapphire crystals.

Type of crystal	YbaCuO	BiSrCaCuO	MgO	$SrTiO_3$
Distance between lattice surfaces	a = 3.8 A	a = 5.4 A	a = 4.2 A	a = 3.9 A
Type of crystal	$LaGaO_3$	$LaAlO_3$	$(1012)Al_2O_3$	Si
Distance between lattice surfaces	a = 3.9 A	a = 3.8 A	a = 5.2 A b = 4.75 A	a = 5.4 A

Figure 16. Lattice Surface Distance Between High-Temperature Oxide Superconducting Crystals and Typical Substrate Crystals

Figure 17 [not reproduced] shows X-ray topography[12] of the MgO substrate crystals currently being used by many firms. This evaluation reveals the presence of micro-angle grain boundaries and highly dense crystal defects. MgO substrate crystals are quite inferior in quality to semiconductor crystals. In addition, where the level of the polishing technology is low (Photo a), layers of surface damage and scratches exist more densely.

If substrate crystals are to be applied to electrons, it is indispensable that inexpensive substrate crystals, with large diameters and satisfactory crystallinity, controlled as are seeded pulled crystals, be developed. Recently, Miyazawa, et al., of NTT LSI Research Laboratory[15] successfully developed $PrGaO_3$ and $NbGaO_3$ substrate crystals, which are superior in lattice matching with yttrium-based crystals, using the Czochralski process. High hopes are being placed on future developments.

4. Technology for Heterojunction With Semiconductor Crystals

Devices with new structures, LSI wires, etc., are manufactured by the heterojunction of high-temperature oxide superconducting crystals with semiconductor crystals, such as Si and GaAs. This is being studied as an application of high-temperature oxide superconducting crystals to electronics. It is also important to study the matching of the superconductor manufacturing process with the semiconductor manufacturing process. It is effective to use inexpensive Si, with its large diameter and good crystallinity, as the crystal growing substrate. A few reports have stated that yttrium-based oxide superconducting crystals have been formed directly on Si crystal substrates. It cannot be said, however, that the crystallinity (formation of SiO_2 on interfaces) and superconducting characteristics of these crystals are fully satisfactory (T_c = 50 K).

There have been many reports of yttrium-based and bismuth-based superconducting crystals being grown by forming buffer layers, such as ZrO_2, MgO, and $SrTiO_3/MgO \cdot Al_2O_3$ on Si crystal substrates. The superconducting characteristics of these crystals are satisfactory (T_c = 60-80 K) compared to when yttrium-based superconducting crystals have been formed directly on Si crystal substrates. The crystallinity of the buffer layers, however, contains mostly multicrystals. There are a few substrate crystals that can be called "substrate crystals with a heteroepitaxial structure," which are formed by full-scale heterojunction with semiconductor crystals.

The author's group has developed oxide crystals, i.e., magnesia spinel ($MgO \cdot Al_2O_3$) crystals by silicon-on-insulator (SOI) forming technology and MgO crystals by the halide CVD technology. The use of these technologies makes it possible to use the full-scale heterojunction of superconductor crystals with semiconductor crystals to obtain crystal substrates with heteroepitaxial structures. Figure 18 [not reproduced] shows an SEM surface photograph and RHEED pattern (a) on a substrate with an $MgO/MgO \cdot Al_2O_3/Si$ heteroepitaxial structure, including an SEM photograph of the cross section. The lattice mismatching of $MgO \cdot Al_2O_3$ crystals with Si and MgO crystals is comparatively small, i.e., 0.8 and 4.1 percent, respectively, with the $MgO \cdot Al_2O_3$ crystals proving effective as buffer layers. After the growth of $MgO \cdot Al_2O_3$ crystals, it is possible to form an SiO_2 layer on the Si interface using the thermal oxidation process, thus enabling thermal stress to be relaxed. It is thought, therefore, that $MgO \cdot Al_2O_3$ crystals can be effectively applied to electronics.

$MgO \cdot Al_2O_3$ crystals can be epitaxially grown on (100) Si substrates at 900°C using the $MgCl_2$-$AlCl_3$-CO_2-H_2 system CVD growth process.[13] MgO crystals can be epitaxially grown at 900°C using the $MgCl_2$-O_2-He system CVD growth process.[4] The lattice mismatching of MgO crystals with bismuth-based crystals is very large, i.e., 25 percent. Bismuth-based crystals, however, are complicated crystals, peculiar to layered structural substances; there are many indefinite points on the bonds of atoms at heterointerfaces. A future task will involve carrying out detailed structural assessments of the crystal interfaces.

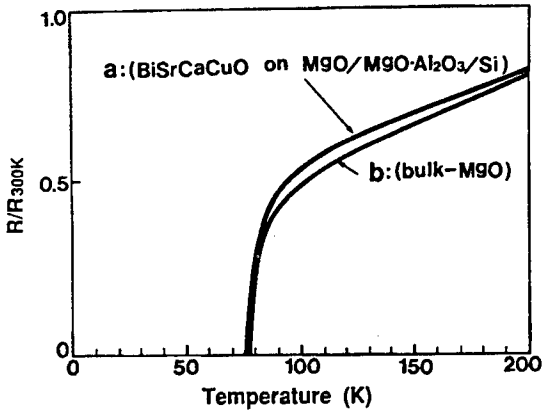

Figure 20. Temperature Dependence of Electrical Resistance of Bismuth-Based Crystals
Curve a shows a substrate with heteroepitaxial structure, while curve b shows a bulk MgO substrate.

Figure 19 [not reproduced] shows an SEM photograph (a) of the surface of bismuth-based as-grown crystals (80 K phase) deposited at 825°C and an SEM photograph (b) of the cross section of crystals with a heteroepitaxial structure. The film thicknesses of the bismuth-based crystals, MgO crystals, and $MgO \cdot Al_2O_3$ crystals are 0.15, 1.5, and 0.3 μm, respectively.

Figure 20 shows the temperature dependence of the electrical resistance of as-grown bismuth-based crystals simultaneously deposited at 825°C.

Curve a indicates the use of a substrate with a heteroepitaxial structure (critical temperature: 75 K), while curve b indicates the use of a bulk MgO crystal substrate (generally used) (critical temperature: 77 K). Thus almost the same characteristics were obtained. The quality of substrate crystals with a heteroepitaxial structure is likely to be upgraded compared with bulk MgO crystals. Therefore, the application of substrate crystals with a heteroepitaxial structure is expected to be enlarged, and will be coupled with the development of crystals with larger areas.

The use of heteroepitaxial growth technology allows $MgO \cdot Al_2O_3$ crystals (with satisfactory crystallinity) to be grown on Si substrate crystals at the considerably high temperature of 900°C. Therefore, it is thought that oxide superconductor crystals are likely to be heteroepitaxially grown directly on $MgO \cdot Al_2O_3$ layers and Si substrate crystals. Where the $MgO \cdot Al_2O_3$ crystal growth technology is used, but where Mg, Al, and oxygen atom compositions are not fully controlled, solid-phase reactions with Si substrate crystals are stronger. As a result, no epitaxial growth is carried out. Therefore, if oxide superconductor crystals are to be grown satisfactorily, it is important that the precise crystal composition control technology be raised to a higher level, and that the crystal growth temperatures be lowered.

5. Conclusion

This report has outlined the crystal growth technology aimed at the application of high-temperature oxide superconductor crystals to electronics, the current status of the raw materials being used, and future problems. If application to electronics is to be achieved, it is indispensable that a completely controlled superconducting thin film crystal growing technology that fully incorporates the various technologies and expertise accumulated in the semiconductor field be developed. It is also necessary for a high-level precise crystal composition control technology and low-temperature crystal growth technology using the CVD growth technology be developed. Along with this, it is necessary to positively proceed with the improvement of the quality of crystal substrates and of the raw materials used to grow crystals, as well as to develop new materials.

References

1. Maeda, H., Tanaka, Y., Fukutomi, M., and Asano, T., JAPANESE JOURNAL OF APPLIED PHYSICS, Vol 27, 1988, p L209.

2. Ihara, M., and Kimura, T., FED HiTcSc-ED 1st Workshop, Miyagi-Zao, 1988, p 137.

3. Kimura, T., Ihara, M., Yamawaki, H., Ikeda, K., and Ozeki, M., ISS 88, Nagoya, 1988, p 495.

4. Ihara, M., Kimura, T., Yamawaki, H., and Ikeda, K., IEEE TRANS. MAG., Vol 25 No 2, March 1989, p 2470.9.

5. Ibid., APPLIED PHYSICS, Vol 58 No 5, 1989, p 751.

6. Ihara, M., Kimura, T., Yamawaki, H., Ueda, O., FED HiTcSc-ED 2nd Workshop, Shikabe-Hokkaido, 1989, p 309.

7. Ihara, M., Yamawaki, H., Kimura, T., and Nakao, H., ISS 89, Tsukuba, PTF-25, 1989, p 222.

8. Nakao, H., Kimura, T., Yamawaki, H., Ihara, K., and Ozeki, M., 37th Appl. Phys. Preliminary Series Draft for Lecture, 1990.

9. Ottosson, M., Andersson, T., Carlsson, J.O., Harsta, A., and Jansson, U., APPLIED PHYSICS LETTERS, Vol 54 No 12, 12 June 1989, p 2478.

10. Yamane, H., Masumoto, H., Hirai, T., Iawasaki, H., Watanabe, K., Kobayashi, N., and Moto, Y., Ibid., Vol 58, 1988, p 1548.

11. Matsuno, S., Uchikawa, F., Yoshizaki, K., ISS 89, Tsukuba, PTF-26, 1989, p 223.

12. Ihara, K., 4th Appl. Phys.-High Temperature Superconductor Research Society OHP Series, Jul 1989.

13. Ihara, M., Arimoto, Y., Jifuku, M., Kimura, T., Kodama, S., Yamawaki, H., and Yamaoka, T., J. ELECTROCHEM. SOC., Vol 129, 1982, p 2570.

14. Ihara, M., Kimura, T., Yamawaki, H., and Ueda, O., FED HiTcSc-ED 2nd Workshop, Shikabe-Hokkaido, 1989, p 135.

15. Miyazawa, S., Mukaida, M., Sasaura, M., and Tazo, Y., J. ELECTROCHEM. SOC., Vol 137 No 4, Apr 1990, p 227C.

Current Status of, Outlook for MBE

916C1001G Tokyo HYOMEN KAGAKU SEMINA in Japanese 27-29 Jun 90 pp 83-94

[Article by Kunimitus Uchinokura, Engineering Department, Tokyo University]

[Text] **1. Introduction**

Success in the semiconductor field (GaAs, etc.) may lead to the achievement of complete crystallinity and a good-quality crystal surface at the atomic level, and also to the artificial manufacture of new substances. These can be said to represent purposes for employing the molecular beam epitaxy (MBE) process.

It should be noted, however, that this process cannot simply be applied to high temperature superconductors for the following reasons:

1) High temperature superconductors are oxides. The method of taking in oxygen, therefore, plays a vital role.

2) GaAs does not naturally deposit layer by layer. Therefore, where GaAs is deposited layer by layer, it is necessary to control the number of atoms per layer. How should the number of atoms be controlled per layer? This represents a significant problem.

3) In connection with 2), the number of elements comprising high temperature superconductors is large. This poses problems.

All these problems are not peculiar to the MBE process. In this paper, however, only the MBE process is discussed. This process uses molecular beams, and a high vacuum state is absolutely necessary. This, however, poses large problems from the standpoint of manufacturing oxides. During the initial stage, thin films were evaporated while there was a shortage of oxygen, amorphous substances (from which oxygen was removed) were prepared, and then the amorphous substances were sintered in oxygen. Even this process enabled the c axis to be well oriented vertically to the substrate. In addition, thin films with zero resistance temperature $T_{c.zero}$ that did not differ greatly from those of bulk specimens were obtained. However, these thin films did not have the characteristics one would expect to result from the use of the MBE process.

Therefore, except for the initial stage, the major problem becomes how to form a high temperature superconducting thin film using the MBE process and growing the thin film in situ by the introduction of oxygen in a high vacuum. In this respect the MBE process undoubtedly represented a disadvantageous process in its early stages, compared with other film forming processes. Sputtering and laser ablation, for example, can form films under high oxygen pressure. Therefore, thin films can be grown in situ in earlier stages. Due to these circumstances, as opposed to the cases in which other processes are used, there are not many reports on the preparation of high temperature superconductor thin films using the MBE process. These disadvantages, however, are being overcome thanks to the recent progress of the active oxygen utilization technology described below. The MBE process is achieving the excellent results originally expected for this process, that are superior to those of other processes. It is expected that the MBE process will progress as a superior high temperature superconducting thin film preparation technology in the future.

Problems with the MBE process and methods of overcoming these problems are described below. The author is currently engaged in the formation of Bi-Sr-Ca-Cu-O MBE thin films using pure ozone (O_3), which is also described in detail.

2. Activation of Oxygen and In-situ Crystal Growth

It is almost impossible to use O_2 oxygen molecules directly for the in situ growth of crystals in a highly vacuum state. Of course, attempts are being made to raise the oxygen pressure solely around the substrate using differential exhaust gases, etc. This measure alone, however, is insufficient for the in situ growth of crystals.

Therefore, other processes that will prove to be more effective than the process in which O_2 oxygen molecules are introduced must be developed. In the other processes, O_2 oxygen molecules are used, but they are changed to the more active O oxygen atoms and ions using any method—Method A. Gases (containing oxygen atoms in molecules) other than oxygen molecules are introduced—Method B. the former method is further classified into Method Aa, in which oxygen molecules are activated in the thin film growing chamber, and Method Ab, in which oxygen molecules are activated before they are introduced into the growing chamber, then activated oxygen molecules are sprayed to substrates. Although such definite classification cannot be applied to all cases, processes are classified as above for convenience. The following active oxygen introduction methods are being used or tested.

[A]

Aa: An RF electromagnetic field is applied to oxygen gases in the growing chamber to produce oxygen plasma and thereby to activate oxygen. This process cannot raise the vacuum much since the production of oxygen plasma and evaporation are carried out in the same area. For this reason, it is difficult to satisfy the molecular beam conditions. This process, therefore, is called the "reactive evaporation process."[1] Figure 1 shows an example.[1] The method using about 5 percent of the ozone O_3 produced in an ozone generator has recently been used.[2]

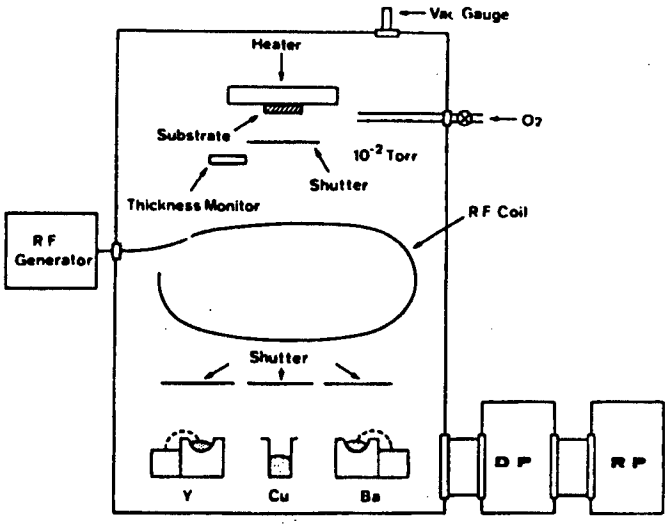

Figure 1. Conceptual Drawing[1] of Reactive Evaporation Process (Where oxygen is activated using RF electromagnetic waves)

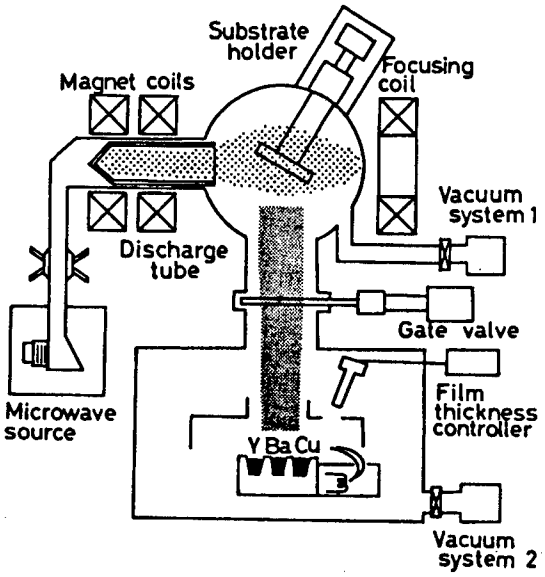

Figure 2. Conceptual Drawing[3] of Evaporation Equipment Using ECR Oxygen Plasma

Ab: Oxygen is activated using an electromagnetic field and activated oxygen is introduced into the growing chamber. If carefully observed, several methods can be used for activating oxygen.

Ab1: Oxygen is activated using ECR plasma. ECR plasma is produced by applying microwaves to oxygen gas in a magnetic field to activate oxygen, as illustrated in Figure 2.[3]

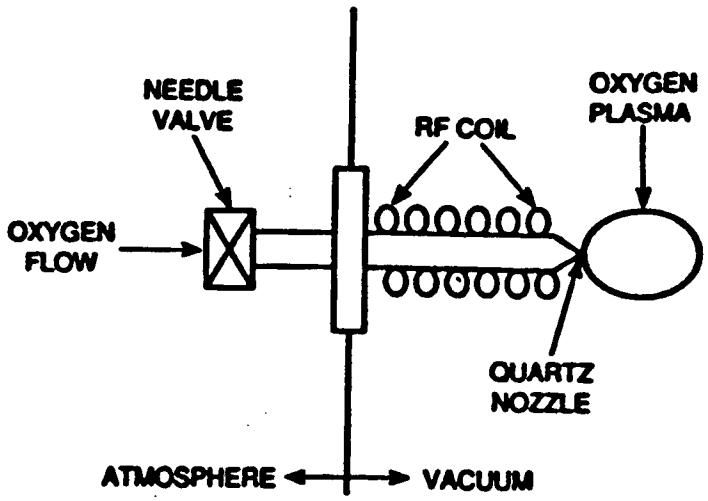

Figure 3. Conceptual Drawing[4] of Oxygen Plasma Source Using RF Electromagnetic Waves

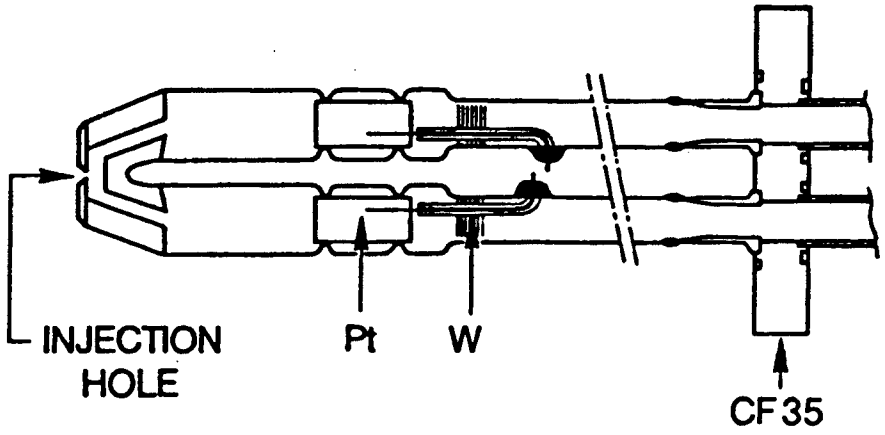

Figure 4. Oxygen Plasma Source Obtained by Applying a dc Voltage[5]

Ab2: Oxygen plasma is produced by RF electromagnetic waves, and excited O and O_2 existing in the oxygen plasma are used, as illustrated in Figure 3.[4]

Ab3: Plasma is produced by applying a dc voltage instead of the above-mentioned RF electromagnetic waves, as illustrated in Figure 4.[5]

B. Processes Introducing Gases Other Than O_2 Oxygen Molecules:

B1: Process using pure or high-concentration ozone O_3. This process was initially used for trial purposes by Berkley, et al., for $YBa_2Cu_3O_y$.[6] This process is described in detail in Section 3.

B2: Process using N_2O. It has been proven that N_2O is very effective when the laser ablation process is used. Although N_2O was used in MBE for trial purposes, there are no reports stating that N_2O is effective for this process.

B3: Process using NO_2. Watanabe, et al.,[7] have reported on the use of this process under a specific system. Currently, however, it is not clear whether this process is generally effective.

3. Bi-Sr-Ca-Cu-O Thin Film MBE In-situ Growth Using Pure Ozone

We are currently preparing (by the MBE process) $Bi_2Sr_2Ca_{n-1}Cu_nO_y$ thin films that use pure ozone, and describe the details below.[8-12]

3.1 Vacuum Evaporation System

We are using a vacuum evaporation system which employs gaskets made of aluminum alloys. Figure 5 shows a conceptual drawing of this system.[8]

The vacuum vessel is exhausted by a cryopump (2,400 ℓ/s) and turbo molecular pump (300 ℓ/s). When no ozone gas is introduced, the system is maintained at a pressure of 4×10^{-6}Pa. Bi, Sr, Ca, and Cu molecular beams are supplied by the Knudsen-cell. PBN is used for the crucibles for Sr, Ca, and Cu, while Ta is used for Bi to keep the volume from expanding and breaking when the Bi solidifies. The cell temperature is always maintained at a constant level. The amount of evaporation is controlled by the opening/closing of the shutter, as will be mentioned later. Further, the substrate temperature is measured by a pyrometer. In order to improve thermal contact, aluminum foil is inserted between the substrate and the substrate holder. Inconel is used for the substrate holder.[11]

3.2 Ozone System

Ozone O_3 gas is used to supply oxygen. The ozone supply system that we used is substantially the same as that initially used by Berkley, et al., for the in-situ growth of $YBa_2Cu_3O_y$. Figure 6 shows a conceptual drawing of our ozone supply system.[11]

A highly pure O_2 oxygen molecule is turned into a gas containing 5 percent O_3 via the ozone generator. Then, only the O_3 is separated and liquefied via the still. Sorption pumps are used for exhausting. It is necessary that the O_3 obtained be as pure as possible. Care must be taken with concentrated ozone because it is likely to explode. We paid attention to the following items.[11]

(1) The mixture of impurities is likely to cause explosions. Therefore, we prepared the ozone system under high vacuum specifications.

(2) A protective shield for explosion protection was provided around the still to prepare for emergencies.

(3) The minimal amount of liquid O_3 necessary was used.

(4) To prevent the decomposition of O_3, only stainless steel, aluminum, glass, and Teflon were used as materials. When silver-coated stainless steel gaskets were used carelessly, thin films grown in situ did not show superconductivity.

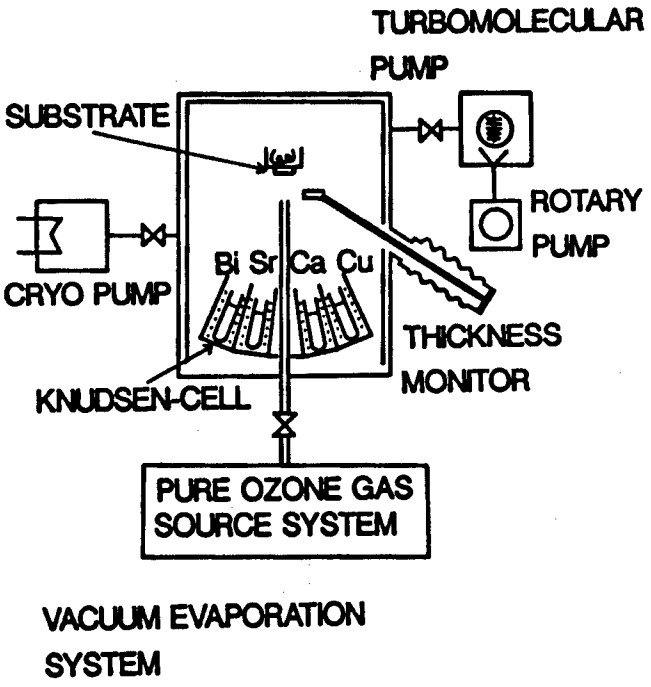

Figure 5. Conceptual Drawing of Vacuum Evaporation System Used[8]

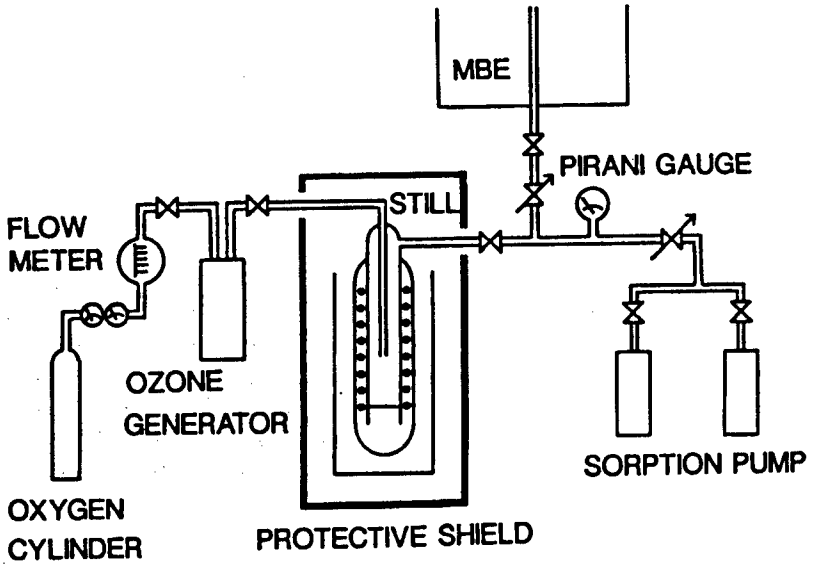

Figure 6. Conceptual Drawing of Pure Ozone Gas Preparation System[11]

(5) The liquefaction of O_2 together with O_3 makes it difficult to remove the O_2. Therefore, conditions should be established in such a way that only the O_3 to be excessively cooled is liquefied (about 94~95 K, 0.5~1 Torr).

(6) After the completion of liquefaction, the He in the sorption pumps and the slight amount of O_2 remaining in the liquid O_3 are fully drawn by the cryopump and turbo molecular pump via the growth chamber before evaporation is conducted.

(7) Unless the O_3 is detected by the four-pole mass analyzer, it does not appear that satisfactory results can be obtained.

During evaporation, liquid O_3 in the still was maintained at 98~99 K and the pressure was maintained at about 66 Pa. Then, O_3 was introduced into the growing chamber. Pure O_3 was introduced through a stainless steel pipe, 8 mm in inner diameter, and discharged toward the substrate located 40 mm away through 20 holes (0.5 mm in diameter, 10 mm in length) parallel to each other.

In another respect, the O_3 is not liquefied, but rather is absorbed by the silica gel, and a highly concentrated O_3 gas is used. This process is also being used.[13]

3.3 Experimental Method

We intended to grow crystals layer by layer and, using a shutter, supply only one kind of each metal element at the same time. O_3 was always supplied during evaporation. Evaporation was started from the Bi layer and completed within the same layer. In the case of $Bi_2Sr_2CaCu_2O_y$, for example, each metal element was evaporated in the order of Bi, Sr, Cu, Ca, Cu, Sr, and Bi, and this process was repeated.

$SrTiO_3$(001) and MgO (001) were used as substrates. After evaporation, the Knudsen cell was promptly returned to room temperature. The substrate temperature was lowered from the temperature T_{sub} of the substrate being evaporated to 200°C in about one hour. During this process, an O_3 pressure of 4×10^{-4}Pa was maintained. When the substrate temperature reached 200°C, the supply of O_3 was stopped. The chemical composition of the thin films evaporated on the MgO was studied by inductively coupled plasma (ICP) atomic emission spectroscopy. Further, the film volume was calculated, as was the number of atoms per layer. When $SrTiO_3$ is used for substrates, the Sr contained in the substrates is detected, and the correct chemical composition of the thin films evaporated on the $SrTiO_3$ substrates cannot be obtained by ICP. The chemical composition, therefore, was assumed to be the same as that of the thin films concurrently evaporated on the MgO substrate.

The typical evaporation conditions are as follows:

The substrate temperature T_{sub} was changed within the range of from 650~800°C. The Knudsen cell was maintained at 491, 489, 530, and 1,080°C for Bi, Sr, Ca, and Cu. The pressure during evaporation was maintained at 4×10^{-4}Pa, which was able to satisfy the molecular beam conditions. The ion electric current of the

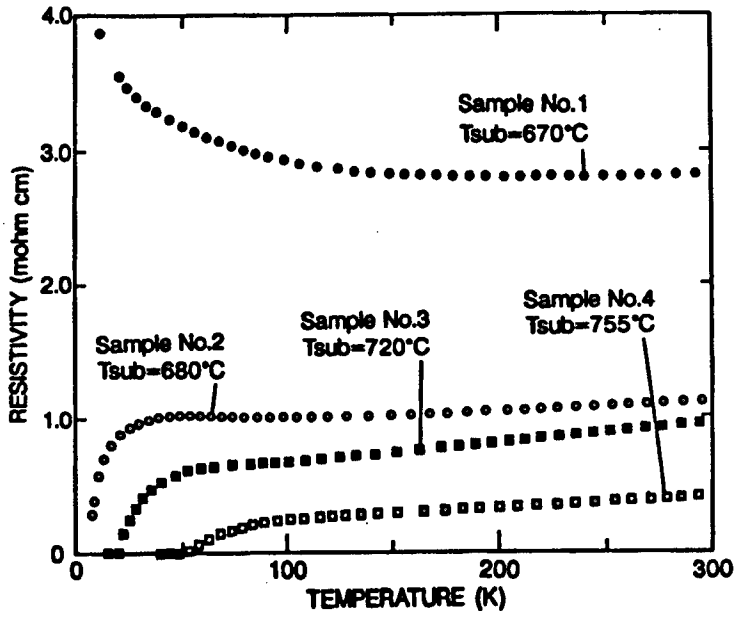

Figure 7. Temperature Dependence of the Resistivity of the as-Deposited Films of $Bi_2Sr_2CaCu_2O_y$ Phase on $SrTiO_3$ (001) Substrates With Various Substrate Temperatures T_{sub}[11]

four-pole mass analyzer was 3 x 10^{-10} and 2 x 10^{-13} A, respectively, for O_2 and O_3. These values do not, of course, give the flow ratio of O_2 to O_3 for the introduced gas. The O_3 is decomposed in the system. Further, when O_3 is ionized in the mass analyzer, it is decomposed and, therefore, the O_3 ion current appears to have become small. When O_3 is not detected, the rate of in situ growth of thin films showing superconductivity decrease greatly. It is effective, therefore, to measure the O_3 by the four-pole mass analyzer. The evaporation time (during which the shutter is opened) of each element was 7.4 s (Bi), 3.7 s (Sr), 4.7 s (Cu), 4.5 s (Ca), 4.7 s (Cu), 3.7 s (Sr), and 7.4 s (Bi), respectively, with respect to one cycle (one-half of unit cell in the c-axial direction) for the case of $Bi_2Sr_2CaCu_2O_y$. When $Bi_2Sr_2Ca_{n-1}Cu_nO_y$ (whose n value differs) is prepared, open shutter conditions were added (removed) to Ca and Cu.

3.4 Results of Experiments[11]

Figure 7 shows the temperature dependence of resistivity of the thin films grown on a $Bi_2Sr_2CaCu_2O_y$ $SrTiO_3$ substrate, with T_{sub} as the parameters.[11] The relationship between T_c^{zero} and T_{sub} is very clear. In other words, as T_{sub} grows, T_c^{zero} grows. Where MgO substrates were used, such a clear relationship was not observed, but T_c^{zero} tended to grow as T_{sub} grew. T_{sub}, therefore, was then set at temperatures ranging from 780~790°C.

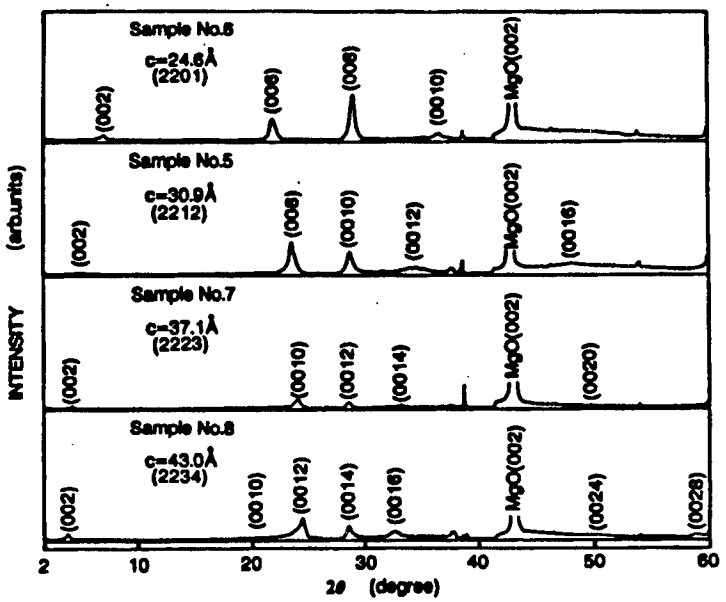

Figure 8. CuK_α X-Ray Diffraction Patterns With θ-2θ Scan of as-Deposited Films for n = 1,2,3, and 4 Phases of $Bi_2Sr_2Ca_{n-1}Cu_nO_y$[11]

When the amount of Bi was varied within the range of $1.30 < x < 2.29$ by expressing the chemical composition as $Bi_2Sr_2CaCu_2O_y$, T_c^{zero} tended to grow along with x. Further, when the amount of Ca was varied within the range of $0.58 < z < 1.70$ by expressing the chemical composition as $Bi_2Sr_2CaCu_2O_y$, T_c^{zero} tended to grow along with z.

Currently, it cannot be said that the evaporation conditions have been optimized. We obtained a maximum T_c^{zero} of 50 K with respect to thin films with the $Bi_2Sr_2CaCu_2O_y$ phase. This figure is considerably lower than that (81 K)[14] of single crystals and MBE thin films obtained by the Stanford [Barian] group which used a similar process. Therefore, efforts to optimize the evaporation conditions are still needed.

Next, we prepared $Bi_2Sr_2Ca_{n-1}Cu_nO_y$ thin films, other than $n \neq 2$, by increasing and decreasing the number of layers containing Cu and Ca while controlling the open/close of the shutter. Figure 8 shows the results of X-ray diffraction of as-grown thin films with a chemical composition of $Bi_2Sr_2Ca_{n-1}Cu_nO_y$ (n = 1,2,3, and 4).[11] As far as X-ray diffraction is concerned, it can be deemed that these thin films are almost single crystals. Thus, we successfully obtained the in situ growth of single phase thin films with a chemical composition of $Bi_2Sr_2Ca_{n-1}Cu_nO_y$ (n = 1,2,3, and 4).

Figure 9 shows changes due to temperature in resistivity of as-evaporated thin films with a chemical composition of $Bi_2Sr_2Ca_{n-1}Cu_nO_y$ (n = 1,2,3, and 4).[11] Thin films with n = 1 showed metallic temperature changes over almost the entire area and their resistivity increased slightly at 20 K or lower; they did not show superconductivity at 4.2 K or higher. Thin films with n = 3 and 4 showed

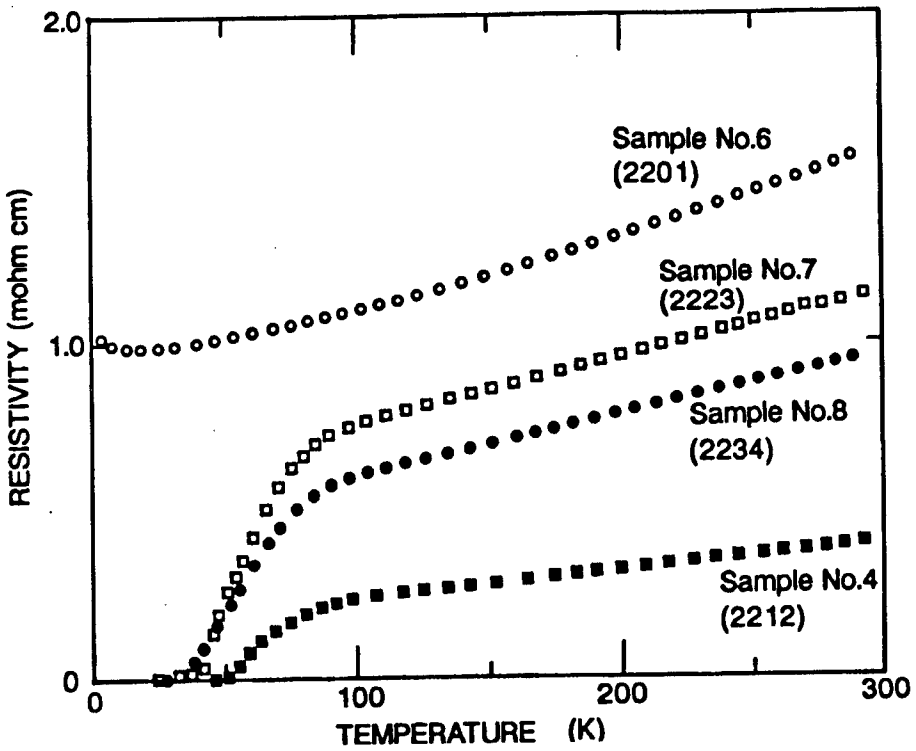

Figure 9. Temperature Dependence of the Resistivity of as-Deposited Films for the n = 1,2,3, and 4 Phases of $Bi_2Sr_2Ca_{n-1}Cu_nO_y$[11]

superconductivity. The superconducting onset temperature and T_c^{zero} of thin films with n = 3 were about 90 K and 40 K, respectively. The superconducting onset temperature and T_c^{zero} of thin films with n = 4 were about 90 K and 33 K, respectively. It does not appear, however, that the temperature dependence of resistivity is peculiar to these phases.

3.5 Physical Properties of Thin films

Electronic Energy Loss Spectral Diffraction (EELS)

It is necessary to study whether thin films obtained through the above processes have the same properties as those of single crystals. Therefore, we studied the electronic conditions of thin films by EELS. Measurements were conducted by the reflection method under the following conditions:

- Incident electrons = 1 keV
- Energy resolution = 0.55 eV
- Incident electron current = 10~20 nA
- Incidence of electron beams on 1 x 1 mm^2 portion of the specimen[11]

Figure 10 shows loss functions $Im(-1/\epsilon(\omega))$ of $Bi_2Sr_2CaCu_2O_y$ thin films, and $Bi_2Sr_2CaCu_2O_y$ and $Bi_2Sr_2CuO_y$ single crystals. $(\epsilon(\omega))$ shows dielectric functions.[11]

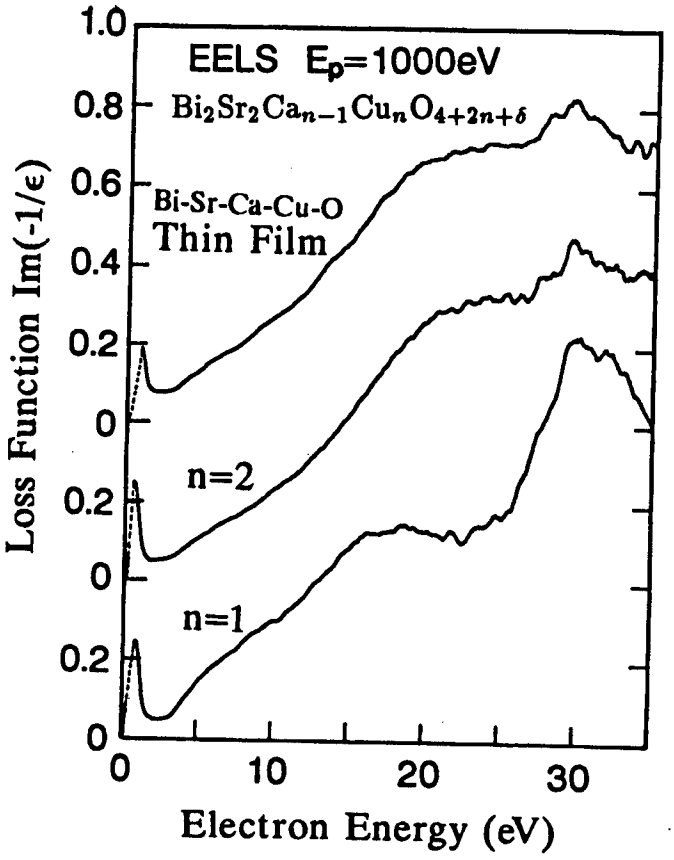

Figure 10. Loss Functions $Im(-1/\epsilon(\omega))$ of as-Deposited $Bi_2Sr_2CaCu_2O_y$ Film, Single-Crystal $Bi_2Sr_2CaCu_2O_y$ and Single-Crystal $Bi_2Sr_2CuO_y$ Obtained From Reflection EELS Measurement[11]

Loss functions were obtained by deducting multiple scattering and quasi-elastic scattering from measured spectrums.[15] Electron energies of 1.5 eV or smaller were extrapolated so that $\epsilon(\omega)$ equals zero at $\omega \to 0$. Loss functions (Figure 3(b) of Reference 16) obtained by optical measurements agreed well with those obtained by EELS (Figure 10). Thus, in order to obtain loss functions in a broad energy region by optical measurement, it is necessary to use several spectro systems, including synchrotron radiation. In reflection EELS, however, it is possible for one item of equipment to easily carry out measurements, thus proving to be very effective. As shown in the figure, the difference between $Bi_2Sr_2CaCu_2O_y$ and $Bi_2Sr_2CuO_y$ single crystals appears markedly near 17~27 eV and 33~35 eV. The former corresponds to the plasma excitation of valence electrons. The broad peak (~20 eV) of valence electron plasmons with n = 2 possesses energy larger than that (~17 eV) of valence electron plasmons with n = 1. This difference reflects the difference in the number of CuO_2 faces. The latter is associated with the Ca^{2+} (3p) core level.

Figure 10 shows that the electronic state of the $Bi_2Sr_2CaCu_2O_y$ thin film is almost the same as that of $Bi_2Sr_2CaCu_2O_y$ single crystals, while the electronic state of this thin film clearly differs from that of $Bi_2Sr_2CuO_y$ single

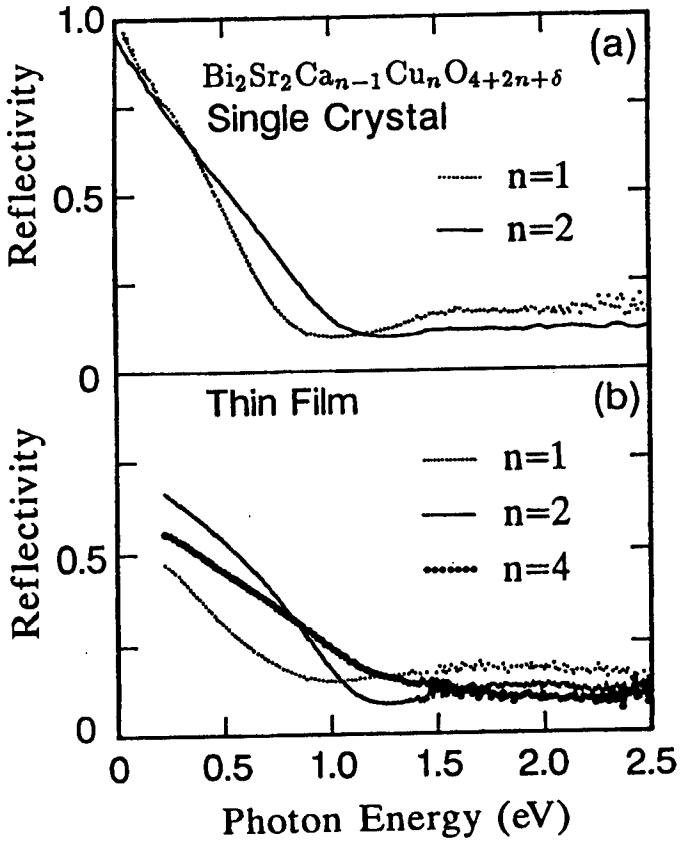

Figure 11. Optical Reflectivity Spectra of (a) Single Crystals With n = 1 and 2 Phases, and (b) as-Deposited Films With n = 1,2, and 4 Phases of $Bi_2Sr_2Ca_{n-1}Cu_nO_y$[11]

crystals. The escape depth of the reflected electrons in the measured energy ranges from 10~20 Å. Therefore, with respect to this measurement, thin films can be deemed as being "bulk" materials. It can be concluded, therefore, that the electronic state of our $Bi_2Sr_2CaCu_2O_y$ thin films remains the same with respect to excitation within the energy range or from 1.5~35 eV.

Optical Reflectivity Spectra

In order to further study the electronic state of thin films, we measured the optical reflectivity spectra. Figure 11 shows the results of the study.[11] The results of experiments on single crystals with n = 1 and 2 phases, are also shown for reference. These results show that while the energy decreases slowly, the reflection factor gradually increases. Such behavior is regarded as common to high temperature superconductors and is frequently deemed to be the plasma reflection of free carriers. Although this behavior has so far been explained using the Drude model, a different explanation has recently appeared.[17] In this experiment, the reflection edge showed almost the same values in both thin films and single crystals (n = 1 and 2), though the absolute value of the reflection factor differs because thin films are exposed to a small amount of transmission light. The experimental results showed that the

energy at the reflection edge grew with the increasing number of CuO_2 faces. This has already been demonstrated in sintered materials with a composition of $Bi_2Sr_2Ca_{n-1}Cu_nO_y$, within the range of from n = 1 to n = 3 (Pb is contained when n = 3).[18]

4. Possibility of MBE Process

As mentioned earlier, thanks to the activation of oxygen, the MBE process is establishing its position as an in situ superconductor growing process that is not inferior to other processes. There is the possibility that the MBE process can perform positive roles in preparing superlattice superconductor thin films or new superconducting substances in the future, utilizing the superior surface smoothness, etc.

References

1. Terashima, T., Iijima, K., Yamamoto, K., Takada, J., Hirata, K., Mazaki H., and Bando, Y., J. CRYSTAL GROWTH, Vol 95, 1989, p 617.

2. Terashima, T., Bando, Y., Iijima, K., Yamamoto, K., Hirata, K., Hayashi, K., Kamigaki, K., and Terauchi, H., "Abstracts of the Second ISTEC Workshop on Superconductivity," Kagoshima, 28–30 May 1990, p 101.

3. Aida, T., Tsukamoto, A., Imagawa, K., Fukazawa, T., Saito, S., Shindo, K., Takagi, K., and Miyauchi, K., JPN. J. APPL. PHYS., Vol 55, 1989, p L635.

4. Budhani, R.C. and Ruchman, M.W., APPL. PHYS. LETT., Vol 55, 1989, p 2354.

5. Touzeau, M., Schuhl, A., Cabanel, R., Luzeau, P., Barski, A., Pagnon, D., Hirtz, J.P., and Creuzaet, G., MRS, Boston, November 1989.

6. Berkley, D.D., Kim, D.H., Johnson, B.R., Goldman, A.M., Macartney, M.L., Beauchamp, K., and Maps, J., APPL. PHYS. LETT., Vol 53, 1988, p 708; Berkley, D.D., Johnson, B.R., Anand, N., Beauchamp, K.M., Conroy, L.E., Goldman, A.M., Maps, J., Mauersberger, K., Macartney, M.L., Morton, J., Tuominen, M., and Zhang, Y-J., Ibid., Vol 53, 1988, p 1973.

7. Watanabe, S., Kawai, M., and Hanada, T., Preprint, Kawai, M., "Abstracts of the Second ISTEC Workshop on Superconductivity," 28–30 May 1990, Kagoshima, p. 109.

8. Nakayama, Y., Ochimizu, H., Maeda, A., Kawazu, A., Uchinokura, K., and Tanaka, S., JPN. J. APPL. PHYS., Vol 28, 1989, p L1217.

9. Nakayama, Y., Tsukada, I., Maeda, A., Uchinokura, K., Ibid., p L1809.

10. Ibid., PHYSICA, Vol C162–164, 1989, p 711.

11. Uchinokura, K., Nakayama, Y., Tsukada, I., Terasaki, I., and Maeda, A., to be published in "Proceedings of the Conference on the Science and Technology of Thin-film Superconductors," Denver, Colorado, USA, Plenum Publishing Co., 30 April-4 May 1990,

12. Uchinokura, K., Nakayama, Y., Tsukada, I., and Maeda, A., "Abstracts of the Second ISTEC Workshop on Superconductivity," Kagoshima, 28-30 May 1990, p 72.

13. Eckstein, J.N., Bozovic, I., von Dessonneck, K.E., Schlom, D.G., and Harris, J.S., Ibid., p 37.

14. Schlom, D.G., Eckstein, J.N., Bozovic, I., Marshall, A.F., Sizemore, J.T., Chen, Z.J., von Dessonneck, K.E., Harris, J.S. Jr., Bravman, J.C., to be published in Proceedings of the Fall MRS Meetings, Symposium M: High Temperature Superconductors, 1989.

15. Terasaki, I., unpublished.

16. Terasaki, I., Tajima, S., Eisaki, H., Takagi, H., Uchinokura, K., and Uchida, S., PHYS. REV., Vol B41, 1990, p 865.

17. For example, Terasaki, I., Nakahashi, T., Takebayashi, S., Maeda, A., and Uchinokura, K., PHYSICA, Vol C165, 1990, p 152.

18. Maeda, A., Hase, M., Tsukada, I., Noda, K., Takebayashi, S., and Uchinokura, K., PHYS. REV., Vol B41, 1990, p 6418.

Current Status of, Outlook for Layered Films

916C1001H Tokyo HYOMEN KAGAKU SEMINA in Japanese 27-29 Jun 90 pp 95-106

[Article by Masao Nakao, Tsukuba Research Laboratory, Sanyo Electric Co., Ltd.]

[Text] **1. Introduction**

The technology for layering dissimilar materials whose physical properties differ plays a very important role in exploring the quantum effects of the electronic system in solids. In other words, layered films make it possible to propose valuable probes capable of grasping microelectronic system behaviors as macro phenomena. This can be recognized from the fact that the research conducted by Ezaki, Giaever, and Josephson (Nobel physics prize winners) was based on semiconductor pn junction, superconductivity/insulator/nonsuperconductivity (SIN) junction, and superconductor/insulator/superconductor (SIS) junction, respectively. These basic studies served to develop new application fields for electronics, such as Josephson devices.

The discovery of oxide superconductors served to greatly enlarge the range of combination of layered films from the material standpoint. So far, cryogenic superconductors and room temperature semiconductors have not been successfully bonded to each other. However, these materials have come to be able to maintain excellent functioning at the liquid nitrogen temperature. The layering of metallic system superconductors with oxide insulators and dielectrics, which was thought to be difficult in metal-based superconductors, can be said to have become easily accomplished. Therefore, in this paper, we would like to report the results of the latest experiments that may result in future applications, while also introducing several new ideas.

2. Thin Film Manufacturing Technology for Layering

New materials are being explored in the search for higher critical temperatures. In conjunction with this, research on processing oxide superconductors into thinner films is being positively conducted. While it is not clear what the final substance will be for commercialization purposes, at the present time the point common to high-temperature superconductors is that they are all copper oxides. It can be said that know-how involving the technology to process copper oxides into thinner films is being steadily accumulated.

As has already been introduced in other lectures, a variety of existing thin film manufacturing technologies are currently being applied to oxide superconductors. Of these technologies, various sputtering processes, laser ablation, chemical vapor deposition (CVD), and vacuum evaporation or a more refined molecular beam epitaxy (MBE) process can be cited as typical processes. Which process is most suitable for oxide superconductors? This cannot yet be answered, but the specific features of the process suited for oxide superconductors can be enumerated. The following can be cited as criteria for judging whether the process concerned is suitable for layering.

- The manufacturing process temperature can be lowered.
- A good matching can be maintained with other material thin film manufacturing technologies.
- Sharp hetero interfaces can be obtained.

The sputtering process is the one being most widely researched in Japan and is the mainstream of oxide superconductor manufacturing processes. It is possible to oxidize metals easily solely by introducing an oxygen gas together with a sputtering gas. Multi-element systems, however, involve difficulties in optimizing target compositions due to differences in the sputtering rate of adhesion rate according to the elements. The multitarget process using several targets, therefore, has been developed. Films are likely to be damaged by ions or the shock of high-speed particles. Therefore, it is necessary to give due consideration to obtaining layered films of good quality.

The laser ablation process can minimize the difference in composition between the target and film, and is not subject to restrictions by the degree of the surrounding vacuum. This process is also said to be able to lower substrate temperatures (~400°C) This process, however, has not yet been used as a thin film manufacturing process for a sufficient amount of time. Research on the depositing mechanism is still being carried out.

The CVD process requires much time for developing raw materials, such as organic metals. This has caused the commencement of research on oxide superconductors to be delayed considerably compared with other processes. Everyone, however, deems that, if the depositing conditions are optimized, the CVD process is the most suitable for mass production. Its future progress as a layering technology deserves attention.

The vacuum evaporation or MBE process can independently control each element and is advantageous for multielement systems. It is unimaginably difficult, however, to feed oxygen to substrates in a highly vacuum state. Metals cannot be oxidized easily solely by introducing oxygen gas using a tube. It is necessary to ionize oxygen, excite oxygen to radicals, or use more active ozone. Evaporation in a low vacuum state was carried out by raising the oxygen pressure only in the vicinity of the substrate. This process, however, is inconsistent with the philosophy of the MBE process used in an ultrahigh vacuum state.

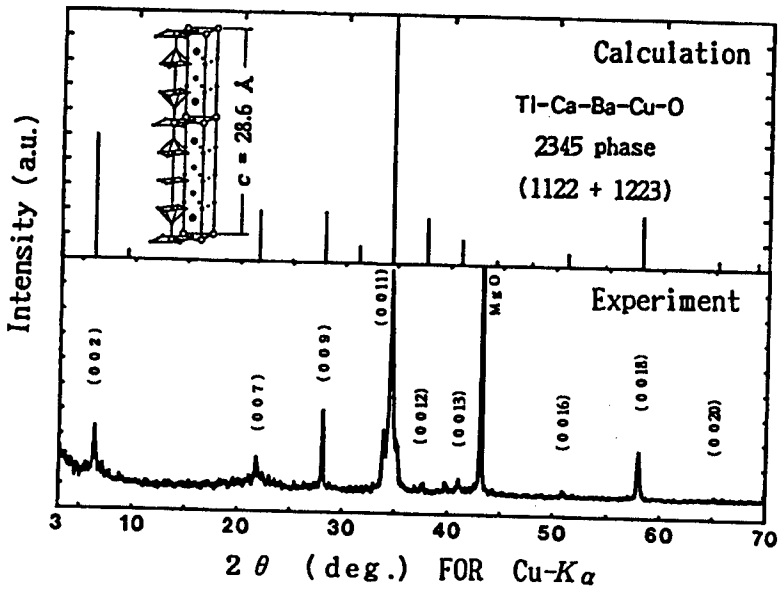

Figure 1. Thallium (Tl)-Based 2 3 4 5 Phase Synthesized by Atomic Layer Control MBE Process

In any event, the final target of these studies is to develop epitaxy technology at the semiconductor level. Is it possible to achieve this target? The success of the development of heteroepitaxy technology, as seen in semiconductor superlattices, depends on whether the substance system concerned can carry out layer-by-layer growth per monatomic layer. It has recently been reported that oxide superconductors grow unit by unit. Someone, however, has doubts about this report, saying that oxide superconductors undergo island growth. However, the preparation of artificial crystals by controlling atomic layers is a dream of researchers. In fact, researchers entered the challenge to prepare artificial crystals using the multitarget process or MBE process in which the shutter is controlled. It has already been discovered that superconducting phases with a new super cycle, as shown in Figure 1, can be synthesized.[1]

3. High-Temperature Superconducting Electronics

The application of metal-based superconducting substances to electronics has to date been confined to very specific fields, as represented by Josephson computers. Josephson devices use macro quantum effects and are thereby provided with excellent characteristics. Josephson devices, however, are substantially diodes (two-terminal devices) and are subject to not a few restrictions for practical application. It can be said that researchers have earnestly desired to develop superconducting transistors (three-terminal devices), superior in characteristics to semiconductor devices.

Table 1. Lattice Constant, Thermal Expansion Rate, and Dielectric Constant Per Material

Material		Crystal system	Lattice constant (Å) a	b	c	Thermal expansion rate (10^{-6}/°C)	Dielectric constant Tc (K)
Super-conductor	La-Ba-Cu-O	Tetragonal	3.779	–	13.171		30
	La-Sr-Cu-O	Tetragonal	3.774	–	13.221	13.8	40
	Y-Ba-Cu-O	Orthorhombic	3.892	3.826	11.68	16.9	94
	Bi-Sr-Ca-Cu-O 2212	Orthorhombic	5.396	5.395	30.643		85
	2223	Orthorhombic	5.396	5.396	37.18		110
	Tl-Ba-Ca-Cu-O 2212	Tetragonal	3.86	–	29.33		110
	2223	Tetragonal	3.85	–	35.66		125
	2234	Tetragonal	3.85	–	42.03		117
	1223	Tetragonal	3.84	–	15.93		116
	1234	Tetragonal	3.85	–	19.11		122
	1245	Tetragonal	3.85	–	22.22		117
Semi-conductor	Si	Cubic	5.43086	–	–	4.2	11.8
	Ge	Cubic	5.65748	–	–	5.8	16
	GaAs	Cubic	5.653	–	–	6.6	10.9
	GaP	Cubic	5.451	–	–	5.9	11.1
	InAs	Cubic	6.095	–	–	5.2	14.5
	InP	Cubic	5.869	–	–	4.8	14.4
	AlAs	Cubic	5.661	–	–	5.2	10.1
	SiC	Cubic	4.358	–	–	3.7	42
	$SrTiO_3$	Cubic	3.905	–	–	11.1	310
	TiO_2	Tetragonal	4.593	–	2.959	9.2	86
	MgO	Cubic	4.213	–	–	14.2	9.65
	YSZ	Cubic	5.139	–	–	10.3	27
	α-Al_2O_3	Triclinic	4.758	–	12.99	7.5	9.34
	BaF_2	Cubic	5.140	–	–	18	
	CaF_2	Cubic	5.4626	–	–	24	6.76
	Quartz	Hexagonal	5.002	–	5.454	0.54	4.5
	$LaGaO_3$	Orthorhombic	5.519	5.494	7.770	12.08	25
	$LaAlO_3$	Hexagonal	5.364	–	13.11		10

The appearance of oxide superconductors has made it possible to use liquid nitrogen as a refrigerant instead of liquid helium. The appearance of oxide superconductors, however, is not confined to such economic advantages. In cooling of semiconductors to 4 K, for example, the carrier loses its thermally excitation (called "freeze"), thus causing the semiconductors to lose their functions. It is known, however, that the cooling of semiconductors to 77 K enables the characteristics to be improved, as can be seen in improved carrier mobility, decreased transistor or sensor noise, etc. This has enabled the establishment of a hybrid combination of semiconductors and superconductors to be achieved. First, it is necessary to prepare a layered structure. To this end, what materials and oxide superconductors should be layered? The combination of appropriate substances is thought to be determined by taking into consideration lattice constants and the thermal expansion rate. Data on oxide superconductors, semiconductors, and insulators have been arranged in Table 1.

The prominent characteristics of oxide superconductors, which differ from those of metal-based superconductors, represent factors attractive for photoelectron spectroscopy. Oxide superconductors have the following characteristics:

(1) The critical temperature is very high.

(2) The upper critical magnetic field is large for a Class 2 superconductor.

(3) Carriers are holes and their concentration is at the level of $10^{21}cm^{-1}$, which is small enough to be comparable to that of highly doped semiconductors.

(4) The energy gap is large enough to be comparable to that of narrow gap semiconductors. (The band gap of semiconductors is in the prill one zone boundary, whereas the superconducting gap is formed on Fermi surfaces.)

(5) The coherence length is very short; it is almost equivalent to the lattice constant.

(6) Substantial electrical, magnetic, and optical anisotropy can be observed.

(7) Oxide superconductors are multielement system compounds and change their shape from insulators to superconductors according to small changes in composition.

How should these characteristics be utilized to create new functions and thereby to achieve the development of devices with new functions? This is an interesting subject for the future development of high temperature superconducting electronics.

4. Layering Involving Insulators

Is it possible to prepare Josephson junctions using oxide superconductors? This is of major concern to those who are engaged in research in the application of oxide superconductors to electronics. It is well known that microcracks and crystal grain boundaries formed in specimens behave as a sort of Josephson junction. To prepare Josephson devices and integrate them, it is indispensable to achieve layered Josephson junctions with uniform characteristics. When the thickness of one layer becomes almost equivalent to the coherence length, Josephson effects will be observable in layered SIS junctions. As for oxide superconductors, however, this is extremely difficult due to characteristic (5) above.

Major materials being currently studied as I [insulator] layers are given in Table 1. here, a somewhat specific example is introduced. Upon its discovery, a YBCO-based superconducting substance was reported to be green. This green colored substance is an insulator phase with a composition of Y_2BaCuO (211) and

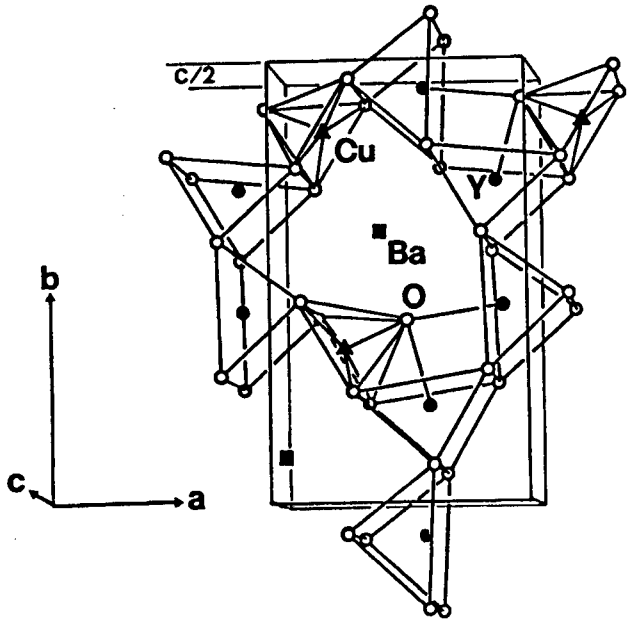

Figure 2. Crystal Structure of Y_2BaCuO_5 Insulating Phase[2,3]

differs from the black-colored superconducting phase $YBa_2Cu_3O_{7-\delta}$ (123). The 211 had already been discovered when 123 was discovered. It is known that 211 has the crystal structure shown in Figure 2.[2,3] Is it possible to form 211 phases into I layers? This is one idea.

There is a peritectic relationship between 211 and 123 in an equilibrium drawing. Crystals separated into two phases are stable thermodynamically. Although 211 and 123 have the same constitutive elements, their relationship can be said to be similar to that of water and oil. Therefore, if crystals are annealed, even after the preparation of a SIS structure, their interfaces become smoother and sharper. It can be expected, therefore, that pinholes, if they exist, are closed. When dissimilar materials are formed into an I layer, they are not permitted to be annealed in view of the mutual diffusion on the interface.

The results of 211 thin films prepared by the magnetron sputtering process are shown in Figure 3.

It has been confirmed that 211 thin films can be grown successfully on magnesia (MgO) substrates and 123 thin films. The crystal orientation of the 211, however, differs between that grown on magnesia substrates and that grown on 123 thin films, i.e., (101) and (041), respectively. This is thought to arise due to the lattice constant differences between magnesia and 123. Further discussions may be required to confirm that thin films were grown epitaxially. We have successfully reduced the thickness of the I layer to about 100 Å, and have also confirmed that the dielectric strength can be significantly improved, as had been estimated by annealing.

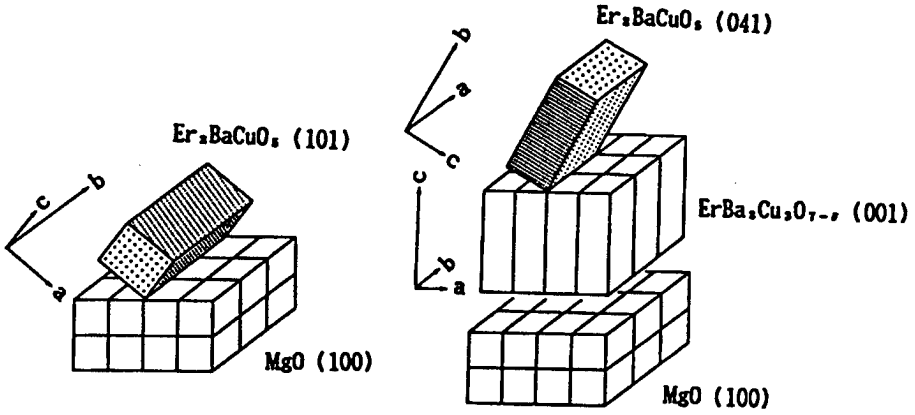

Figure 3. Crystal Orientation Relationship Between Y_2BaCuO_5 on a Magnesia Substrate and U_2BaCuO_5 on a $YBa_2Cu_3O_{7-\delta}$ Thin Film

5. Semiconductor Layering

Extremely high-quality and inexpensive silicon (Si) wafers are used as substrates to form superconducting thin films. This process is currently being widely studied. The lattice constant of silicon is quite close to that of superconducting thin films and, therefore, epitaxial growth was expected. However, as was made clear quite long ago, this involves several problems. In other words, 1) if the substrate temperature is raised, silicon is easily diffused into superconducting thin films. As a result, the superconductivity of the thin films is lost; 2) there is a large difference in the thermal expansion rate between superconductors and semiconductors. Microcracks, therefore, occur during cooling after the formation of thin films; and 3) silicon is likely to be oxidized and insulating SiO_2 is formed on the interface. In other words, silicon restores oxide superconductors and breaks their superconductivity. It is necessary, therefore, to use the process at lower temperatures (600°C or less), sandwich a buffer layer between interfaces, etc.

Experiments involving the formation of semiconductor thin films on superconductor thin films have just been started. Kobayashi, et al., of Osaka University indicated the possibility that germanium (Ge) could be grown epitaxially on YBCO thin films, and conducted experiments. Rare metal-based superconductors, however, involve problems with orthorhombic-tetragonal transition due to the lack of oxygen. It is also necessary to grow thin films at low temperatures, ranging from 200~250°C, to prevent mutual diffusion. Kobayashi, et al., therefore, have not yet successfully realized epitaxial growth. Later, bismuth-based superconductors (Bi-Sr-Ca-Cu-O), resistive to the lack of oxygen, were discovered, and research entered a new phase. Table 2 presents the lattice mismatching between bismuth-based superconductors and major semiconductors.

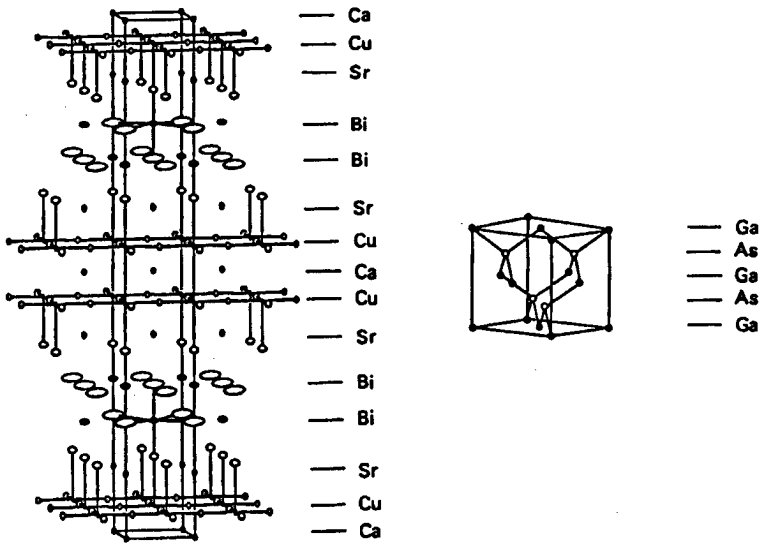

Figure 4. Crystal Orientation in Which the Lattice Between the Bismuth-Based Superconductor and Gallium Arsenide Matches

Table 2. Lattice Mismatching Between Bismuth-Based Superconductors and Semiconductors

	Ge	Si	GaAs	GaP	InAs	AlAs
Mismatching (%)	4.8	0.65	4.8	1.0	1.3	4.9

Gallium arsenide (GaAs) is layered on bismuth-based superconductors. This represents a new concept. The crystal orientation in which the lattice between the bismuth-based superconductor and GaAs matches is shown in Figure 4. GaAs, a compound semiconductor, plays a vital role in practical application. Therefore, the low-temperature growth technology using MBE, etc., has been well established for GaAs. However, even if GaAs is oxidized, good-quality insulators, such as SiO_2, cannot be obtained. This has so far made it impossible to manufacture MOS transistors with good characteristics and difficult to carry out planar integration. These features, however, may have advantageous effects on the layering of oxide superconductors and semiconductors. This is the aspect of this idea that we must consider.

Figure 5 shows the superconducting characteristics of a substrate bismuth-based layer before and after GaAs is deposited.

The bismuth-based superconducting layer[5] was the so-called "low-temperature phase (2212 phase)" and, therefore, the zero resistance temperature remained about 83 K. It should be noted here that the zero resistance temperature of the substrate superconducting layer rose from 71 K to 83 K after GaAs was layered. There is fairly good strategy in this respect.

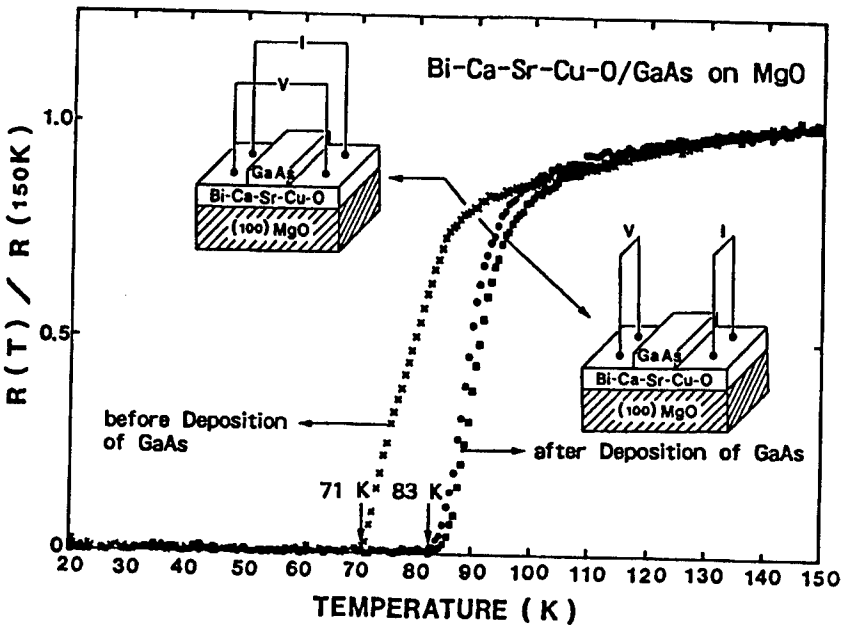

Figure 5. Superconducting Characteristics of Substrate Bismuth-Based Layer Before and After GaAs Is Deposited

It is known that there is a relationship, such as that shown in Figure 6, between the critical temperature (T_c) and oxygen composition in bismuth-based superconductors. In other words, there is an optimum oxygen composition that results in the highest T_c. The T_c decreases if the oxygen composition either exceeds or is lower than this optimum oxygen composition.

It has already been made clear that the characteristics of superconducting layers deteriorate chiefly due to the lack of oxygen caused by heating substrates during deposition. The strategy[6] is to supply the superconducting layer with an excessive amount of oxygen before deposition.

Figure 7 shows the results of X-ray diffraction of the above deposited films. When the substrate temperature was 450°C, deposited films demonstrated the most satisfactory crystallinity. The figure shows that when bismuth-based monocrystals were used for the substrate, GaAs was beautifully oriented (111). It is estimated, however, that the (100) orientation results in good lattice matching. This should be deemed a natural orientation.

6. Planar-Type SNS Junction

Planar-type SNS junctions can achieve Josephson junctions more simply than can layering sandwiched structures. In other words, a superconducting microbridge, in which microscopic grooves are cut, is prepared, and a metal or a semiconductor is layered on the microbridge. This process requires the application of the layering process only once, but necessitates the use of lithographic technology with a high resolution. The microscopic processing technology

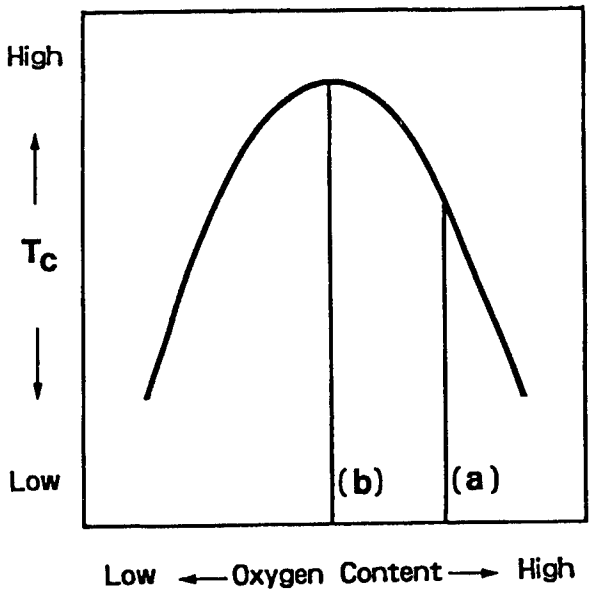

Figure 6. Relationship Between Critical Temperature (T_c) and Oxygen Composition in Bismuth-Based Superconductor

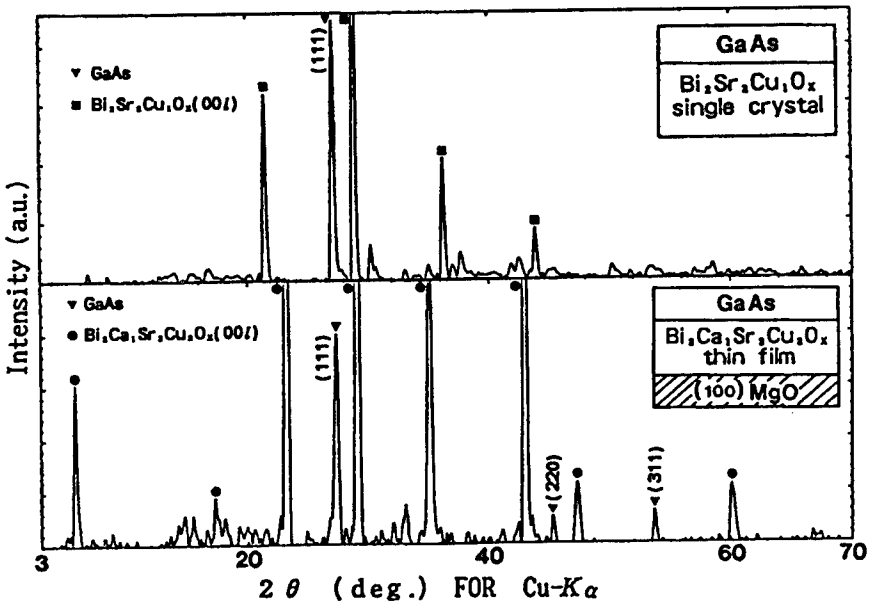

Figure 7. X-Ray Diffraction Pattern of Bismuth-Based Superconductor/Gallium Arsenide Deposited Film

already developed in the semiconductor field has reached the 0.1 μm (maximum) level. SIS junctions, however, cannot yet be prepared by such technology. Meanwhile, the characteristics of SNS junctions using proximity effects are determined by the coherence length of the N layers. The use of general metals or semiconductors as N layers, therefore, is likely to achieve SNS junctions.

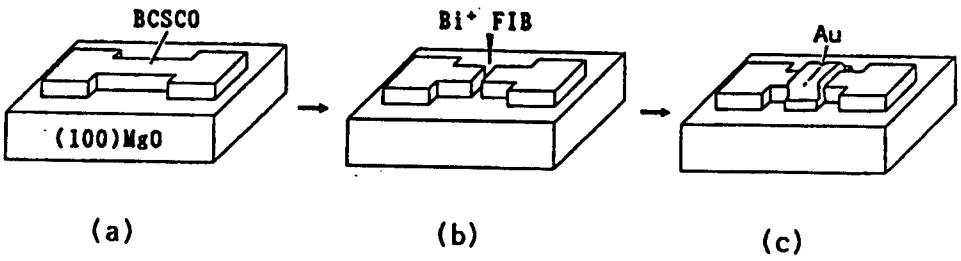

Figure 8. Planar SNS Junction Preparation Process
(a) Bismuth-based thin film formation
(b) Gap etching
(c) N layer evaporation

Is it possible to apply the microscopic semiconductor processing technology to oxide superconductors without modifications? Using focused ion beam (FIB), planar SNS junctions were manufactured on a trial basis and an example of this trial experiment is introduced here. The use of FIBs[7] allows a processing accuracy of the 0.1 μm level to be maintained. Superconducting thin films around the portion being processed, however, are damaged by ion beams during processing; this causes areas to appear in which superconductivity has been lost. If such areas are annealed, they can restore the lost superconductivity. In this case, however, elements used as ions diffuse as impurities. The necessary measure to be taken here is to process bismuth-based superconducting thin films using bismuth ions (Bi^+) as the FIB.

Can an element be used as an FIB? This question depends on whether the liquid metal ion source can be prepared by the metal or the alloy. The melting point of the metals or alloys must be comparatively low and the steam pressure must not be very high. These are major requirements. Bismuth completely satisfies these requirements and does not become an impurity in bismuth-based superconductors. Figure 8 shows the planar SNS junction preparation process using the said technique.

A groove of about 0.2 μm in gap width was etched at the microbridge portion using Bi^+ FIBs, then an N layer was evaporated on the etched groove. Gold (Au) was used for the N layer in this example. GaAs, etc., can be thought of as prospective N layer materials. In particular, semiconductors are larger in coherence length than metals and their carrier concentration can be controlled. Semiconductors, therefore, may have a larger range of application. Although there are many problems to be resolved in the future, current-voltage characteristics, as shown in Figure 9, have already been obtained.

7. Future Outlook

It is very difficult to estimate the future of "seeds" searching-type research, like that involving high temperature superconductors. New substances with higher critical temperatures may be discovered. New uses that have not yet been envisioned may be found suddenly. It is important, however, to proceed with research on thin films and layering for the following two reasons.

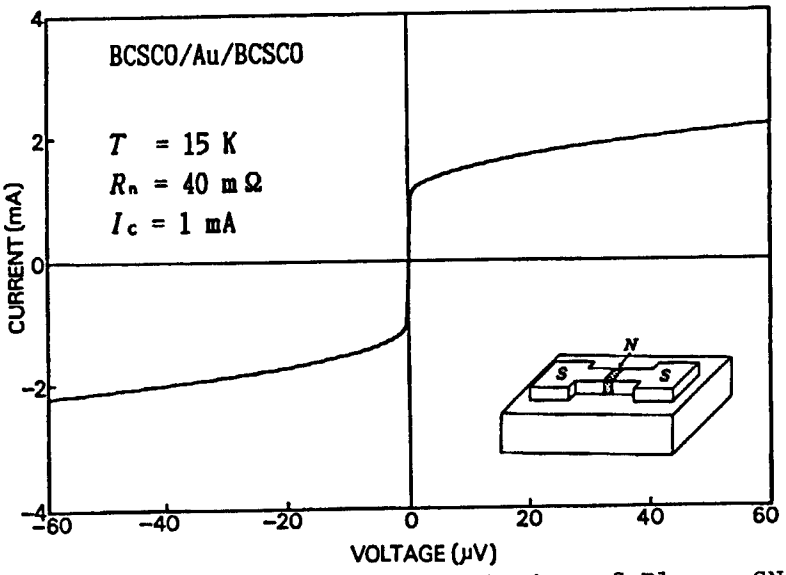

Figure 9. Current-Voltage Characteristics of Planar SNS Junction

On the basis of atomic layer control epitaxy concepts, new substances are being synthesized on a trial basis. This attempt may provide guidelines for the search for new substances. Further, it can be expected that unknown quantum effects will be discovered, with layered structures serving as probes. In the latter case, the preparation of Josephson junctions can be said to be the hurdle that researchers must first jump over.

It has become possible to use superconductors and semiconductors within the same temperature region. This is the most important concept when applying superconductors to electronics. Two types of substances, that were respectively thought to represent a phenomena in different regions, have come to be bonded to each other via the liquid nitrogen temperature. Compared with semiconductor technology, superconducting technology has only specific applications. This general concept appears to have so far exercised great influence. This is because superconductors are accompanied by a handicap, that is, the absolute necessity for cryogenic temperatures. Meanwhile, the appearance of high temperature superconductors does not eliminate the necessity for cooling. The critical temperature has become much higher and, therefore the currently available refrigerating technology can fully comply with the requirements. For example, it is possible to cool microcomputer chips easily at home using a refrigerator that is equivalent to an outdoor airconditioning unit. As refrigerators become further miniaturized, the bonding of oxide superconductors to semiconductors will certainly develop more attractive and new electronic fields.

References

1. Furukawa, H. and Nakao, M., "Proc. Tsukuba Seminar on High T_c Superconductivity," 1989, pp 155–160.

2. Michel, C. and Raveau, B., J. SOLID STATE CHEM., Vol 43, 1982, p 73.

3. Hazen, R.M., Finger, L.W., Angel, R.J., Prewitt, C.T., Ross, N.L., Mao, R.K., and Hadidiacos, C.G., PHYS. REV., Vol B35, 1987, p 7238.

4. Nemoto, M., Matsuta, Y., Yuasa, R., and Nakao, M., "Proc. Int. Superconductivity Electronics Conf.," 1989, pp 24–27.

5. Nakao, M., "Ext. Abs. 6th Int. Workshop on Future Electron Devices," 1989, pp 411–414.

6. Kuwahara, H. and Nakao, M., "Proc. Int. Superconductivity Electronics Conf., 1989, pp 28–31.

7. Fujiwara, S., Yuasa, R., Kuwahara, H., Nakao, M., and Suzuki, S., "Proc. 2nd Int. Symp. on Superconductivity," 1989, in press.

Thin Films for Optical Applications

916C1001I Tokyo HYOMEN KAGAKU SEMINA in Japanese 27-29 Jun 90 pp 107-123

[Article by Keichi Tanabe, NTT Electronic Application Research Laboratory]

[Text] **1. Introduction**

Josephson devices composed of superconducting thin films show phenomena peculiar to macro quantum effects, such as photon induced tunneling, the appearance of shapiro steps, and nonequilibrium phenomena due to interaction with electromagnetic waves. The use of these phenomena may result in achieving the development of electromagnetic wave detection devices that are superior to conventional semiconductor detection devices in a wide wavelength region ranging from microwaves to X-rays. This has already been demonstrated in the devices using low T_c superconductors. Josephson devices, however, are currently being used only for superconductor-insulator-superconductor (SIS) quasi-particle mixers in electric wave astronomy due to cooling problems. The appearance of high temperature superconductors, however, may resolve problems involved with cooling using liquid helium and may also improve the device performance. It can be expected that the application field of electromagnetic wave/photoelectric detection devices will be expanded rapidly.

In this paper, we first describe the principles and features of various types of detection devices using superconductors, introduce the current status of research aimed at the application of high temperature superconducting thin films, and then discuss problems involving materials and thin films. In the latter half of this paper, we introduce in detail the latest results of our research on detection devices using nonequilibrium phenomena.

2. Type and Features of Electromagnetic Wave/Photoelectric Detection Device Using Superconducting Thin Films

2.1 Classification

Figure 1 shows the classification of electromagnetic wave/photoelectric detection devices using superconductors and the current status of major studies, mainly being conducted in Japan.

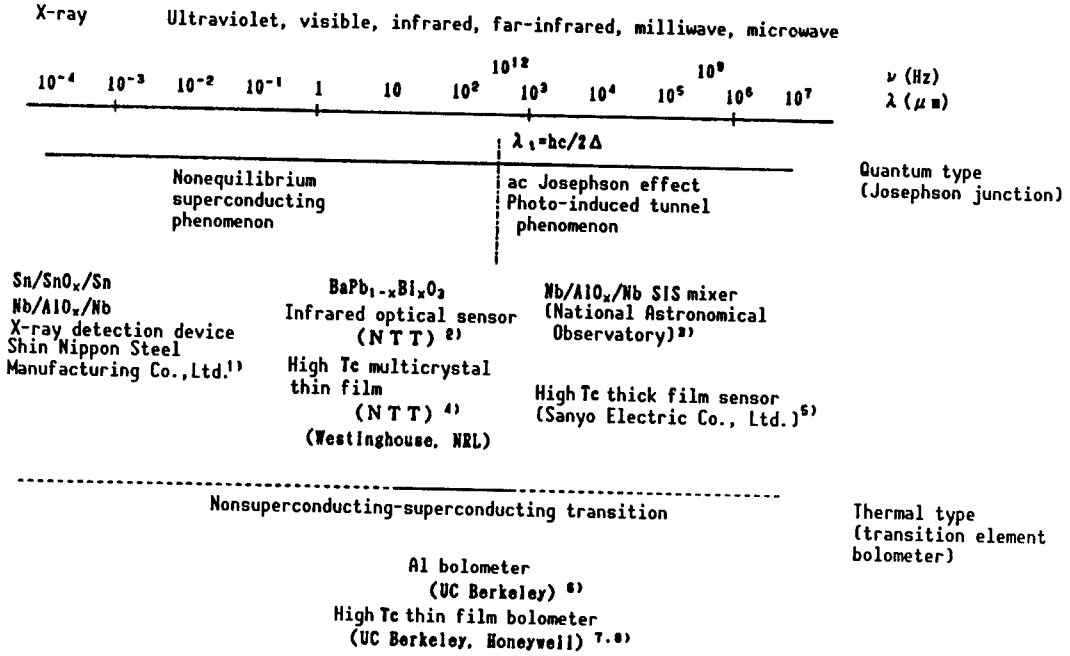

Figure 1. Classification of Electromagnetic Wave/Photoelectric Detection Devices

As is the case with semiconductor detection devices, superconductor detection devices can be classified roughly into two types, that is, the thermal type that detects rising thin film temperatures by irradiating electromagnetic waves, and the quantum type that uses carrier (quasi-particles in superconductors) excitation and Josephson effects.

The mainstream of the thermal type involves utilizing rapid changes in the electric resistance of thin films near the superconducting transition temperature. This is referred to as a "transition-edge bolometer." This type device is not superior to the quantum-type device, but exhibits comparatively high sensitivity; the sensitivity demonstrates little wavelength dependence. The response speed is generally slow.

Quantum-type devices can be further classified into two types according to the relationship in magnitude between the photon energy ($h\nu$) detected and the superconductor gap energy (2Δ). In $h\nu<2\Delta$, that is, in the long wavelength region, quantum effects peculiar to Josephson devices, such as photon induced tunnel phenomenon and the appearance of shapiro steps, can be used to detect responses. This type of device makes it possible to mix frequencies, demonstrating ultrahigh-speed response. Therefore, it may be applied to the communications field. Meanwhile, on the short wavelength side, i.e., $h\nu>2\Delta$, Cooper pairs (superconducting electron pairs) in superconductors break due to the absorption of photons, thereby producing quasi-particles. As a result, nonequilibrium phenomena occur. The quantum type devices are used to detect such phenomena. This type of device enables responses to be photoelectrically detected at high sensitivities and comparatively high speeds of 1 ns or less

by selecting appropriate device materials. The wavelength ($\lambda t = hc/2\Delta$) at the boundary between the two types was 200~600 μm (ν~1 THz) for low T_c superconductors, while it was 30 μm (ν~10 THz) for high temperature (90 K class) superconducting materials. Thus, the wavelength shifted by about one digit on the short wavelength side.

The individual detection devices are described below in detail.

2.2 Thermal Type Device (Transition-edge bolometer)

Transition-edge bolometers are of a basic structure, in which an electromagnetic wave absorber and superconducting thin films (used to detect changes in temperature) are connected by thermal conductivity G in a hot bath at a temperature T_0 that is lower than T_c. As absorbers, superconductors or nonsuperconducting metals (Bi, etc.) are used. The latter is called the "complex type." In order to operate bolometers at the T_c, the design is carried out in such a manner that the relationship $G = P_{IR}/(T_c-T_0)$ can be satisfied. P_{IR} is the background radiation power irradiated by the bolometers and is given by the Planck radiation formula. The bolometer sensitivity, S, can be represented as follows:

$$S = \frac{I_B R \alpha \eta}{G(1+\omega^2\tau^2)^{1/2}} \qquad (1)$$

where I_B = bias current
R = resistance of superconducting thin film at T_c midpoint
η = absorptivity of electromagnetic waves
ω = chopping frequency
τ = bolometer response time

If the heat capacity of the absorber and superconducting thin film is assumed to be C, the following equation can be given.

$$\tau = C/G \qquad (2)$$

Further, $\alpha = d \ln R(T)/dT$ is the variation rate of resistance arising from the temperature. In the case of superconductors, this variation rate is approximated as $\alpha \sim (\delta T_c)^{-1}$. δT_c is the transition width of the electric resistance. Good-quality high temperature superconducting thin films show a δT_c of about 2 K and the variation rate becomes $\alpha \sim 0.5\ K^{-1}$. α as measured by the bolometer using nonsuperconducting metals such as Bi is on the order of 10^{-3} at the highest. This shows that transition-edge bolometers make it possible to obtain sensitivities that are higher by two digits or more than those of bolometers using nonsuperconducting metals.

Complex-type bolometers using Al with T_c = 1.3 K have already been developed as transition-type bolometers using low T_c superconductors.S6 The following performance has been reported:

- Equivalent noise power
  (NEP = Vn/S; Vn = noise voltage): 1.7×10^{15} $WHz^{-1.2}$
- Response time: 83 ms

However, since there is no large difference in sensitivity between the complex-type bolometers and semiconductor bolometers cooled to the same temperature, they are not currently being used.[9]

Meanwhile, after the discovery of high-temperature Y-based superconductors, Richards, et al., of the University of California estimated the performance of transition-edge bolometers which used Y-based superconducting materials. Then, they emphasized that these bolometers are superior to conventional detection devices in the far-infrared ray region of $\lambda > 13$ μm.[7] The NEP of a transition-edge bolometer can be represented as follows.

$$NEP = (NEP_{phot}^2 + NEP_{phon}^2 + NEP_{John}^2 + NEP1/f^2 + NEP_{amp}^2)^{1/2} \quad (3)$$

The first through third terms are the contribution of photon noise, phonon noise, and Johnson noise from the respective backgrounds. The fourth term is the contribution of thin film 1/f noise. In the multicrystal thin film of high temperature superconductors, magnetic flux quantum trapped by crystal grain boundaries move in a hopping manner due to bias current, etc., thereby producing a large amount of 1/f noise. This phenomenon has already been reported.[10] It has also been made clear that this 1/f noise can be greatly reduced by using high quality c-axis oriented films. The fifth term is the distribution of the amplifier noise, which can be disregarded at temperature equivalent to 90 K. According to their studies, it is possible to design conductance G on a smaller side by selecting substrate materials whose heat capacity is small, thereby controlling the contribution of the phonon noise and 1/f noise to the same level as that of the Johnson noise. For example, a $SrTiO_3$ substrate with an area of 1 x 1 mm^2 and a thickness of 20 μm shows C~20 $\mu J/K$. In this case, 2.2×10^{-11} $WHz^{-1/2}$ was obtained as NEP. An ideal case using Si and BN membranes shows C~0.1 $\mu J/K$ and, therefore, a NEP of approximately 1.3×10^{-12} $WHz^{-1/2}$ can be expected (Richards, et al.). Figure 2 compares the estimated specific detection capacity D^* ($= A^{1/2}/NEP$) of a high T_c bolometer with that of the conventional type detector.[11]

In the $\lambda > 20$ μm region, optical conduction type semiconductor detection devices exhibit sensitivity as high as those used after being cooled to temperatures of about 4.2 K or lower. There are no good detection devices that operate at temperatures exceeding 4.2 K. High T_c bolometers are expected to demonstrate sensitivities in the said region, which are higher by at least one digit than those of pyroelectric sensors operating at room temperature.

U.S. research institutes have recently reported the manufacture of high T_c transition-edge bolometers. Stratton, et al., of Honeywell Inc., for example, grew $DyBa_2Cu_3O_y$ thin films (by the reactive evaporation process) on a substrate obtained by depositing Si_3N_4 and YSZ as a buffer layer on an Si wafer. Then, they removed Si from the light reception portion by etching and manufactured thermally isolated bolometers with small C and G. They obtained a sensitivity of S~800 V/W and τ~1 ms, but have not reported on the NEP.[8]

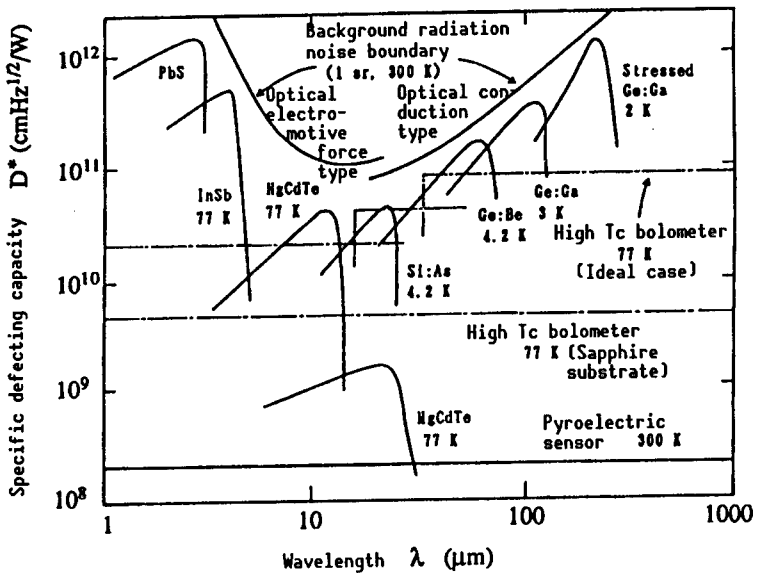

Figure 2. Comparison of Estimated Specific Detection Capacity of High T_c Bolometers With Specific Detection Capacity of Conventional Detection Devices

The response speed of bolometers is generally slow. The volume of the substrate thermally linked with thin films decreases by reducing the size of the light reception portion. As a result, it is possible to make fast response speeds compatible with high sensitivity. In this case, both C and G become smaller. However, since C and G are scaled by raising size L to the third power and the first power, respectively, the cutoff frequency f_c (=G/C) increase is inversely proportional to the second power of L, i.e., the area. This concept regarding micro bolometers has already been applied to bolometers that use Bi and are operated at room temperature.[12] Richards, et al., recently predicted the performance of micro bolometers using high temperature superconducting thin films.[13] They have assumed 5 x 1 x 0.02 μm^3 as the size of the bolometer thin film. A lens made of, for instance, Teflon, and Bow-Tie and Spiral antennas are used to effectively couple electromagnetic waves to bolometers, which are smaller than the electromagnetic wavelength. Although the characteristics of thin films depend greatly on the substrate materials, they have estimated the following values:

- For MgO substrates capable of easily forming high-quality thin films:

  $f_c = 2.6 \times 10^8$ Hz
  NEP ($f \ll f_c$) ~$4 \times 10^{-11} WHz^{-1/2}$

- For YSZ substrates with lower thermal conductivity:

  $f_c = 8.6 \times 10^5$ Hz
  NEP ~2.5×10^{-12} $WHz^{-1/2}$

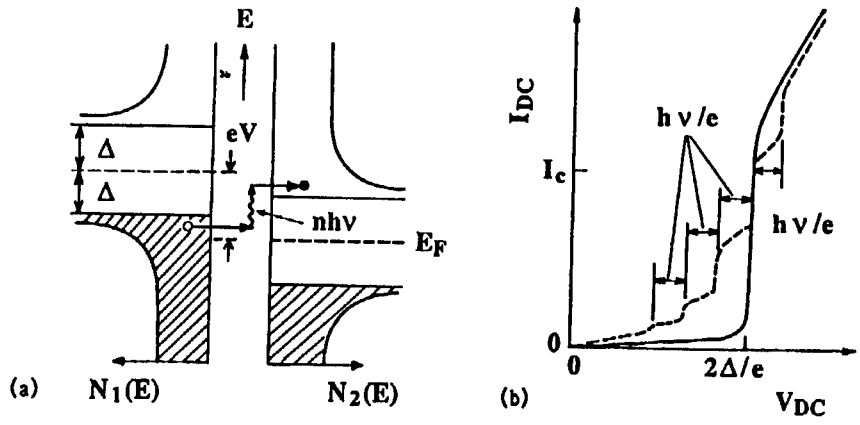

Figure 3. Energy Drawing Indicating Tunneling Process in SIS Tunnel Junction and Current Voltage Characteristics

Micro bolometers can be arrayed easily. They can also be operated at high frequencies that are not affected by the 1/f noise. However, the bias current density necessary to achieve high sensitivity S becomes $10^6 A/cm^2$ or larger. Therefore, the use of high-quality (high J_c) thin films capable of firmly pinning magnetic flux is thought to be indispensable.

2.3 Quantum Type Device (SIS quasi-particle, Josephson detection device)

Figure 3 shows the energy conditions and current-voltage characteristics of a superconductor-insulator-superconductor (SIS) type tunnel junction, in which two superconducting thin films are separated from each other using an extremely thin (1~2 nm) insulation layer barrier.

In the superconducting state, electrons form Cooper pairs, and an energy gap of 2Δ is formed at the Fermi level. At a bias voltage of $V < 2\Delta/e$, only a small number of quasi-particles (nonpair electrons), which are thermally excited, tunnel the junction and, therefore, only little current flow. At a voltage of $2\Delta/e$, quasi-particles (formed as a result of the Cooper pairs having been broken) tunnel the junction in large quantities and, therefore, the current increases rapidly. As a result, large nonlinear current-voltage characteristics appear, as shown in (b). If photons are irradiated to the tunnel junction, energy equivalent to n number of photons is given to the tunnel junction, even at a bias voltage of $2\Delta/e$ or smaller. Then, quasi-particles tunnel the junction. This is called the "photon induced tunnel phenomenon." The current-voltage characteristics undergo modulation, as indicated by the broken lines in (b). In other words, steps appear on both sides of the gap voltage at intervals of $h\nu/e$.

Therefore, if the application of a fixed amount of bias current to the tunnel junction is maintained, changes in voltage can be observed by irradiating photons, and so-called "video detection" can be carried out. In addition, it is possible to carry out the mixing (heterodyne detection) of electromagnetic waves using a marked modulation of current-voltage characteristics. This SIS quasi-particle mixer can obtain conversion gains from signal frequency to

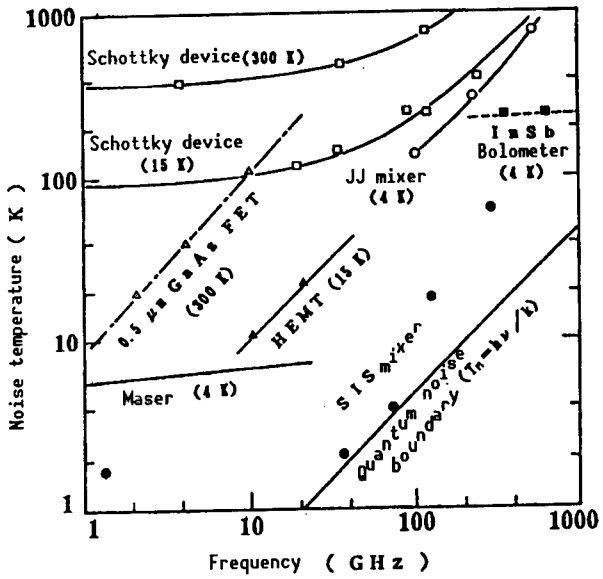

Figure 4. Frequency Dependence of Equivalent Noise Temperature of Various Mixers and Detection Devices

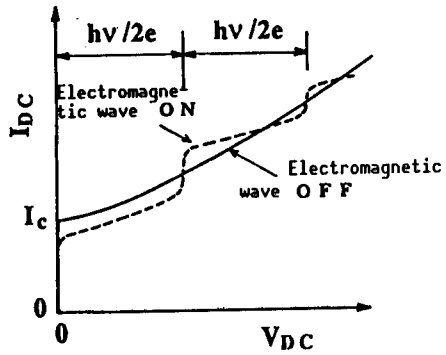

Figure 5. Changes in Current-Voltage Characteristics of Weakly Coupled Josephson Device Due to Irradiation of Electromagnetic Waves

intermediate frequency thanks to the quantum effect. This mixer is also characterized by extremely low noise. Figure 4 shows the frequency dependence of the equivalent noise temperature (temperature when noise is assumed to be equivalent to the thermal noise arising from the input resistance of the mixer) of various types of mixers and detection devices.[14]

SIS quasi-particle mixer noise is low to the extent that it nearly corresponds to the quantum noise boundary ($T_M = h\nu/k_B$) at 100 GHz or lower frequencies, based on the quantum mechanical uncertainty of incident photons. SIS quasi-particle mixers are the best detectors in the extremely high frequency band and have been put to practical use for the observation of space electric waves. In Japan, mixers using $Nb/AlO_x/Nb$ tunnel junctions have been developed and are being used at the National Nobeyama Astronomical Observatory.[3]

Meanwhile, changes in the current-voltage characteristics of a Josephson weakly coupled device (whose superconductivity was weakened by very finely processing a part of the superconducting thin films) due to the irradiation of electromagnetic waves are shown schematically in Figure 5.

Under the limited voltage state, an ac supercurrent of $\nu_j = 2eV_{DC}/h$ in frequency flows. If electromagnetic waves (frequency ν_s) are irradiated, due to the synchronization effect, dc current steps (shapiro step) occur at the bias voltage that satisfies $\nu_j + n\nu_s = 0$. The use of this effect makes it possible to carry out video detection and heterodyne detection (mixing). As shown in Figure 4, the noise temperature of Josephson mixers is considerably higher than that of SIS quasi-particle mixers. This is because the noise

component in a high frequency region, mixed with locally sent electric waves and their harmonics and also Josephson sent electric waves, appears as intermediate frequency band noise. This mechanism is called "noise down conversion." (SIS mixers can control this mechanism by the junction capacity.[15]) However, Josephson mixers are small in capacity compared with SIS mixers and, therefore, can respond to electromagnetic waves with higher frequency. In other words, Josephson mixers are characterized by the fact that they can respond at ultrahigh speed (high band). The cutoff frequency of Josephson mixers can be given by the following equation:

$$f_c = 2eRI_c/h,$$

where R = nonsuperconducting resistance of device
I_c = maximum dc Josephson current

I_cR products are proportional to energy gap Δ. Therefore, it is expected that mixers capable of responding to frequencies (~10 THz) that are higher by one or more digits than can be handled by conventional detection devices can be developed by applying high temperature superconductors.

No studies have yet been conducted on the application of high temperature superconductor to SIS quasi-particle detection devices since high-quality tunnel junctions have not yet been achieved. Difficulties in the manufacture of junctions arise from characteristics peculiar to high temperature superconductors, such as extremely short coherence length, surface instability, and layered structure. It is a major project to establish a method for selecting and forming tunnel barrier materials that are free from pinholes and do not involve changes in the surface chemical conditions.

Meanwhile, the crystal grain boundaries of high temperature superconductors multicrystal thin films show weak bonding characteristics. The application of such multicrystal thin films to Josephson-type detection devices, therefore, has been studied from early on. Sobolewski, et al., reported on video detection and heterodyne detection at 77 K using a $YBa_2Cu_3O_y$ (YBCO) multicrystal thin film (3 x 1 mm) with low J_c, which was prepared by the magnetron sputtering process.[16]. The results of studies conducted in Japan concerning detection devices using YBCO films (prepared by the coprecipitation process) have indicated that highly sensitive mixing can be carried out at the 20 GHz band.[5] Studies are also being conducted concerning the response to ultrahigh frequencies, which is aimed at application to communications (e.g., inter-satellite) at the THz band. For example, it has been confirmed that an Nb point contact junction formed on YBCO thin films (prepared by the chemical vapor deposition (CVD) process) shows shapiro steps when electromagnetic waves (far infrared rays) of 1.29 THz (λ = 233 μm) are irradiated.[17] How can the superiority in characteristics (noise and gain) of Josephson mixers (using high temperature superconducting materials) over other detection devices be proved in the 100 GHz and smaller bands? This is a subject to be resolved. Another major topic appears to be the establishment of the technology for preparing high-quality weak coupling type devices with low capacity and large I_cR product at ultrahigh frequency bands of more than several hundred GHz.

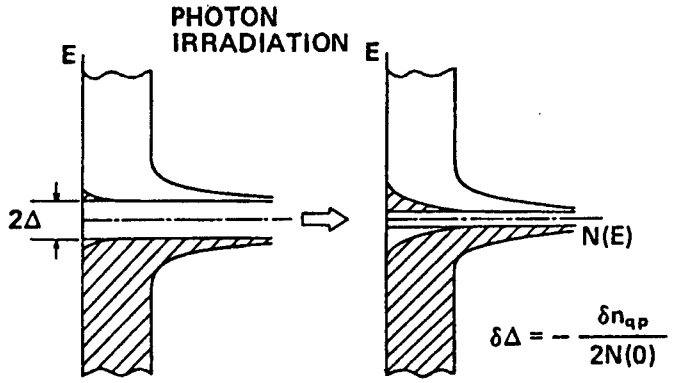

Figure 6. Energy Phase Diagram of Nonequilibrium Phenomena

2.4 Nonequilibrium Device

Figure 6 is a conceptual drawing explaining the principle of detection by nonequilibrium devices.

If photons with energy larger than a gap energy of 2Δ are incident on superconducting thin films, Cooper pairs are broken, and electron-shaped and hole-shaped quasi-particles are thus formed in large quantities. These quasi-particles lose energy due to inelastic scattering with other quasi-particles and lattice defects, the release of phonons, etc., and are relaxed to the gap edge. Then, they are recombined with each other and become Cooper pairs. The process from excitation to recombination requires a period of 1 ps to 1 ns. Therefore, the density of quasi-particles in thin films irradiated with photons exceeds that of the quasi-particles thermally excited in an equilibrium state. Such a state offset from the equilibrium state is referred to as a "nonequilibrium state." In such a nonequilibrium state the gap energy value decreases. This is because the gap energy has become an order parameter for the phase transition phenomenon termed "superconductivity," which differs greatly from semiconductors. The gap variation can be approximated by means of the following equation:

$$\delta\Delta = \frac{-\delta n_{qp}}{2N(0)} \tag{4}$$

where δn_{qp} = excessive quasi-particle density
$N(0)$ = state density (value in a nonsuperconducting state) at the Fermi level
$2n(0)\Delta$ = density of Cooper pairs

A certain number of Cooper pairs existing in an equilibrium state are broken by the light irradiation and turned into quasi-particles. The right side of equation (4) corresponds to the rate of Cooper pairs thus broken and turned into quasi-particles.

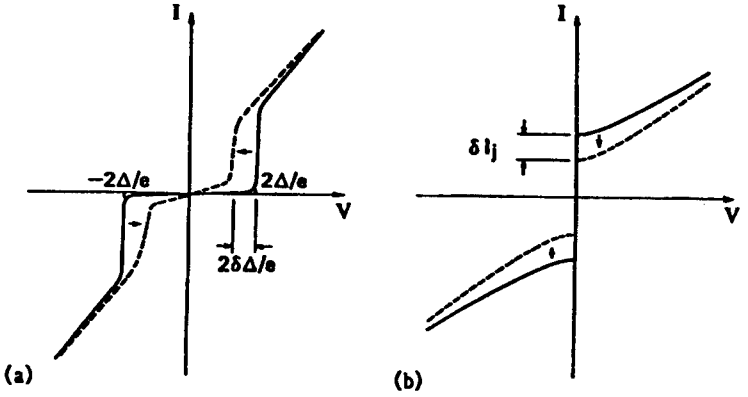

Figure 7. Changes in Current–Voltage Characteristics of Tunnel and Weakly Coupled Josephson Device in Nonequilibrium State

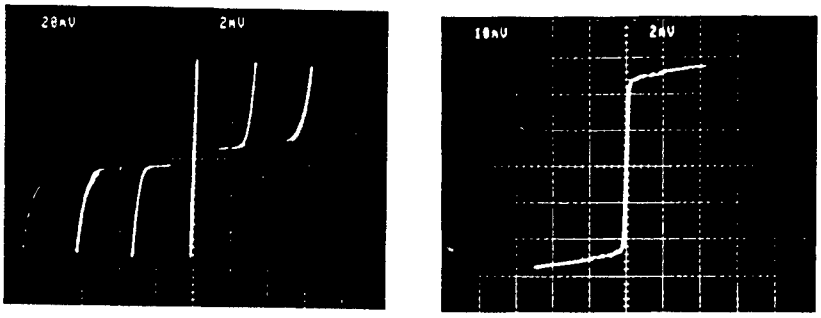

Figure 8. Current–Voltage Characteristics (the axis of abscissas: 2 mV/div.) Observed for Constricted Structure Using a $BaPb_{0.75}Bi_{0.25}O_3$ Multicrystal Thin Film

The gap energy decreased by light irradiation can be detected easily using Josephson junctions. For example, the current–voltage characteristics of the tunnel junction shown in Figure 7(a) change like the wave lines. Decreases in gap energy, therefore, can be detected as changes in voltage if the application of a constant bias current is maintained. Meanwhile, in weakly coupled devices, there is a proportional relationship, i.e., $I_c = \pi\Delta/2eRn$, between the dc Josephson current I_c and gap energy. Decreases in gap energy, therefore, appear as decreases in I_c and can be detected as changes in voltage if a constant bias current is continuously applied to the junction.

It has been discovered that devices using $BaPb_{0.75}Bi_{0.25}O_3$ multicrystal thin films show high sensitivity and high-speed response to infrared light. As a result, the usefulness of nonequilibrium devices has been made clear for the first time.[2] $BaPb_{0.75}Bi_{0.25}O_3$ (BPBO) is a perovskite type oxide superconductor which is a leading high temperature superconducting material, exhibiting a T_c of about 13 K. For example, thin films prepared on a sapphire substrate by the magnetron sputtering process using a sintered target are composed of multicrystals whose average particle size ranges from 200~300 nm. If a constructed

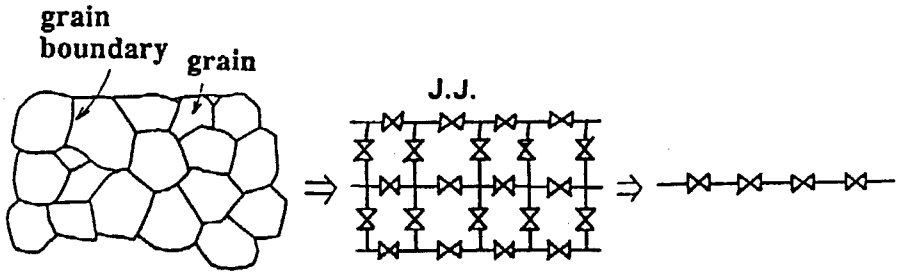

Figure 9. $BaPb_{0.75}Bi_{0.25}O_3$ Multicrystal Thin Film Equivalent Circuit

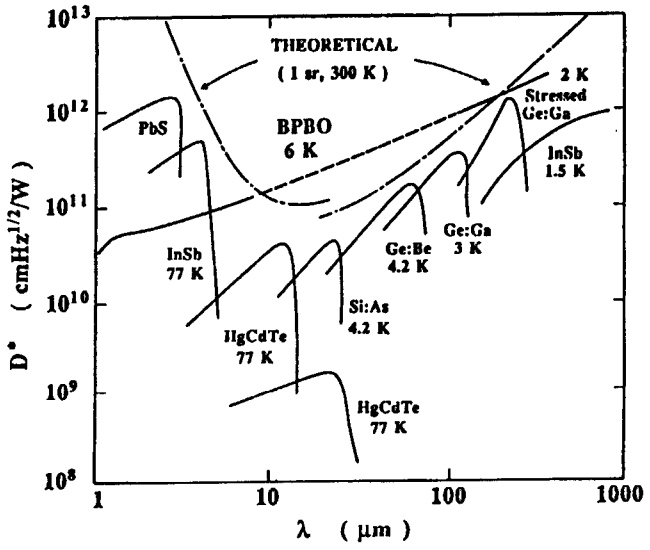

Figure 10. Comparison of Specific Detection Capacity Between BPBO Thin Film Detection Device and Conventional Detection Device

structure of 10~50 μm in width and length is formed, the current-voltage characteristics shown in Figure 8 can be observed.

In other words, characteristics at temperatures near T_c resembled weakly coupled devices, whereas characteristics at lower temperatures closely resemble those of tunnel junctions connected in series. This is because a Boundary Josephson Junction (BJJ) is naturally formed at crystal grain boundaries due to the lack of oxygen, etc., and the constricted structure can be deemed an equivalent junction row, as shown in Figure 9.[18]

The detection device (10 x 10 μm^2 in size) using BPBO multicrystal thin films demonstrated a high sensitivity to an infrared light of λ = 1.3 μm, as described below.[2]

- NEP = $2 \times 10^{-14} WHz^{-1/2}$
- D^* = $5 \times 10^{10} cmHz^{1/2}/W$
- S = 10^4 V/W

These values were obtained at an operating temperature of 6 K, at which characteristics like weakly coupled devices can be observed. It has also been discovered that sensitivity S grows in proportion to $\lambda^{0.5\sim1}$ on the long wavelength side. On the basis of these results, the wavelength dependence of D^* of a BPBO thin film detection device was compared with that of the conventional detection device. The results are shown in Figure 10.

Some semiconductor detection devices, when cooled to cryogenic temperatures, show a high sensitivity near the theoretical limit (background radiation noise limit). These devices have already been developed, although the wavelength region in which such high sensitivity can be obtained is narrow. Meanwhile, it is known that BPBO thin film detection devices demonstrate high sensitivity, approaching the theoretical limit, in a wide wavelength region of $5\ \mu m < \lambda < 500\ \mu m$. The following have been cited as factors allowing such high sensitivity to be obtained.[2]

(1) The carrier density is about $5 \times 10^{21} cm^{-3}$, which is two digits lower than that of metal superconductors such as Nb. Therefore, the reflection factor in the infrared light region is small, and light is absorbed effectively.

(2) The density of states N(0) is smaller than that of metal superconductors and, consequently, large changes in voltage appear due to nonequilibrium phenomena (Equation (4)).

(3) A detection voltage is added and observed ($\delta V_T = N\delta V$; N = number of arrays ~100) due to the effect of the serial connection (array) of grain boundary Josephson junctions. Noise is added to the incoherence and the signal to noise ratio (S/N) grows in proportion to $N^{1/2}$.

(4) The gap energy 2Δ is 3 meV, which is smaller by two or three digits than that of semiconductors. BPBO thin film detection devices, therefore, are highly sensitive to light with a long wavelength (cutoff wavelength: $2_t \sim 500\ \mu m$).

Further, BPBO thin film detection devices are characterized by the fact that their response time is comparatively fast, i.e., 0.5 ns. The response time of a nonequilibrium device can be given by the following effective quasi-particle recombination time:

$$\tau_{eff} = \tau_R \left(\frac{1+\tau_{es}}{\tau_B} \right) \tag{5}$$

where τ_R = recombination time of quasi-particles existing at gap edge
τ_B = time required for phonons (produced during quasi-particle energy relaxation) to break Cooper pairs again
τ_{es} = time required for phonons to begin to escape into the substrate and refrigerant

τ_{es} can further be expressed as follows:

$$\tau_{es} = \frac{4d}{\eta C_s}$$

where C_s = acoustic velocity of superconductor thin film
d = film thickness
η = reflection factor of phonon at thin film interface

τ_R and τ_B are inversely proportional to the third power of T_c.[19] As for BPBO thin films with T_c ~10 K, τ_R and τ_B are estimated to be about 10~50 ps. When the film thickness is 150 nm, τ_{es} can be estimated at 0.5 ns. A τ_{eff} of 1 ns or less can ultimately be achieved.

As mentioned above, nonequilibrium detection devices using BPBO multicrystal thin films are excellent devices, capable of achieving both high sensitivity and high-speed response over a wide wavelength region of far-infrared rays, although their 6 K operating temperature is low. No advanced technologies for preparing oxide superconductor thin films had been established at the time high temperature superconducting materials were discovered. Nonequilibrium detection devices using BPBO multicrystal thin films, therefore, have not yet been put into practical use.

3. Response of High-Temperature Superconductor Thin Film to Infrared Light

3.1 State of Research

With a view to developing infrared light detection devices (based on the nonequilibrium phenomena) that are highly sensitive, respond at high speed, and are operated at high temperatures, such as the liquid nitrogen temperature, research on the response of superconductor thin films to light has been positively promoted, mainly in the United States, since the discovery of high temperature superconductors. This is because high temperature superconducting materials have characteristics similar to those of BPBO, such as low carrier density and the presence of grain boundary Josephson junctions. Typical examples of these studies are given in Table 1.

The technology for preparing high-quality thin films has already been established for YBCO thin films, which, therefore, have mostly been used for studies. There are many examples of research on the response of epitaxial thin films with higher current density J_c to light, in addition to those on multicrystal (granular) thin films similar to BPBO.

With respect to YBCO thin films, no high response sensitivity comparable to that of BPBO has yet been reported at T_c or lower temperatures, in spite of the initial expectations. Most results of research on the response of epitaxial thin films to light show that the peak of the sensitivity is observed solely in the electric resistance transition region near T_c.[20,21] The relaxation time of these responses is small, i.e., 1 μs~0.1 s. Therefore, these responses have been concluded to be bolometric responses that result from rising thin film temperatures, as discussed in Section 2.2. Frenkel, et al., of Bellcore have recently reported that high-quality, very thin films (40 nm thick) show a high-speed response of about 1 ns on the lower temperature side from the

Table 1. Major Examples of Research on Response of YBCO Thin Films to Light

(Epitaxial thin films)

Researchers/ research institutes	Wave-length (μm)	Sensi-tivity (V/W)	Temper-ature region	Response speed	Detection mechanism, etc.
Forrester, et al. (Westinghouse)[20]	0.63 1.06	$4x10^3$	$T \sim T_c$ (50~60 K)	μs – 0.1s	Bolometric d~350 nm
Brockelsby, et al. (AT&B Bell)[21]	0.63 1.06	0.1	$T \sim T_c$ (80 K)	10~100 ns ("ON")	Bolometric d~280 nm
Frenkel, et al. (Bellcore)[22]	1.06	0.03	$T \sim 0.5\ T_c$ (40~60 K)	~1 ns	Nonequi-librium? d~40 nm
Zeldov, et al. (IBM Yorktown)[23]	0.63	~0.25	$T < T_c$ (80~85 K)	< 0.1 ms ?	Optically induced flux-creep

(Granular thin films)

Wilson, et al. (Hughes)[24]	800 K BBDY	3×10^3	$T < T_c$ (60,10 K)	< 0.1 ms	Bolometric + nonequi-librium?
Culbertson, et al. (NRL)[25]	900 K BBDY 0.58	~10	$T \ll T_c$ (~10 K)	~ 10 ns	Nonequi-librium? (KT tran-sition)

resistance transition region, although the sensitivity is low, i.e., 0.03 V/W.[22] They insist that this high-speed response is caused by the nonequilibrium phenomena. The response of high-quality c-axis oriented films at T_c or lower temperatures indicates a temperature dependence that is different from differential resistance (dR/dT). In this regard, Zeldov, et al., of IBM reported on the presence of nonbolometric response components.[23] They also suggested a new mechanism, in which the magnetic flux creeps causing the so-called "bottom" portion of electric resistance in high temperature superconductors are facilitated by the light irradiation.

With respect to granular thin films, several sensitivity peaks were observed on the low temperature side, as well as near T_c.[24-27] So far, it has been stressed that these responses on the low temperature side are caused by the decomposition (related to Kosterlitz-Thouless transition)[25] of restrained magnetic flux pairs peculiar to two-dimensional superconductors and phase slip[26] peculiar to granular thin films. Thus, the response mechanism of high temperature superconductor thin films to light has to date represented a major

issue. It has been indispensable, therefore, to clarify this mechanism in order to obtain guidelines to achieve the development of highly efficient light detection devices as well. Described below are the results of studies we conducted to explain this response mechanism.

3.2 Experimental Methods

We took the following approaches to explain the said mechanism. First, to clarify differences due to materials, we studied the response of $La_{2-x}Sr_xCuO_4$ (LSCO) thin films to light, in addition to that of YBCO thin films. By taking the analogy of BPBO thin films, it was estimated that granular thin films (most multicrystal thin films with weak orientation) could obtain a higher sensitivity. However, in view of the fact that the characteristics can be easily controlled, we used epitaxial thin films whose crystals were oriented uniformly. In this case, two types of crystal grains whose orientations in the c-axis substrate surface cross at right angles were present (the so-called "mosaic" structure), for example, that found in (100) oriented thin films. This caused weak bonding between the crystal grains, and the current density J_c became comparatively low. With respect to YBCO thin films, we also studied the response of variously oriented thin films, as shown in Table 2 below.

Table 2. Characteristics of Thin films Whose Response to Light Was Studied

	LSCO(100)	EBCO(001)	YBCO(103) //[010]	//[301]	YBCO(113)
Substrate	$SrTiO_3$ (100)	MgO(100)	$SrTiO_3$ (110)	—	$SrTiO_3$ (111)
Thickness (nm)	400	110	100	100	100
T_c (K)	18	82	81	79	71
J_c(0 K) (A/cm^2)	3×10^5	1.0×10^7	1.2×10^7	3×10^6	8×10^5

The J_c of these thin films increases in the order of YBCO(113) <YBCO(103) ($j \| c$) < YBCO(103) ($j \perp c$)~EBCO($EuBa_2Cu_3O_y$)(001). These thin films were deposited by magnetron sputtering and reactive evaporation using sintered targets, and their orientations were controlled based on such conditions as the type and temperature of the substrate, and the gas pressure.[28-30] The film thickness was controlled to values equivalent to or less than the light immersion depth (LSCO(100): 500 nm; other thin films: about 100 nm).

Figure 11 shows a light response experiment schematic layout.

Using the said thin films, we prepared a construction of 13 x 13 μm by means of the general photo process and Ar ion milling process. The experiment layout was devised so that semiconductor laser beams (λ = 1.3 μm) could be vertically

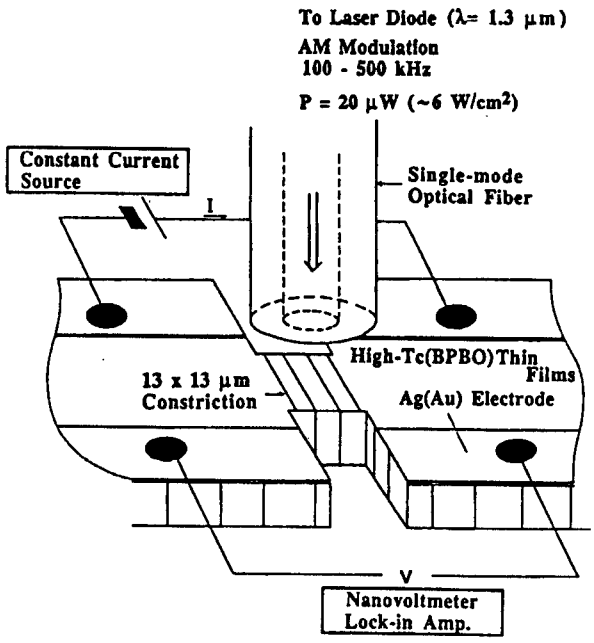

Figure 11. Schematic Drawing of Light Response Experimental Layout

incident upon the constriction, using single-mode optical fibers introduced into the inside of the cryostat. A constant bias current flow was maintained in the thin films. Then, a voltage shift occurring when infrared light (strength = ~20 μW), whose amplitude was modulated by sine waves (wavelength = 100~500 kHz) was irradiated, was observed using lock-in amplifiers, etc.

3.3 Results of Experiments and Studies

Figure 12 shows the bias current dependence of the voltage shift (response voltage) due to light irradiation as observed in LSCO(100) thin films. The detection voltage rises rapidly from a point exceeding the critical current of the thin film constriction and peaks, then decreases slowly. This trend can be markedly observed on the low temperature side, in particular. Such a bias current dependence closely resembles that observed in BPBO thin films. Meanwhile, the bolometric response voltage does peak but, in many cases, grows monotonously with respect to the bias current.

In Figure 13, LSCO(100) thin film response voltages have been plotted in regard to measured temperatures, with the bias current as the parameter. The response voltage peaks at the T_c or lower temperatures. When a low bias current flows, the response voltage peak is low and exists at a point near T_c. As the bias current grows, the response voltage peak shifts on the low temperature side and increases. The highest sensitivity near a measured temperature of 5 K is about 20 V/W, which is two digits smaller than the sensitivity observed by the BPBO thin film detection device. In the figure, changes in the temperature differential coefficient dR/dT of electrical resistance at the largest bias current are shown by broken lines. Where a bolometric response is assumed, the response voltage δV is represented as:

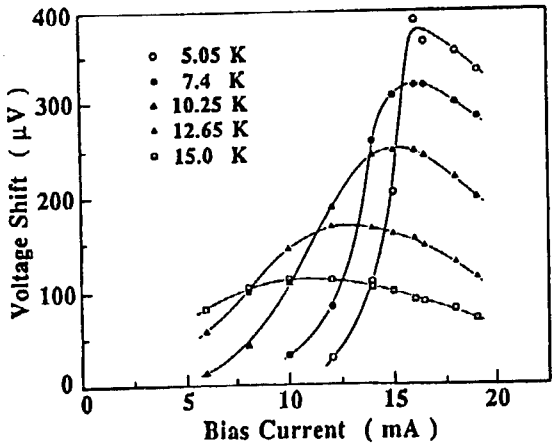

Figure 12. Bias Current Dependence of Response Voltage in LSCO(100) Thin Film (f = 300 kHz, P = 20 μW)

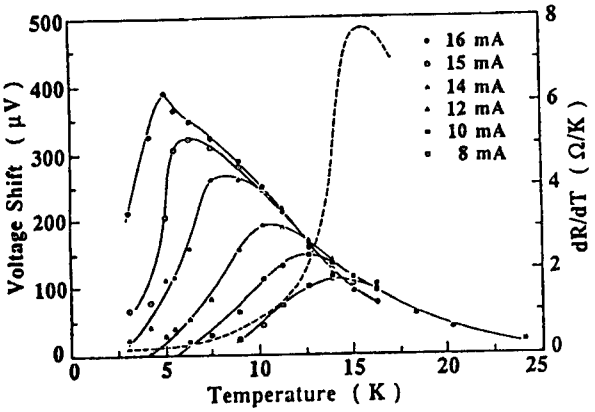

Figure 13. Temperature Dependence of Response Voltage of LSCO(100) Thin film (wave lines show temperature dependence of dR/dT)

$$\delta V = I_B(dR/dT)\ \delta T$$

where I_B = bias current
δT = rate of increase in thin film temperature

When δT is constant, the response voltage must show the same temperature dependence as that of dR/dT. In fact, a large response voltage has been observed at low temperatures, where dR/dT becomes very small. These results clearly indicate that the response is based on a nonbolometric mechanism.

Figure 14 shows the temperature dependence of the response voltage observed in YBCO(103) oriented thin films exhibiting a comparatively high J_c. With respect to a bias current of 2 mA, the peak of the response voltage exists near the transition region of the dc voltage (electrical resistance) indicated by a line alternating long and short dashes. The response appears to be bolometric. If observed carefully, however, it can be seen that a large response exists even in the resistance transition bottom region. To ensure that the presence of this large response can be easily observed, the response voltage is shown in Figure 15 using values standardized by dV/dT.

If the response is bolometric, these standardized values correspond to rising thin film temperatures. In fact, it is known that these values are constant in the region exceeding T_c and that the response is bolometric. It is also known that in the temperature region below T_c, the standardized response grows as the temperature decreases and the nonbolometric response gradually becomes dominant. A very similar trend has been observed for other thin films (given in Table 2) whose orientation and J_c differ. The sensitivity values of YBCO thin film are about 1~5 V/W, which are smaller than those of LSCO thin films.

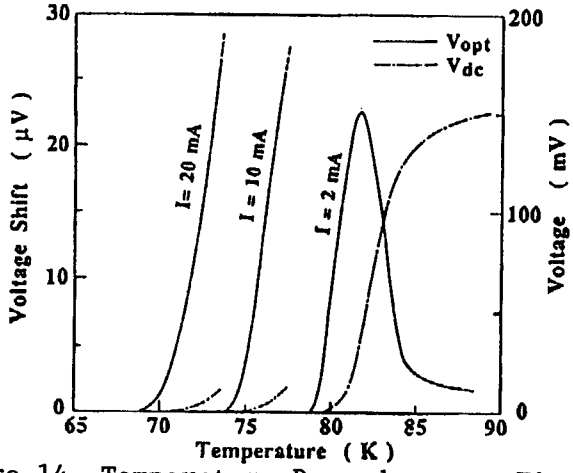

Figure 14. Temperature Dependence (f = 110 kHz, P = 20 μW) of Response Voltage (solid lines) and dc Voltage (alternate long and shortdash line) in YBCO(103) Thin Film (j⊥c)

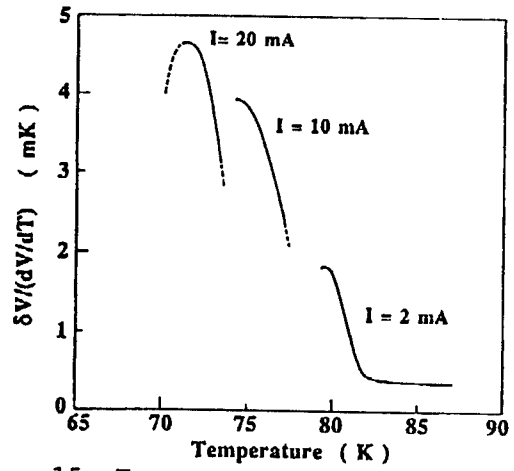

Figure 15. Temperature Dependence of Standardized Response With Respect to YBCO(103) Thin Film (j⊥c)

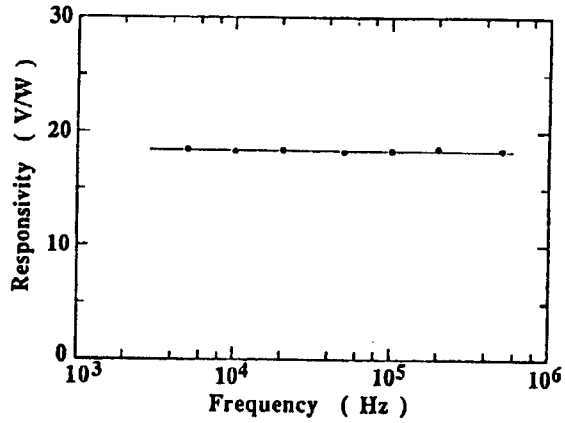

Figure 16. Modulation Frequency Dependence of Response Sensitivity to LSCO(100) Thin Films

Figure 16 shows the modulation frequency dependence of the response sensitivity to LSCO(100) thin films. The figure shows that the sensitivity is constant with respect to modulations up to 500 kHz, and that the response time is shorter than a μs. There is little change in the sensitivity of other thin films in this frequency range. These results have been obtained. A future task will be to resolve problems involving the unwanted capacity and contact resistance of the contact part, thereby measuring the high-speed response using pulsed light.

As mentioned above, the nonbolometric response becomes dominant in both LSCO and YBCO thin films in the region of temperatures below the T_c. The nonequilibrium phenomenon, as that found with BPBO thin films, can initially be considered to be the mechanism for this response. Sensitivity based on the nonequilibrium phenomenon can generally be represented as follows:

$$\tau_{NE} = \frac{\partial V}{\partial I_c}\Big|_{I_B} \frac{\partial I_c}{\partial \Delta}\Big|_T \frac{\partial \Delta}{\partial n_{qp}}\Big|_T \frac{\delta n_{qp}}{P}. \quad (7)$$

where I_c = critical current
δn_{qp} = excessive quasi-particle density
P = incident light power

The first term indicates the bias current dependence. Where this term is assumed to have been optimized, the magnitude of sensitivity is controlled by the third and fourth terms. Where quasi-particles of $h\nu/\Delta$ in quantity are assumed to have been ideally produced by photons with an energy of $h\nu$, the excessive quasi-particle density of the fourth term is proportional to τ_{eff}/Δ. τ_{eff} is an effective recombination time given by Equation (5). τ_R and τ_B are inversely proportional to the third power of T_c. Therefore, these values become quite small in high temperature superconducting materials, compared with τ_{es}, and τ_{es} is thought to control τ_{eff}. τ_{es} of an oxide superconductor of about 100 nm in thickness shows a small dependence on materials, and is estimated to reach about 1 ns. Meanwhile, the third term can be approximated as 1/2N(0) (N(0): density of states). The sensitivity is ultimately inversely proportional to $2N(0)\Delta$, that is, the pair electron density. Where the quantum efficiency is otherwise assumed to decrease against photons with high energy, it can be concluded that the sensitivity is inversely proportional to N(0).

Physical properties and response sensitivity observed for BPBO, LSCO, and YBCO are given in Table 3.

Table 3. Physical Parameter and Response Sensitivity of Various Oxide Superconductors

Material		BPBO	LSCO	YBCO
T_c	(K)	12	38	92
n	$(10^{21}cm^{-3})$[31]	4	2	5
N(0)	$(10^{21}$ states/eV $cm^3)$[32]	1.9	27	102
r	V/W	10^3~10^4	10~20	1~5
r_N	(mK)		10^2	10

n: carrier density
r_N: normalized response = $\delta V/(dV/dT)$

The number of carriers of Cu-based superconducting materials greatly resembles that of BPBO. However, the density of states of LSCO and YBCO, calculated based on the electron specific heat coefficient γ, is about 15 times and 50 times, respectively, that of BPBO. In other words, the density of states of LSCO and YBCO is larger by one or two digits than that of BPBO.[31,32] This difference between the two groups is thought to be closely related to the superconductivity mechanism. The response sensitivity observed is larger in the order of BPBO > LSCO > YBCO, which nearly agrees with the said theoretical

estimate. $Ba_{1-x}K_xBiO_3$(BKBO) thin films have a T_c of about 30 K, but their N(0) is estimated to be about two times that of BPBO. We have recently measured the response of these thin films and obtained a sensitivity which is larger by one or two digits than that of Cu-based high temperature superconductors.[33] Thus, since there is a strong correlation between response sensitivity and the density of states, it can be concluded that the nonbolometric response observed in LSCO and YBCO is based on the nonequilibrium phenomenon.

We have thus found that the use of materials whose density of states is small, such as BKBO, has proven to be effective in achieving the development of highly sensitive nonequilibrium detection devices. In addition, where materials whose density of states is large, such as YBCO, are used, it is thought to be necessary to have more control over the escape of phonons to substrates (in this case, approaching bolometers) or to improve the quasi-particle density by using extremely thin films.

4. Conclusion

The above-mentioned transition-edge bolometers, quasi-particle Josephson mixers, and nonequilibrium device are each based on different principles. As can be seen in these devices, however, the practical use of electromagnetic wave/light detection devices which utilize the characteristics of high temperature superconducting materials and oxide superconducting materials has already been proposed. These devices have high potential for greatly surpassing detection devices using conventional semiconductors, although no characteristics allowing practical use have yet been indicated. Therefore, proving the superior potentials of these devices represents a major topic that requires immediate attention. This is thought to be the first step to developing new application fields and achieving dreams, as represented by communications in the THz band. It is hoped that this goal will be achieved concurrently with progress in the technologies for manufacturing thin films, junctions, etc., as well as with the classification of the physical properties of high temperature superconductors.

References

1. Kurakado, M. and Matsumura, A., JAPANESE JOURNAL OF APPLIED PHYSICS, Vol 28, 1989, p L459.

2. Enomoto, Y., et al., Ibid., Vol 23, 1984, p L333; Enomoto, Y. and Murakami, T., J. APPL. PHYS., Vol 59, 1986, p 3807.

3. Kumagawa, et al., Electronic Information Communications Society Meeting, 22-5, 1987.

4. Tanabe, K., et al., JAPANESE JOURNAL OF APPLIED PHYSICS, Vol 29, 1990, p L466.

5. Niki, et al., "Electronic Information Communications Society Technological Study Report," SCE90-8, 1990.

6. Clarke, J., et al., J. APPL. PHYS., Vol 48, 1977, p 4865.

7. Richards, P.L., et al., APPLIED PHYSICS LETTERS, Vol 54, 1989, p 283.

8. Stratton, T.G., et al., Proc. SC GLOBAL 90, Long Beach, 1990 (Superconductor Applications Association, El Toro, 1990).

9. Richards, P.L. and Qing Hu, PROC. IEEE, Vol 77, 1989, p 1233.

10. Ferrari, M.J., et al., APPLIED PHYSICS LETTERS, Vol 53, 1988, p 695; Ferrari, M.J., et al., IEEE TRANS. MAGN., Vol MG-25, 1989, p 806.

11. NIKKEI SUPERCONDUCTOR, 10 July 1989, p 8.

12. Tien-Lai Hwang, et al., APPLIED PHYSICS LETTERS, Vol 34, 1979, p 773.

13. Qing Hu and Richards, P.L., Ibid., Vol 55, 1989, p 2444.

14. Nisenoff, M., CRYOGENICS, Vol 28, 1988, p 47.

15. For example, "Superconducting Electronics," (edited by H. Hara, Ohm Co., Ltd.) 1985.

16. Sobolewski, R., et al., PHYSICA C, Vols 153-155, 1988, p 1431; Konopka, J., et al., APPLIED PHYSICS LETTERS, Vol 53, 1988, p 796.

17. Sugawara, et al., "Electronic Information Communications Society Technological Study Report," SCE90-2, 1990.

18. Enomoto, Y., et al., JAPANESE JOURNAL OF APPLIED PHYSICS, Vol 21, 1982, p L384.

19. Kapalan, S.B. et al., PHYS. REV. B, Vol 14, 1976, p 4854.

20. Forrester, M.F., et al., APPLIED PHYSICS LETTERS, Vol 53, 1988, p 1332.

21. Brocklesby, W.S., et al., Ibid., Vol 54, 1989, p 1175.

22. Frenkel, A., et al., Ibid., p 1594.

23. Zeldov, E., et al., PHYS. REV. LETT., Vol 62, 1989, p 3093.

24. Wilson, J.A., et al., Paper A2, presented Mtg. IRIS Specialty Group on Infrared Detectors, Baltimore, August 1988.

25. Culbertson, J.C., et al., PHYS. REV., Vol B39, 1989, p 12359.

26. Leung, M., et al., APPLIED PHYSICS LETTERS, Vol 51, 1987, p 2046.

27. Osterman, D.P., et al., IEEE TRANS. MAGN., Vol MAG-25, 1989, p 1323.

28. Suzuki, M. and Murakami, T., PHASE TRANSITIONS, Vol 15, 1989, p 201.

29. Asano, H., et al., JAPANESE JOURNAL OF APPLIED PHYSICS, Vol 28, 1989, p L981.

30. Kubo, et al., 1990 Spring Applied Physics Lecture Meeting Preliminary Draft, p 123.

31. Kitazawa, Kishio, APPL. PHYS., Vol 57,1988, p 1644.

32. Batlogg, B., "Mechanism of High Temperature Superconductivity," H. Kamimura and A. Oshiyama, ed., Springer-Verlag, Berlin-Heidelberg, 1989, p 326.

33. Tanabe, et al., Pending contribution of article by periodical.

Thin Films for Magnetic Applications

916C1001J Tokyo HYOMEN KAGAKU SEMINA in Japanese 27-29 Jun 90 pp 125-127

[Article by Ushio Kawabe, Hitachi Central Laboratory, Hitachi, Ltd.]

[Text] **1. Introduction**

High temperature superconducting thin film formation technologies have to date been studied in various manners, and good quality thin films have already been prepared. The magnetic properties of high temperature superconductors have already been made clear. Therefore, the application of high temperature superconductors to the magnetic field using these properties has been reported at several academic society meetings. This paper outlines the latest status of and outlook for the application of thin films to the magnetic field.

2. Magnetic Properties of High Temperature Superconducting Thin Film

As a magnetic field is applied to high temperature superconducting thin films, superconducting condensation is released; this phenomenon appears markedly at higher temperatures. Therefore, the process of the invasion of a magnetic field into high temperature superconductors varies with magnetic fields and temperatures. This phenomenon can be represented by the state variables of magnetic field and temperature based on the GLAG phenomenon theory[1] for metal group superconductors. In particular, the GL parameters κ of high temperature superconductors are two digits smaller than those of metal superconductors. In addition, the magnetic fields and temperatures of high temperature superconductors are one digit larger than those of metal group superconductors. New unusual phenomena, therefore, are appearing. Nelson, et al.,[2] have roughly classified three regions whose magnetic properties differ from each other. When magnetic field is applied to high temperature superconducting thin films, a completely diamagnetic Meissner region appears. This region is very narrow because Hc_1 is small. In this case, magnetic flux invades only the surface layer (depth: magnetic field invasion length λ) of high temperature superconductors. As a result, high temperature superconducting thin films, as a whole, demonstrate complete electric conductivity, and the surface resistance is extremely small. Further, when the size of the magnetic field exceeds Hc_1, vortexes with a threadlike core (core radius = coherence length ξ) placed in a nonsuperconducting state invade the inside of the superconductor in the

magnetic field direction and form triangular crystal lattices.[3] In this case, magnetic flux invades only the threadlike core portion placed in a nonsuperconducting state. The thin films do not exhibit complete electric conductivity, but possess a small amount of a resistance component. In this region, magnetic flux creeps that vary with the passage of time are likely to occur. As the magnetic field continues to grow, the triangular crystal lattices encounter problems and begin to partially scatter and melt. They soon assume an amorphous or fluidic state. This phenomenon is accelerated when the temperature is high, even though the magnetic field is small. There is an example in which this phenomenon began to occur in YBCO at 60 K. In this temperature region, the invasion of magnetic flux becomes irregularly disordered, and irreversible changes occur. If an electric current is applied to the superconductor placed in such an irreversible state, a large magnetic flux flow and marked abnormality in resistance, associated with the two-dimensional structure, appear.[4] The appearance of these phenomena is noticeable near the critical temperature, even though the magnetic field is weak. Thus, the superconducting thin films, having undergone this process, exceed the critical value Hc_2, and finally, through phase transition, enter into a nonsuperconducting state. This is an ideal magnetic property of high temperature superconductors. Actual materials, however, are mixed with defects and inhomogeneous points of the third phase. These inhomogeneous points themselves have the effect of pinning the magnetic flux, and this effect operates in the direction in which the thin films try to maintain their superconducting state against the invasion of the large magnetic flux. However, if this effect is excessive, an unstable magnetic field is formed. The magnetic properties of thin films with good crystallinity depends on the anisotropy of crystals. It is necessary to study the application of high temperature superconducting thin films to the magnetic field, taking these characteristics into consideration.

3. Application of High-Temperature Superconducting Thin Film to Magnetic Field

Regarding the application of high temperature superconducting thin films to magnetic fields using their magnetic properties, the following examples have already been reported:

(1) Use of the magnetic field dependence of high temperature superconducting thin films characteristics I–V near critical temperature.[5]

(2) Use of high temperature superconducting thin film magnetic flux flow.

(3) Use of grain boundary Josephson junction characteristics IV, quantum interference phenomena, and V–ϕ characteristics.[6]

(4) Use of S (Pb alloy)/N(ag)/S(YBCO) junction and proximity effects.[7]

(5) dc transformer connection using the superconducting phenomena.[8]

(6) Use of YBCO/PrBCO/YBCO heteroepitaxial structure and superlattice structure.[9]

(7) Magnetic shield and trap using Meissner effect and pinning effect.[10]

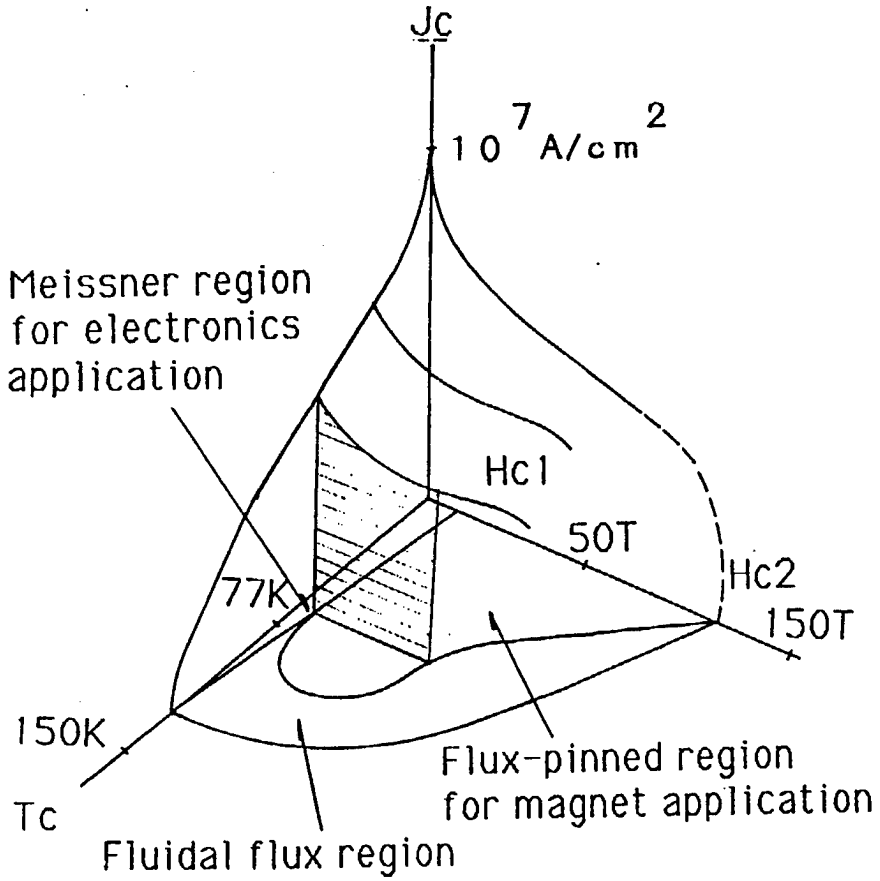

Figure. Three states of Superconductor in Space Surrounded by Critical Temperature, Critical Magnetic Field, and Critical Current

4. Outlook

The application of high temperature superconducting thin films to the magnetic field set forth in (1) through (6) above employs the sharp changes which occur in the order of the coherence length on high temperature superconducting thin film interfaces. If the surface and interface of high temperature superconducting thin films can be controlled, hopes will be able to be placed on dreamlike O_3s at the liquid nitrogen temperature by extracting specific features involving the application of high temperature superconducting thin films to the magnetic field. The key technology in this field is the low temperature thin film formation process technology at the atomic level.

References

1. Gorkov, L.P., SOVIET PHYS., Vol JETP9, 1959, p 1364.

2. Nelson, D.R., Proceedings of M2-THSC Meeting, Stanford, 1989; PHYSICA, Vols C162-164, 1989, p 1156.

3. Abrikosov, A.A., SOVIET PHYS., Vol JETP5, 1957, p 1174.

4. Ban, M., Ichiguchi, T., and Onogi, T., PHYS. REV., Vol 40B, 1989, p 4419.

5. Nojima, H., et al., FEDHiTcSc-ED2nd Workshop, Hokkaido, 1989.

6. Koch, R.H., et al., APL, Vol 54, 1989, p 951.

7. Nishino, T., et al., To be published in APL in 1990.

8. Tarutani, Y., et al., MRS Int'l. Meeting on Advanced Materials, Tokyo, 1989.

9. Rogers, T., et al., APL. LETT., Vol 55, 1989, p 2032.

10. Tanaka, S., 2nd ISTEC Workshop on Superconductivity, Kagoshima, 29 May 1990.

- END -

NTIS
ATTN: PROCESS 103

5285 PORT ROYAL RD
SPRINGFIELD, VA 22161

This is a U.S. Government publication. Its contents in no way represent the policies, views, or attitudes of the U.S. Government. Users of this publication may cite FBIS or JPRS provided they do so in a manner clearly identifying them as the secondary source.

Foreign Broadcast Information Service (FBIS) and Joint Publications Research Service (JPRS) publications contain political, military, economic, environmental, and sociological news, commentary, and other information, as well as scientific and technical data and reports. All information has been obtained from foreign radio and television broadcasts, news agency transmissions, newspapers, books, and periodicals. Items generally are processed from the first or best available sources. It should not be inferred that they have been disseminated only in the medium, in the language, or to the area indicated. Items from foreign language sources are translated; those from English-language sources are transcribed. Except for excluding certain diacritics, FBIS renders personal and place-names in accordance with the romanization systems approved for U.S. Government publications by the U.S. Board of Geographic Names.

Headlines, editorial reports, and material enclosed in brackets [ ] are supplied by FBIS/JPRS. Processing indicators such as [Text] or [Excerpts] in the first line of each item indicate how the information was processed from the original. Unfamiliar names rendered phonetically are enclosed in parentheses. Words or names preceded by a question mark and enclosed in parentheses were not clear from the original source but have been supplied as appropriate to the context. Other unattributed parenthetical notes within the body of an item originate with the source. Times within items are as given by the source. Passages in boldface or italics are as published.

SUBSCRIPTION/PROCUREMENT INFORMATION

The FBIS DAILY REPORT contains current news and information and is published Monday through Friday in eight volumes: China, East Europe, Soviet Union, East Asia, Near East & South Asia, Sub-Saharan Africa, Latin America, and West Europe. Supplements to the DAILY REPORTs may also be available periodically and will be distributed to regular DAILY REPORT subscribers. JPRS publications, which include approximately 50 regional, worldwide, and topical reports, generally contain less time-sensitive information and are published periodically.

Current DAILY REPORTs and JPRS publications are listed in *Government Reports Announcements* issued semimonthly by the National Technical Information Service (NTIS), 5285 Port Royal Road, Springfield, Virginia 22161 and the *Monthly Catalog of U.S. Government Publications* issued by the Superintendent of Documents, U.S. Government Printing Office, Washington, D.C. 20402.

The public may subscribe to either hardcover or microfiche versions of the DAILY REPORTs and JPRS publications through NTIS at the above address or by calling (703) 487-4630. Subscription rates will be provided by NTIS upon request. Subscriptions are available outside the United States from NTIS or appointed foreign dealers. New subscribers should expect a 30-day delay in receipt of the first issue.

U.S. Government offices may obtain subscriptions to the DAILY REPORTs or JPRS publications (hardcover or microfiche) at no charge through their sponsoring organizations. For additional information or assistance, call FBIS, (202) 338-6735,or write to P.O. Box 2604, Washington, D.C. 20013. Department of Defense consumers are required to submit requests through appropriate command validation channels to DIA, RTS-2C, Washington, D.C. 20301. (Telephone: (202) 373-3771, Autovon: 243-3771.)

Back issues or single copies of the DAILY REPORTs and JPRS publications are not available. Both the DAILY REPORTs and the JPRS publications are on file for public reference at the Library of Congress and at many Federal Depository Libraries. Reference copies may also be seen at many public and university libraries throughout the United States.